Numerical Study on Tsunami Disaster Mitigation around Aceh Province, Indonesia

（インドネシア・アチェ州周辺における津波減災に関する数値解析）

July, 2019

Doctor of Philosophy (Engineering)

Teuku Muhammad Rasyif
（テウク　モハマド　ラシフ）

Toyohashi University of Technology

Abstract

Dreadful damages was caused by tsunami waves in several coastal areas in this world. Especially tsunami in 2004, the tsunami gave damage to infrastructures in coastal area and caused about 230,000 numbers of human casualties at several countries such as Indonesia, Sri Langka, Thailand, and India. One decade after the 2004 tsunami, about seven big earthquake such as the Nias and Simeulu tsunami on 2005, Mentawai island tsunami on 2010, and on 2012 have been occurred in Sumatra subduction zone. That tsunamis caused different impact in Indonesia especially along the coastal areas of Aceh Province. The reflected tsunami wave in Pulo Raya Island during the 2004 tsunami able to caused massive impact toward the lee side of the island. The tsunami wave amplification have been happened toward several cities in western coast of Aceh such as Meulaboh, Tapaktuan, and Singkil due to influence of small island that located in front of the cities.

The tsunami waves also have caused significantly morphological changes in coastal area such as could separate a mainland and leave the small amount of the mainland at the sea which change it become a new small island. This indicated the tsunami waves have the strong force which it could be erode the sediment at the bottom of the sea and the land. The form of dark-murky water which witnesses by the local community who survive from the Indian Ocean Tsunami evidences that tsunami waves which come to the shore brought the large number of sediment to mainland while run-up.

Following this series of tragic events, which caused huge losses of life and enormous damage to infrastructure, several researchers developed a numerical model to gain a greater understanding of tsunami wave process from its generation until inundation to the coastal areas. The numerical simulation becomes one method which widely was used by several researchers to investigate

tsunami wave impact toward the coastal area. Therefore, several mitigation process were derived from the simulation results such as estimated of inundation area (EIA) and estimated time of arrival (ETA). The EIA and ETA data were used by several country to create tsunami hazard map and incorporate with the tsunami early warning system. However, other tsunami mechanism such as sediment transport is rather not consider in the tsunami simulation model. The sediment transport is one of important things in process of tsunami mitigation such as to study about the coastal morphological changes, recovery process after tsunami, and tsunami deposit.

Chapter One illustrates the impact from tsunami wave toward coastal area of Aceh Province. The previous studies on tsunami wave impact, the reflected wave effect, the small island influence, and morphological changes are summarized.

In Chapter Two, a general information about numerical model and equations such as shallow water, sediment transport, and bottom level changes formula that applied are summarized. Several cities in Aceh Province such as the western coast of Aceh Province and Pulo Raya island as a large domain and Banda Aceh as a small domain were used as study case. The large domain was investigated by observing the wave propagation process toward the coastal area by using the COMCOT model. The coastal morphological changes was investigated by coupling a hydrodynamic model with a sediment transport module on Banda Aceh city as the small domain. The Cornell Multigrid Coupled Tsunami Model (COMCOT) was coupled with the XBeach Model to simultaneously simulate sediment transport and the hydrodynamic process during the tsunami. The coupled model is known as COMCOT-SED.

In Chapter Three, the numerical simulation of the 2004 Indian Ocean Tsunami were validated, analyzed, and discussed. The satellite measurement,

field observation, and geospatial information data were applied to validate the simulation results for large and small domain. The results show that the simulation results have a good agreement with the observation data. The propagation process results also show different characteristic toward the western cities and Pulo Raya island as the large domain. The COMCOT-SED model indicated that coastal area of Banda Aceh city as the small domain received massive morphological changes impact due to the 2004 tsunami.

In Chapter Four, the influence of the small island against tsunami wave is investigated through a numerical simulations. Past and hypothetical earthquake have been applied to investigate the influence of the small island. Small changes of the location of epicenter in future tsunami will result in different tsunami impact along Sumatra Island due to the influence of small island. The hydrodynamic processes of reflected tsunami waves and their impact on Pulo Raya Island are also investigated with the numerical model. The simulation confirms eyewitness accounts that it was not the initial run-up, but the reflected waves that devastated the worst-hit areas of the island.

In Chapter Five, major findings, conclusions, and recommendation obtained in this study are summarized.

Dedication

This study is dedicated to the people who have never failed to give me moral support, especially my dearest wife, and daughter.

Acknowledgements

Bismillahhirrahmannirrahim

First of all, I am grateful to the almighty Allah for making all of things possible so this thesis could be finish in time. Secondly, I would like to express a sincere gratitude to my parent, my family, and my brothers who always pray and encourage me to finish this research.

I would dedicate sincere thankfulness and gratitude to my supervisor Prof. Shigeru Kato for interminable guidance, help and support throughout the period of research. He has devoted much of his valuable time, for accepting me to carry out the research in their areas of jurisdiction and for providing accommodation. His assistance have been vital for the research.

I also express my gratitude to Prof. Takanobu Inoue and Prof. Kuriko Yokota as the committee members who kindly read my thesis and gave many suggestions.

I am deeply grateful to Dr.Eng Syamsidik, who has helped me in many ways.

I would also like to acknowledge with much appreciation for the crucial friendship of the member of Coastal and Hydraulics Engineering Laboratory in Japan and Indonesia respectively, for their kindness, cooperation and friendship. Their support and pray made it possible through to the end. Many more persons participated in various ways to ensure my research succeeded and I

am thankful to them all.

Finally, I have to express my gratitude to the Ministry of Education, Culture, Sports, Science and Technology of Japan (MEXT) Scholarship which has supported my study by providing the scholarship in Toyohashi University of Technology.

Teuku Muhammad Rasyif

Toyohashi, Japan

July, 2019

Contents

List of Figures

List of Tables

Chapter 1

Introduction

1.1 Backgrounds

Tsunamis have caused significant damages to coastal areas worldwide. The big earthquake that generates destructive tsunami was occurred on December, 26th 2004 with magnitude about $M_W = 9.1$. This quake was occurred after about 100 year since the big earthquake in 1907 at the Sumatra subduction zone. Along that time, the quake with magnitude $M_W > 7.5$ did not occurred. Less information and education regarding this mega disaster had caused massive damaged infrastructures in coastal area and caused about 230,000 fatalities mainly in Indonesia, Sri Lanka, Thailand, and India.

Less than 3 months after the big tsunami in 2004, an earthquake occurrence does not start to stop. The stress given by the great earthquake on 2004 activated an adjacent segment of the fault on 2005. In just a decade based on the historical data (USGS, 2014), the number of earthquakes around Sumatra subduction zone that occurred within the time period 2004-2014, with magnitude greater than $M_W > 5$, and hypocenters shallower than 40 km were about

3395 as shown in Figure 1.1. Among these earthquakes, four big tsunamigenic earthquakes with magnitude over $M_W > 8$ as indicated by red circle in Figure Figure 1.1 were occurred along Sumatra subduction zone such as the Indian Ocean tsunami on December 26, 2004, the Nias and Simeulu islands tsunami on March 21, 2005, the Mentawai island tsunami on October 25, 2010, and the

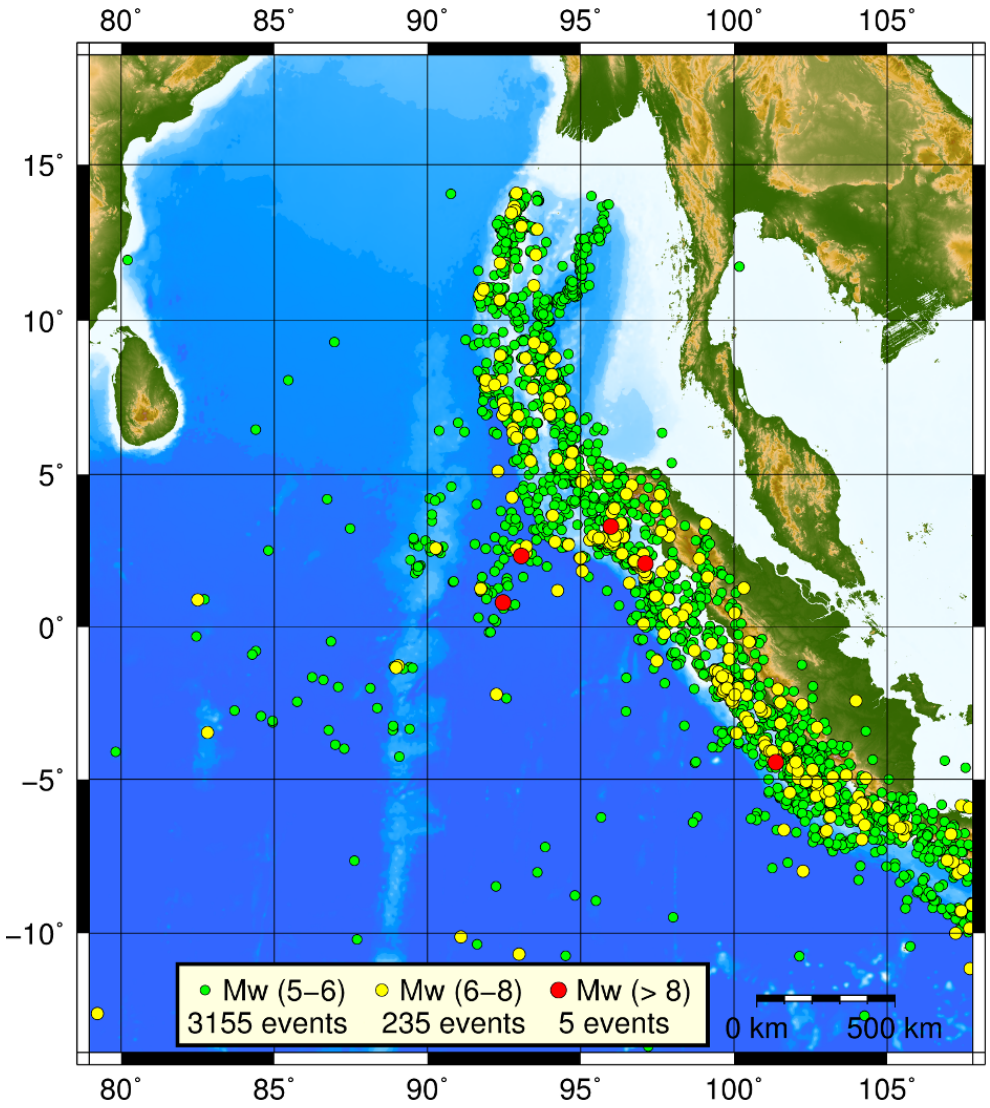

Figure 1.1: Historical earthquakes within the time period 2004-2014 (USGS, 2014).

biggest strike-slip earthquake on November 4, 2012 (Duputel et al., 2012).

The earthquakes that occurred at Sumatra subduction zone itself caused different impact along the coastal area in Aceh Province. Such as at the western cities of Aceh namely: Meulaboh, Tapaktuan, and Singkil, The tsunami wave in 2004 and 2005 did not give significant damage on Tapaktuan city due to existing of the small island. In another hand, the tsunami waves in 2004 and 2005 were caused massive damage in Meulaboh and Singkil. This condition caused difficulty to carry out any disaster mitigation program such as prepares an escape route, an escape building, etc in order to prevent the tsunami hazard at Tapaktuan city (Syamsidik et al., 2015b).

Minor mitigation activity from the local government can decrease awareness and preparedness of local community at Tapaktuan toward the tsunami disaster. A study to understand the impact of the tsunami wave at the mainland due to existing of the small island is necessary to be resolved. Few research to date has discussed on the influence of an isle group especially an island with a long shape such as the Simeulu Island which located in front of Tapaktuan toward the tsunami wave. The recent researches showed that the small offshore island can be act as an amplification of wave energy to the mainland. This condition was proofed by the Mentawai Island tsunami on 2010 as shown in Figure 1.2 (Hill et al., 2012).

The tsunami waves impacted not only mainland areas but also small islands many of which experienced major damage. Impacts of the 2004 Indian Ocean tsunami on small islands often received less attention than the mainland area. Tsunami mitigation on small islands is difficult. These islands offer limited evacuation areas and are located close to tsunamigenic sources. In some cases,

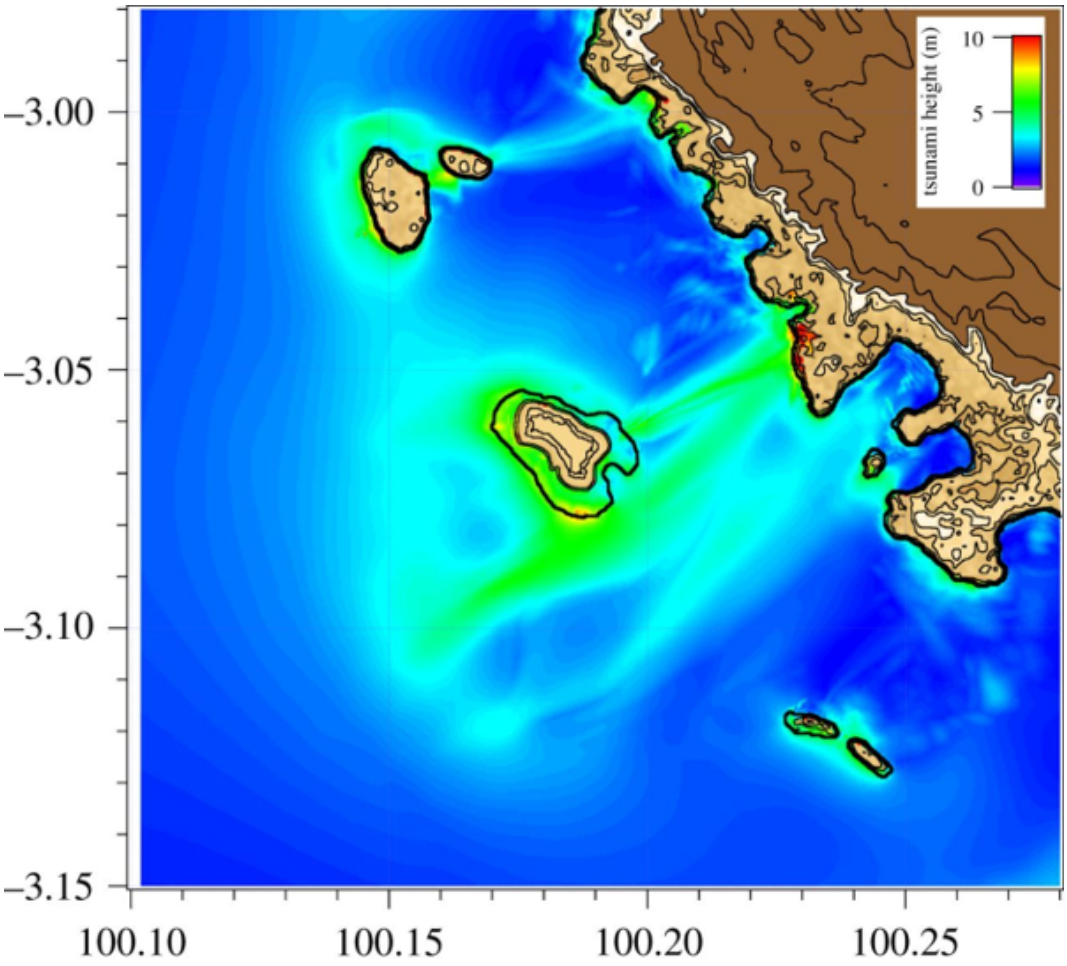

Figure 1.2: Simulation of the maximum wave height during the Mentawais 2010 tsunami. Significant run-up is observed on the coastal areas behind the small offshore islands (Hill et al., 2012).

small islands in Indonesia are even isolated from the national tsunami early warning system (Syamsidik and Istiyanto, 2013). Past tsunami events, such as the 1992 Flores Island tsunami and the 1993 Hokkaido Island tsunami, caused massive damage on the lee sides of small islands (Yeh et al., 1993, 1994; Liu et al., 1995). Post-tsunami survey data showed that the tsunami runup was significantly higher on these islands. By using numerical simulation and observation data, (Imamura et al., 1995) found that the reflected tsunami

waves were the main cause of the worst impacts on the southern coast of Babi Island during the Flores Island tsunami as indicated in Figure 1.3. The tsunami that hit the Mentawai Islands in 2010 had the same impacts as those that hit the Flores and Hokkaido islands. The tsunami waves were amplified around the lee side of the small island instead of being reduced by the island.

Tsunami wave also can cause severe change to coastal morphology. Nev-

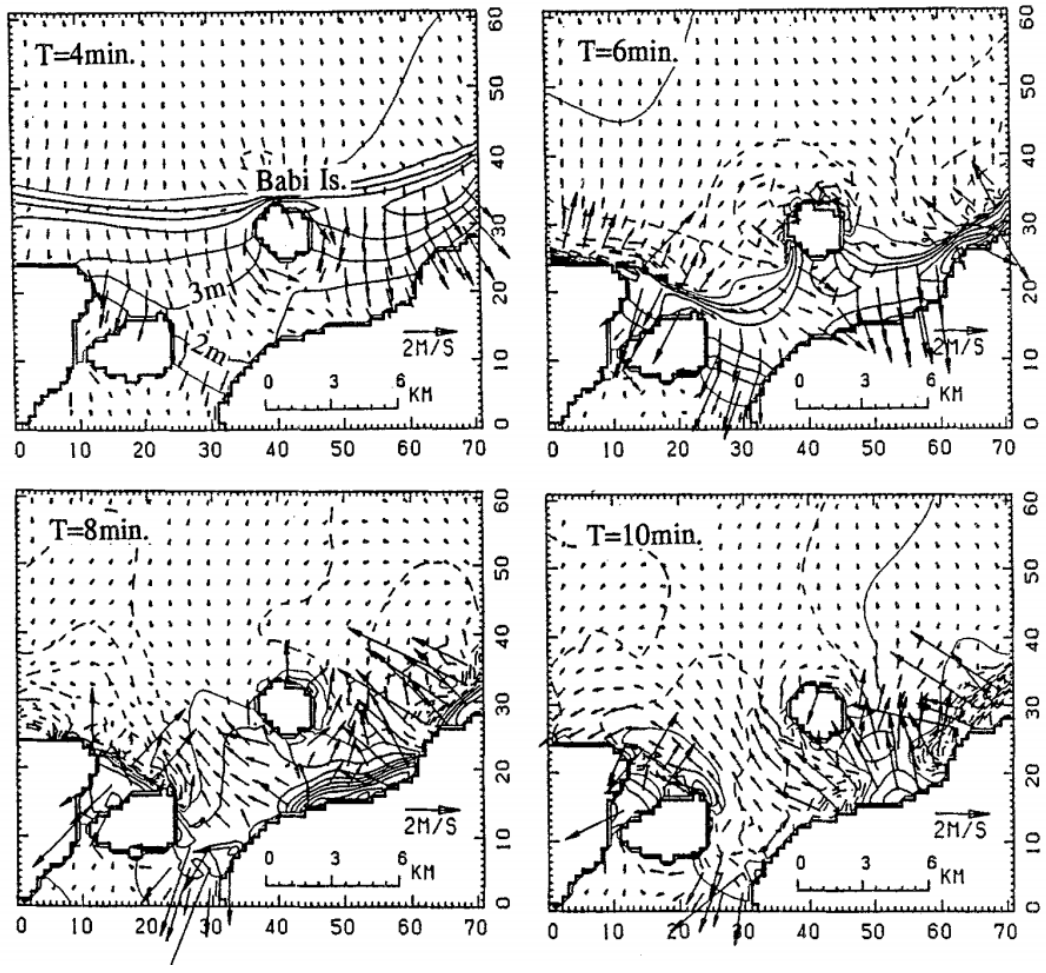

Figure 1.3: Water elevation contours with intervals of 1 m and current vectors around Babi Island. The first wave was reflected along the northern shore of Flores Island 8 minutes after the earthquake and attacked the southern coast of Babi Island (Imamura et al., 1995).

ertheless the latest developments in tsunami engineering, we still do not fully understand the massive sediment transport that occurs during tsunami waves. The 2004 Indian Ocean tsunami that eroded a large part of coastal areas in affected coasts provides important evidence on tsunami sediment transport. However, large-scale simulations investigating the sediment transport process are still rare. The hydrodynamics of tsunami waves can result in massive destruction of coastal areas (Sugawara et al., 2014; Gusman et al., 2018; Ontowirjo et al., 2013). Previous research has mainly focused on morphological changes from the tsunami wave by observing the change based on satellite images, aerial photo, and field measurements (Richmond et al., 2012; Tappin et al., 2012; Tanaka et al., 2012; Syamsidik et al., 2017a). On the other hand, very few numerical investigations of beach profile changes caused by tsunami waves have been performed (Ramalho et al., 2018; Yamashita et al., 2016).

In recent decades, tsunami numerical simulations have been developed by applying a hydrodynamic model to simulate a tsunami wave, from its generation and propagation until inundation, such as Method of Splitting Tsunami (MOST) (Titov and Synolakis, 1998), Tohoku University's Numerical Analysis Model for Investigation of Near-field tsunamis (TUNAMI-N2) (Goto et al., 1992), Cornell Multigrid Coupled Tsunami Model (COMCOT) (Liu et al., 1995; Wang, 2009). These model were open sorece models and developed based on Shallow Water Equations (SWE). However, MOST model did not consider a bottom friction. Therefore, this model usually used for worst case scenario. In another hand, TUNAMI-N2 and COMCOT models have been applied the bottom friction in its calculation.

Several benchmark studies for COMCOT model were conducted in previous studies to evaluate the numerical model's validity with analytical solution,

laboratory, and field measurements (Wijetunge et al., 2008; Wijetunge, 2009; Liu et al., 1995; Wang, 2009; Wang and Liu, 2007; Megawati et al., 2009). The COMCOT model has been used to estimate the inundation area and time of arrival known as Estimate of Inundation Area (EIA) and Estimated Time of Arrival (ETA), which contributes to the mitigation concept of creating a tsunami hazard map and incorporation with a tsunami early warning system (Syamsidik et al., 2015b).

However, these model such as COMCOT and TUNAMI-N2 did not consider the morphological changes and sediment transport when the tsunami wave propagate in nearshore area in it's calculation. Many tsunami witnesses and measurement studies were observed that the tsunami wave able to bring the sediment in high velocity (Lavigne et al., 2009; Bourgeois, 2009). Currently, there are several the tsunami models that employed the sediment transport to investigate the morphological changes due to tsunami wave such as the model that developed by (Simpson and Castelltort, 2006; Xiao et al., 2010; Sugawara, 2004; Takahashi et al., 2001; Goto and Imamura, 2007; Apotsos et al., 2011; Nakamura et al., 2009). These model have been validated by using laboratory experiment and real case event.

Nonetheless, there are several demerit from the previous model such as cannot handle mixed grain sizes, the large and small domain are simulated separately which apply just hydrodynamic and both of hydrodynamic and sediment transport, and limited to be used for small and moderate tsunami with wave height around 5-10 m. The COMCOT-SED model that developed by (Li et al., 2012) was applied to simulate the tsunami wave induced sediment transport. This model have been improved from the previous study such as able to simulate the tsunami wave induced sediment transport with mix grain

size, simulate with multi grid size simultaneously, and able to simulate with tsunami wave height more than 15 m.

Unlike the 2011 Great East Japan Earthquake and Tsunami that motivated a number of sediment transport studies, the effects of the 2004 Indian Ocean tsunami waves on Banda Aceh's coastal morphology have not been fully analyzed despite the severe damage. So far, the coastal morphological changes in Banda Aceh have been analyzed by observing the change from the satellite imagery and measurement data as shown in Figure 1.4 (Meilianda et al., 2010; Griffin et al., 2013; Syamsidik et al., 2015a, 2017b).

The 2004 Indian Ocean tsunami has been studied to examine the effects of severe coastal erosion (Paris et al., 2009; Goto et al., 2011). It detached a headland and created a small island in the case of Ujong Seudeun of Aceh Al'ala et al. (2015) and Pulo Raya Island (Rasyif et al., 2016). A coastal area, which had been occupied by a local community in Pulo Raya Island, was eroded by the tsunami wave. After the 2004 disaster, these areas were left unpopulated because the local community felt that returning was unsafe (Rasyif et al., 2016). This shows that the morphological changes due to the tsunami resulted in dramatic changes that affected the coastal community (Rasyif et al., 2016).

Considering the above condition such as small island influence, reflected wave effect in Pulo Raya Island, and morphological changes that happened in Aceh Province, tsunami mitigation is especially important. In Indonesia, most of the small islands such as the Weh, Pulo Aceh, Banyak, Mentawai, and Enggano islands are populated. There are a lot of cities in the main island that located behind of the small offshore island. Almost coastal areas in Aceh Province is still in natural condition without any protection. The local

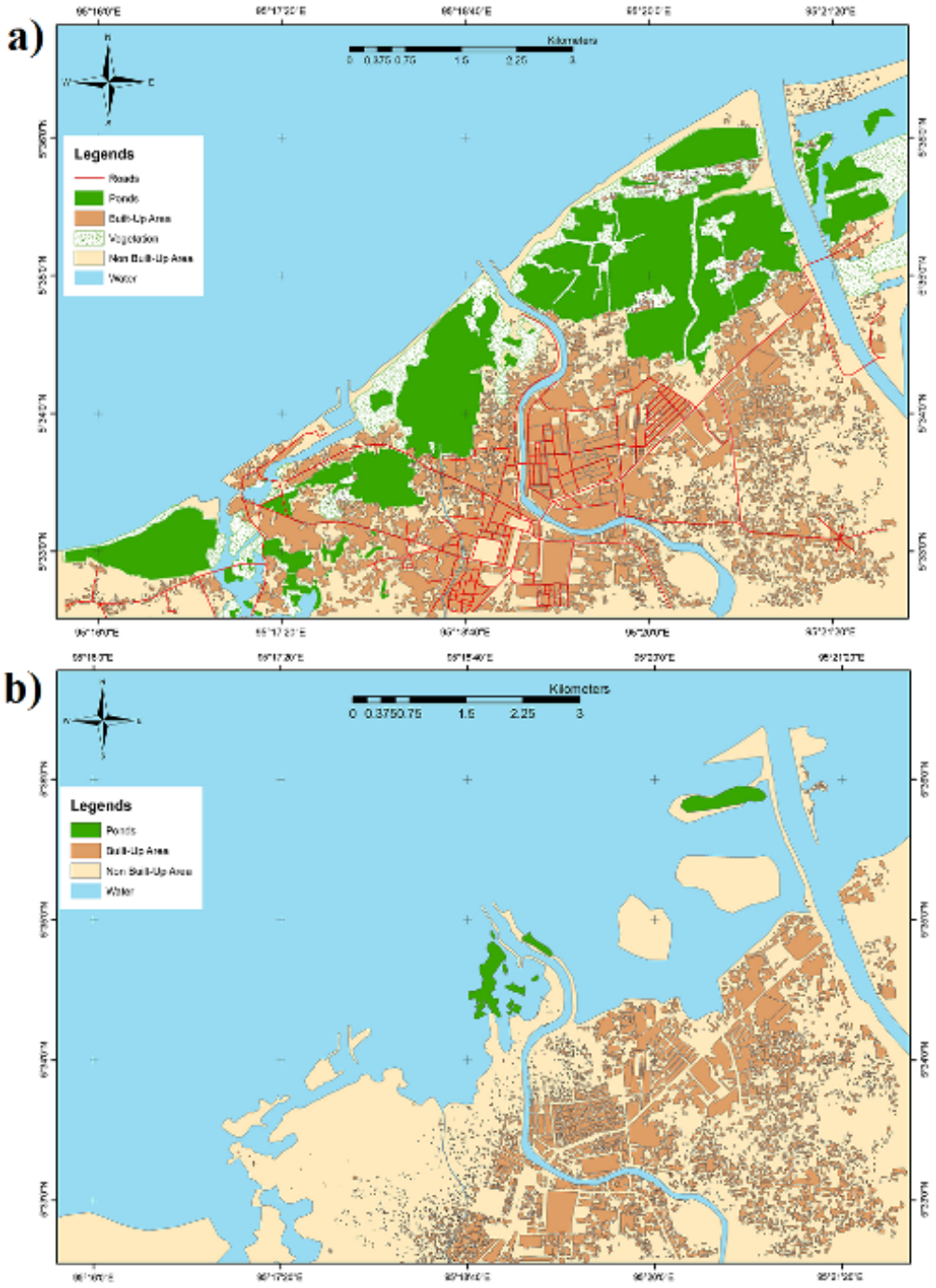

Figure 1.4: Land use of Banda Aceh in 2004: a) before and b) after the Indian Ocean tsunami (Syamsidik et al., 2017b).

community also settled near to the coastal areas.

1.2 Purpose of the Research

The goal of this study is to enhance the local community awareness and preparedness toward the tsunami hazard especially in Aceh province, Indonesia. Therefore, this study aims as follows:

1. To performing a comprehensive investigation of the effects of the small island on the tsunami wave height at the mainland which is directly protected by the isle.
2. To investigate the hydrodynamic process of reflected tsunami wave on small islands.
3. To investigate the morphological changes in Banda Aceh city as small domain due to the tsunami wave in 2004.

1.3 Outline of Thesis

The outline of this thesis is as follows.

- Chapter 1 describes overall thesis contents, which includes the background for doing research in the field of tsunami numerical simulation and briefly explains the purpose of the research.
- Chapter 2 describes general information about numerical model, study area, and input data that used for simulation.
- Chapter 3 describes about verification process and investigate the Indian Ocean tsunami impact toward Aceh Province for large and small domain.

- Chapter 4 investigates the influence of small island and reflected wave along Sumatra island based on the numerical simulation for tsunami disaster reduction.
- Chapter 5 is the final chapter. It describes the conclusion that can be drawn based on the results and also followed by the potential future work.

References

Al'ala, M., Rasyif, T. M., and Fahmi, M. (2015). Numerical simulation of ujong seudeun land separation caused by the 2004 indian ocean tsunami, aceh-indonesia. *Science of Tsunami Hazards*, 34(3):159–172.

Apotsos, A., Gelfenbaum, G., and Jaffe, B. (2011). Process-based modeling of tsunami inundation and sediment transport. *Journal of Geophysical Research: Earth Surface*, 116(F1):p. F01006.

Bourgeois, J. (2009). Geologic effects and records of tsunamis. *Bernard, E. N and Robinson, A. R., eds*, 15:55–92.

Duputel, Z., Kanamori, H., Tsai, V. C., Rivera, L., Meng, L., Ampuero, J.-P., and Stock, J. M. (2012). The 2012 sumatra great earthquake sequence. *Earth and Planetary Science Letters*, 351:247–257.

Goto, C., Ogawa, Y., Shuto, N., and Imamura, F. (1992). Numerical method of tsunami simulation with the leap-frog scheme. *Translated for the TIME project by N Shuto*.

Goto, K. and Imamura, F. (2007). Numerical models for sediment transport by tsunamis. *Quat Res*, 46(6):463–475.

Goto, K., Takahashi, J., Oie, T., and Imamura, F. (2011). Remarkable bathymetric change in the nearshore zone by the 2004 indian ocean tsunami: Kirinda harbor, sri lanka. *Geomorphology*, 127(1-2):107–116.

Griffin, C., Ellis, D., Beavis, S., and Zoleta-Nantes, D. (2013). Coastal resources, livelihoods and the 2004 indian ocean tsunami in aceh, indonesia. *Ocean & coastal management*, 71:176–186.

Gusman, A. R., Goto, T., Satake, K., Takahashi, T., and Ishibe, T. (2018). Sediment transport modeling of multiple grain sizes for the 2011 tohoku tsunami on a steep coastal valley of numanohama, northeast japan. *Marine Geology*, 405:77–91.

Hill, E. M., Borrero, J. C., Huang, Z., Qiu, Q., Banerjee, P., Natawidjaja, D. H., Elosegui, P., Fritz, H. M., Suwargadi, B. W., and Pranantyo, I. R. (2012). The 2010 m_w 7.8 mentawai earthquake: Very shallow source of a rare tsunami earthquake determined from tsunami field survey and near-field gps data. *Journal of Geophysical Research: Solid Earth*, 117(B6):p. B06402.

Imamura, F., Gica, E., Takahashi, T., and Shuto, N. (1995). Numerical simulation of the 1992 flores tsunami: Interpretation of tsunami phenomena in northeastern flores island and damage at babi island. *Pure and Applied Geophysics*, 144(3):555–568.

Lavigne, F., Paris, R., Grancher, D., Wassmer, P., Brunstein, D., Vautier, F., Leone, F., Flohic, F., De Coster, B., and Gunawan, T. (2009). Reconstruction of tsunami inland propagation on december 26, 2004 in banda aceh, indonesia, through field investigations. *Pure and Applied Geophysics*, 166(1-2):259–281.

Li, L., Qiu, Q., and Huang, Z. (2012). Numerical modeling of the morphological change in lhok nga, west banda aceh, during the 2004 indian ocean tsunami: understanding tsunami deposits using a forward modeling method. *Natural Hazards*, 64(2):1549–1574.

Liu, P. L.-F., Cho, Y.-S., Briggs, M. J., Kanoglu, U., and Synolakis, C. E. (1995). Runup of solitary waves on a circular island. *Journal of Fluid Mechanics*, 302:259–285.

Megawati, K., Shaw, F., Sieh, K., Huang, Z., Wu, T.-R., Lin, Y., Tan, S. K., and Pan, T.-C. (2009). Tsunami hazard from the subduction megathrust of the south china sea: Part i. source characterization and the resulting tsunami. *Journal of Asian Earth Sciences*, 36(1):13–20.

Meilianda, E., Dohmen-Janssen, C. M., Maathuis, B., Hulscher, S. J., and Mulder, J. (2010). Short-term morphological responses and developments of banda aceh coast, sumatra island, indonesia after the tsunami on 26 december 2004. *Marine Geology*, 275(1-4):96–109.

Nakamura, T., Mizutani, N., and Yim, S. C. (2009). A three-dimensional coupled fluid-sediment interaction model with bed-load/suspended-load transport for scour analysis around a fixed structure. *Journal of Offshore Mechanics and Arctic Engineering*, 131(3):031104.

Ontowirjo, B., Paris, R., and Mano, A. (2013). Modeling of coastal erosion and sediment deposition during the 2004 indian ocean tsunami in lhok nga, sumatra, indonesia. *Natural Hazards*, 65(3):1967–1979.

Paris, R., Wassmer, P., Sartohadi, J., Lavigne, F., Barthomeuf, B., Desgages, E., Grancher, D., Baumert, P., Vautier, F., and Brunstein, D. (2009). Tsunamis as geomorphic crises: lessons from the december 26, 2004 tsunami

in lhok nga, west banda aceh (sumatra, indonesia). *Geomorphology*, 104(1-2):59–72.

Ramalho, I., Omira, R., El Moussaoui, S., Baptista, M., and Zaghloul, M. (2018). Tsunami-induced morphological change–a model-based impact assessment of the 1755 tsunami in ne atlantic from the morocco coast. *Geomorphology*, 319:78–91.

Rasyif, T. M., Al'ala, M., and Fahmi, M. (2016). Numerical simulation of the impacts of reflected tsunami waves on pulo raya island during the 2004 indian ocean tsunami. *Journal of Coastal Conservation*, 20(6):489–499.

Richmond, B., Szczuciński, W., Chagué-Goff, C., Goto, K., Sugawara, D., Witter, R., Tappin, D. R., Jaffe, B., Fujino, S., and Nishimura, Y. (2012). Erosion, deposition and landscape change on the sendai coastal plain, japan, resulting from the march 11, 2011 tohoku-oki tsunami. *Sedimentary Geology*, 282:27–39.

Simpson, G. and Castelltort, S. (2006). Coupled model of surface water flow, sediment transport and morphological evolution. *Computers & Geosciences*, 32(10):1600–1614.

Sugawara, D., Goto, K., and Jaffe, B. E. (2014). Numerical models of tsunami sediment transport current understanding and future directions. *Marine Geology*, 352:295–320.

Sugawara, M. (2004). Basic study on sand sedimentation by a tsunami on an uniform slope. *Tohoku Journal of Natural Disaster Science*, 40:265–270.

Syamsidik, Fahmi, M., Fatimah, E., and Al'ala, M. (2017a). A decade process of coastal land use changes in peukan bada-aceh after the 2004 indian

ocean tsunami. *IOP Conference Series: Earth and Environmental Science*, 56(1):012012.

Syamsidik, Iskandar, A., and Rasyif, T. M. (2015a). Progress of coastal line rehabilitation after the indian ocean tsunami around banda aceh coasts. *In: Shaw R (ed) Recovery from the Indian Ocean Tsunami, disaster risk reduction*, pp:175–189.

Syamsidik and Istiyanto, D. C. (2013). Tsunami mitigation measures for tsunami prone small islands: lessons learned from the 2010 tsunami around the mentawai islands of indonesia. *Journal of Earthquake and Tsunami*, 7(01):1350002.

Syamsidik, Oktari, R. S., Munadi, K., Arief, S., and Fajri, I. Z. (2017b). Changes in coastal land use and the reasons for selecting places to live in banda aceh 10 years after the 2004 indian ocean tsunami. *Natural Hazards*, 88(3):1503–1521.

Syamsidik, Rasyif, T. M., and Kato, S. (2015b). Development of accurate tsunami estimated times of arrival for tsunami-prone cities in aceh, indonesia. *International Journal of Disaster Risk Reduction*, 14:403 – 410.

Takahashi, T., Shuto, N., Imamura, F., and Asai, D. (2001). Modeling sediment transport due to tsunamis with exchange rate between bed load layer and suspended load layer. In *Proceedings of the International Conference on Coastal Engineering*, pages 1508–1519.

Tanaka, H., Tinh, N. X., Umeda, M., Hirao, R., Pradjoko, E., Mano, A., and Udo, K. (2012). Coastal and estuarine morphology changes induced by the 2011 great east japan earthquake tsunami. *Coastal Engineering Journal*, 54(01):1250010.

Tappin, D. R., Evans, H. M., Jordan, C. J., Richmond, B., Sugawara, D., and Goto, K. (2012). Coastal changes in the sendai area from the impact of the 2011 tōhoku-oki tsunami: Interpretations of time series satellite images, helicopter-borne video footage and field observations. *Sedimentary Geology*, 282:151–174.

Titov, V. V. and Synolakis, C. E. (1998). Numerical modeling of tidal wave runup. *Journal of Waterway, Port, Coastal, and Ocean Engineering*, 124(4):157–171.

USGS (2014). Nthe largest earthquakes in the world since 1900. available from: http://earthquake.usgs.gov/earthquakes/world/10_ largest_world.php. last accessed: 2014, augustus 10.

Wang, X. (2009). User manual for comcot version 1.7 (first draft). *Cornel University*, 65.

Wang, X. and Liu, P. L.-F. (2007). Numerical simulations of the 2004 indian ocean tsunamis30,fe,ff0"80"94coastal effects. *Journal of Earthquake and Tsunami*, 1(03):273–297.

Wijetunge, J., Wang, X., and Liu, P. L.-F. (2008). Indian ocean tsunami on 26 december 2004: numerical modeling of inundation in three cities on the south coast of sri lanka. *Journal of Earthquake and Tsunami*, 2(02):133–155.

Wijetunge, J. J. (2009). Field measurements and numerical simulations of the 2004 tsunami impact on the south coast of sri lanka. *Ocean Engineering*, 36(12-13):960–973.

Xiao, H., Young, Y. L., and Prévost, J. H. (2010). Hydro-and morpho-dynamic

modeling of breaking solitary waves over a fine sand beach. part ii: Numerical simulation. *Marine Geology*, 269(3-4):119–131.

Yamashita, K., Sugawara, D., Takahashi, T., Imamura, F., Saito, Y., Imato, Y., Kai, T., Uehara, H., Kato, T., and Nakata, K. (2016). Numerical simulations of large-scale sediment transport caused by the 2011 tohoku earthquake tsunami in hirota bay, southern sanriku coast. *Coastal Engineering Journal*, 58(04):1640015.

Yeh, H., Imamura, F., Synolakis, C., Tsuji, Y., Liu, P., and Shi, S. (1993). The flores island tsunamis. *Eos, Transactions American Geophysical Union*, 74(33):369–373.

Yeh, H., Liu, P., Briggs, M., and Synolakis, C. (1994). Propagation and amplification of tsunamis at coastal boundaries. *Nature*, 372(6504):353.

Chapter 2

Numerical Model for Tsunami

2.1 General Information about Numerical Model

The sediment transport is simulated by applying the XBeach model. XBeach model is open source code that had been developed by (Roelvink et al., 2010). Such as the COMCOT, XBeach model able to simulate wave propagation and inundation. An advantage over COMCOT, XBeach model also capable to simulate the sediment transport and morphological changes under various wave and flow condition. Several analytical solutions, large scale laboratory experiments, and several field observation had been applied to testing the model validity. However due to its high demand on computer resources for high spatial resolution, XBeach is just adopted for small areas.

COMCOT model is coupled with XBeach model by (Li et al., 2012b) to simulate the tsunami wave hydrodynamic process and sediment transport with high efficiency and accuracy. Therefore, COMCOT-SED model is capable to

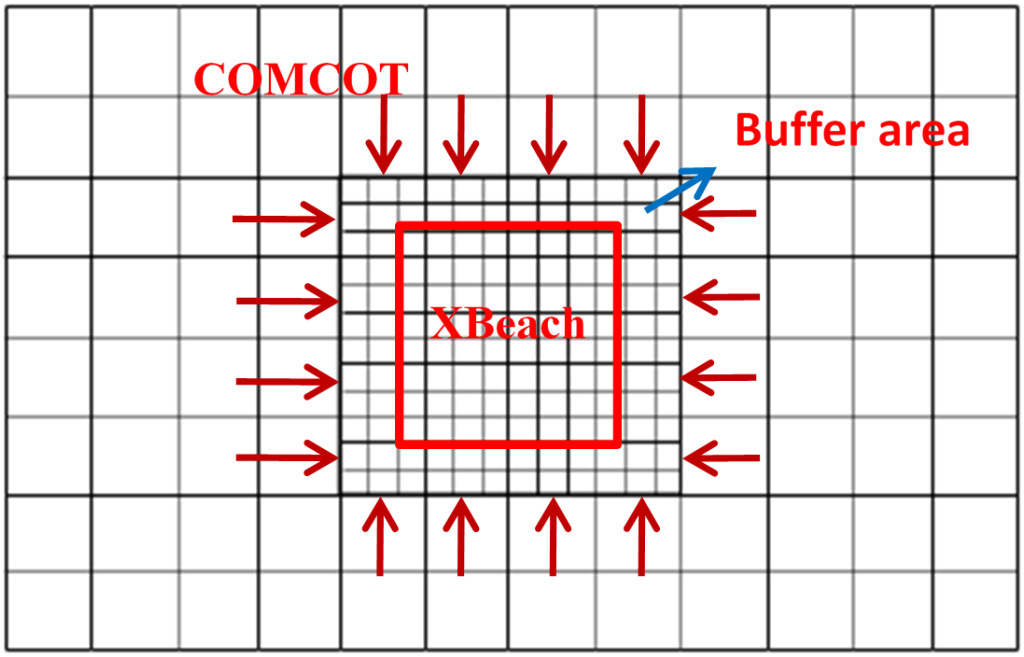

Figure 2.1: Skech of nested grid setup in COMCOT-SED model.

simulate the tsunami wave from its generation, propagation, inundation, and morphological changes. The coupled model is named as COMCOT-SED. The sediment transport calculation in XBeach model is included into the inner most layer of COMCOT model. A sketch of nested grid setup in COMCOT-SED model can be seen in Figure 2.1. A buffer area is applied as a transitional area to minimize a sudden change effect on the boundary between the innermost and its parent layer.

2.1.1 Shallow water equations

A set of linear and non-linear shallow water equations (SWEs) were applied to the COMCOT-SED model to calculate the water surface elevation and volume flux. Both equations are available with spherical or cartesian coordinate systems. In the linear SWEs with spherical coordinates in a large area, the

Coriolis effect due to the earth's rotation is included. In the local simulation area, the non-linear SWEs with the cartesian coordinate system is adopted. The cartesian coordinates, with non-linear SWEs on the innermost layer, must be used to apply the sediment calculation in the COMCOT-SED model. The linear SWE equation for cartesian coordinate system formulated in COMCOT is as follows (the detail equations can be see in (Wang, 2009)):

$$\frac{\partial \eta}{\partial t} + \frac{\partial (Hu)}{\partial x} + \frac{\partial (Hv)}{\partial y} = -\frac{\partial h}{\partial t} \tag{2.1}$$

$$\frac{\partial Hu}{\partial t} + gh\frac{\partial \eta}{\partial x} = 0 \tag{2.2}$$

$$\frac{\partial Hv}{\partial t} + gh\frac{\partial \eta}{\partial y} = 0 \tag{2.3}$$

$$H = \eta + h \tag{2.4}$$

where η represents the water surface elevation. h is the water depth. H is the total water depth. u and v are depth averaged velocities in the x and y direction, respectively. g is the gravitational acceleration. t is time.

Meanwhile, the nonlinear SWEs employed by COMCOT-SED are formulated as follows:

$$\frac{\partial \eta}{\partial t} + \frac{\partial (Hu)}{\partial x} + \frac{\partial (Hv)}{\partial y} = -\frac{\partial h}{\partial t} \tag{2.5}$$

$$\frac{\partial u}{\partial t} + u\frac{\partial u}{\partial x} + v\frac{\partial u}{\partial y} + F_x = -g\frac{\partial \eta}{\partial x} \tag{2.6}$$

$$\frac{\partial v}{\partial t} + u\frac{\partial v}{\partial x} + v\frac{\partial v}{\partial y} + F_y = -g\frac{\partial \eta}{\partial y} \tag{2.7}$$

$$F_x = \frac{gn^2}{H^{4/3}} u\sqrt{u^2 + v^2} = 0 \tag{2.8}$$

$$F_y = \frac{gn^2}{H^{4/3}} v\sqrt{u^2 + v^2} = 0 \tag{2.9}$$

where F_x and F_y represent the bottom friction in the x and y direction. n is Manning's coefficient for bottom roughness.

2.1.2 Moving boundary scheme

The moving boundary scheme just able to be used for non-linear calculation in COMCOT-SED model. The initial conditions for water level and volume flux is zero in COMCOT-SED model. In the COMCOT-SED, the water area indicates with positive value. While, the land area indicates with negative value. Several algorithms will be determine whether a calculation point is dry or submerged by evaluating the value of total water level (H). Figure 2.2 illustrates the logic in model when the total water level at the shoreline have value more than zero ($H > 0$). Several logic that will be happened are as following:

- If $H_{i+1} < 0$ and $h_{i+1} + \eta_i \geq 0$, then the shoreline remains between grid points i and $i + 1$ and the volume flux $Hu_{i+1/2}$ remains zero (Figure 2.1a);
- If $H_{i+1} \leq 0$ and $h_{i+1} + \eta_i > 0$, then the shoreline moves to between grid points $i + 1$ and $i + 2$ and the volume flux $Hu_{i+1/2}$ may have a nonzero value, while $Hu_{i+3/2}$ is assigned to be zero. The flooding depth is $H_f = H_{i+1} + \eta_i$ (Figure 2.1b);

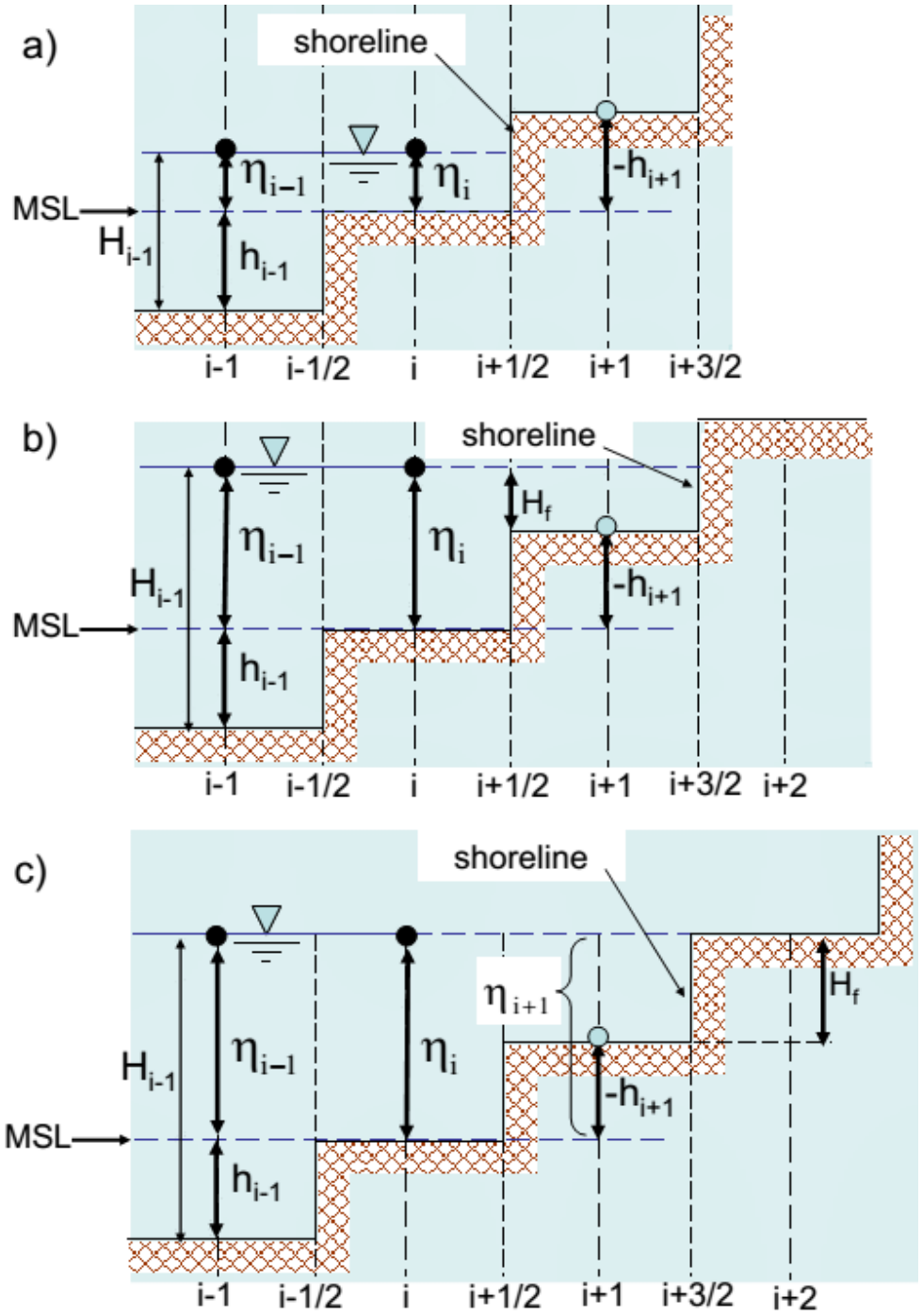

Figure 2.2: A sketch of moving boundary scheme (Wang, 2009).

- If $H_{i+1} > 0$, then the shoreline moves to between grid points $i + 1$ and $i + 2$. The volume flux $Hu_{i+1/2}$ and $Hu_{i+3/2}$ may have a nonzero value. The flooding depth is $H_f = \max(H_{i+1} + \eta_i,\ H_{i+1}\ \eta_+\ \eta_i + 1)$ (Figure 2.1c).

2.1.3 Sediment Model

The sediment calculation is based on the XBeach Model version 6 (Roelvink et al., 2010). Xbeach is applied to a depth-averaged advection–diffusion equation according to (Galappatti and Vreugdenhil, 1985) to calculate a sediment concentration as shown in Equation (2.8).

$$\frac{\partial HC}{\partial t} + \frac{\partial HCu}{\partial x} + \frac{\partial HCv}{\partial y} + \frac{\partial}{\partial x}\left(D_h H \frac{\partial C}{\partial x}\right) + \frac{\partial}{\partial y}\left(D_h H \frac{\partial C}{\partial y}\right) = \frac{HC_{eq} - HC}{T_s} \tag{2.10}$$

where C represents the depth-averaged concentration of suspended sediment; D_h is the sediment diffusion coefficient. A default value of $D_h = 1.0$ was selected. T_s is the adaptation time of sediment concentration that is calculated based on total water depth (H) and sediment fall velocity (w_s) as in the following equation:

$$T_s = max\left(f_{Ts}\frac{H}{w_s}, T_{s,min}\right) \tag{2.11}$$

where f_{Ts} is a correction and calibration factor. f_{Ts} has a range and a default value of about 0.01–1 and 0.1, respectively. The default value of $f_{Ts} = 0.1$ was adopted in the simulation. $T_{s,min}$ is the minimum adaptation time. $T_{s,min}$ has a range and a default value of about 0.01–10 and 0.5, respectively. $T_{s,min} = 0.2$ was adopted in the simulation. These parameters were applied following previous studies (Li et al., 2014; Li and Huang, 2013).

C_{eq} represents the equilibrium sediment concentration calculated according to (Li et al., 2012a) as the following approximation:

$$C_{eq} = \frac{q_s + q_b}{|u|H} \tag{2.12}$$

where q_s is the sediment volume flux for the suspended load, q_b is the sediment volume flux for the bed load, and $|u|$ is the magnitude of the depth-average velocity. The volume fluxes for the suspended and bed loads were calculated based on (Soulsby, 1997) as the following expressions:

$$q_s = 0.012|u|H\left(\frac{|u| - u_{cr}}{[(s-1)\,gd_{50}]^{1/2}}\right)^{2.4}\left(\frac{d_{50}}{H}\right)D_*^{-0.6} \tag{2.13}$$

$$q_b = 0.005|u|H\left(\frac{|u| - u_{cr}}{[(s-1)\,gd_{50}]^{1/2}}\right)^{2.4}\left(\frac{d_{50}}{H}\right)^{1.2} \tag{2.14}$$

where $D_* = [(s-1)g/\nu^2]^{1/3}d_{50}$ is the dimensionless particle diameter. ν is kinematic viscosity. d_{50} is the median grain size. u_{cr} is the critical depth-averaged flow velocity that was calculated according to (Soulsby, 1997) as the following:

$$u_{cr} = 0.19\,(d_{50})^{0.1}\log\,(12H/3d_{90}) \tag{2.15}$$

when $0.0001(\mathrm{m}) \leq d_{50} \leq 0.0005(\mathrm{m})$ and

$$u_{cr} = 8.5\,(d_{50})^{0.6}\log\,(12H/3d_{90}) \tag{2.16}$$

when $0.0005(\mathrm{m}) \leq d_{50} \leq 0.002(\mathrm{m})$. where $d_{90} = 1.5d_{50}$ represents the diameter where 90% of the distribution has a smaller particle size.

2.1.4 Bottom Change Model

Equation (2.17) shows the mass-balance for bed-level changes used to update the bottom elevation. This can be expressed in the form of a partial differential equation describing the process of the sediment transport rate in the x and y directions, respectively. z_b represents the bottom elevation that changes with time. p is the bed material porosity. q_x and q_y represent the sediment transport rates in the x and y directions, respectively (Roelvink et al., 2010).

$$\frac{\partial z_b}{\partial t} + \frac{1}{1-p}\left(\frac{\partial q_x}{\partial x} + \frac{\partial q_y}{\partial y}\right) = 0 \tag{2.17}$$

$$q_x = \frac{\partial HCu}{\partial x} + \frac{\partial}{\partial x}\left(D_h H \frac{\partial C}{\partial x}\right) \tag{2.18}$$

$$q_y = \frac{\partial HCv}{\partial y} + \frac{\partial}{\partial y}\left(D_h H \frac{\partial C}{\partial y}\right) \tag{2.19}$$

2.1.5 Fault model

There are two categories of model in COMCOT to calculate seafloor displacement. They are an instantaneous and a transient deformation based on duration of seafloor motion. A model that has been used in this research is the instantaneous deformation model. This model calculates seafloor disturbance by elastic finite fault plane theory. Originally, the model is based on the theory of (Mansinha and Smylie, 1971). Later (Okada, 1985) improved the model. This model has been developed based on the assumption that a fault plane (a rectangular fault plane) is buried in semi-infinite elastic half plane. It is also assumed that the sea level will mimic deformation of the seafloor caused by

the earthquake.

The fault plane is the plane between the subduction plate and the impacted major plane. The fault plane and surface subduction plate (red color) can be seen in Figure 2.3. There are nine parameters to implement fault models in COMCOT-SED model such as latitude and longitude of epicenter, focal depth, length and width of fault, dislocation, strike angel, angel slip and dip angel. A dislocation is defined as the relative motion distance between the lower and upper fault block on the fault plane. The Strike θ is the angle measured from the north clockwise to the strike direction ($0° < \theta < 360°$). The dip δ is the angle measured from the horizontal top surface to fault plane ($0° < \delta < 90°$). The slip λ is the angle measured anti-clockwise from the strike direction to black arrow ($0° < \lambda < 180°$).

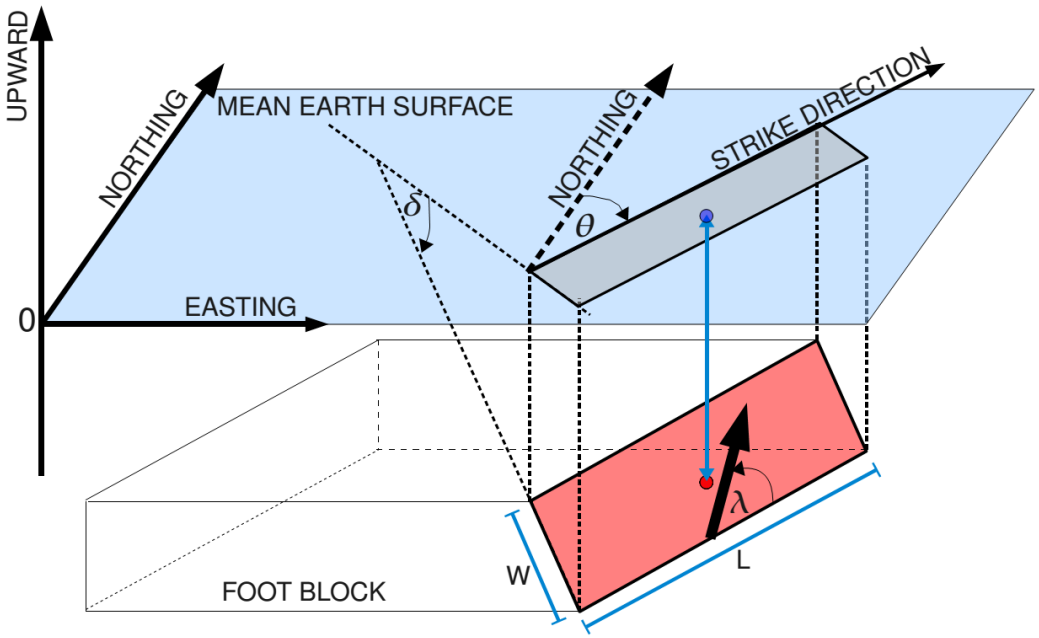

Figure 2.3: Sketch of a Fault Plane (Wang, 2009).

Table 2.1: List of Multi Fault Parameters for Tsunami on 2004.

No	Coordinate		Fault parameters			D	Depth	W	L
	Long(°)	Lat (°)	Strike(°)	Dip(°)	Slip (°)	(m)	(km)	(km)	(km)
1	94.57	3.83	323	12	90	18	25	220	130
2	93.9	5.22	348	12	90	23	25	150	130
3	93.21	7.41	338	12	90	12	25	390	120
4	92.6	9.7	356	12	90	12	25	150	95
5	92.87	11.7	10	12	90	12	25	350	95

Several past earthquake scenarios such as the tsunami in 2004, 2005, and 2012 were adopted with single and multi fault model. Occasionally, a single fault model is unable to represent a complex rupture mechanism such as a big earthquake in 2004. The aftershock faults line area was extended over 1200 km from earthquake epicenter in the northwest of Sumatra to the Andaman island (Ammon et al., 2005). Therefore, several researchers proposed a multi fault model to represent the complex rupture. The multi fault model has been used for the big earthquake event in 2004 and 2005. The tsunami in 2012 were generated by applying an analysis of relationship between a magnitude and a rupture dimension (Wells and Coppersmith, 1994) for single fault model.

The fault parameters published by (Grilli et al., 2007) were applied in this study to generate the bottom deformation as an initial trigger for the tsunami in 2004. The source was divided into five segments with a total seismic moment equivalent to $M_w = 9.22$ (Fault parameters can be seen in Table 2.1). The fault parameters were validated by comparing the simulation results to satellite transect, tide gauge, and run-up height measurements near the Banda Aceh coast (Grilli et al., 2007). This is the same model that was used to investigate the morphological changes to the Khao Lak coast in Thailand during the 2004 tsunami (Li et al., 2014).

The tsunami in 2005 was generated based on Banerjee et al. (2007). The

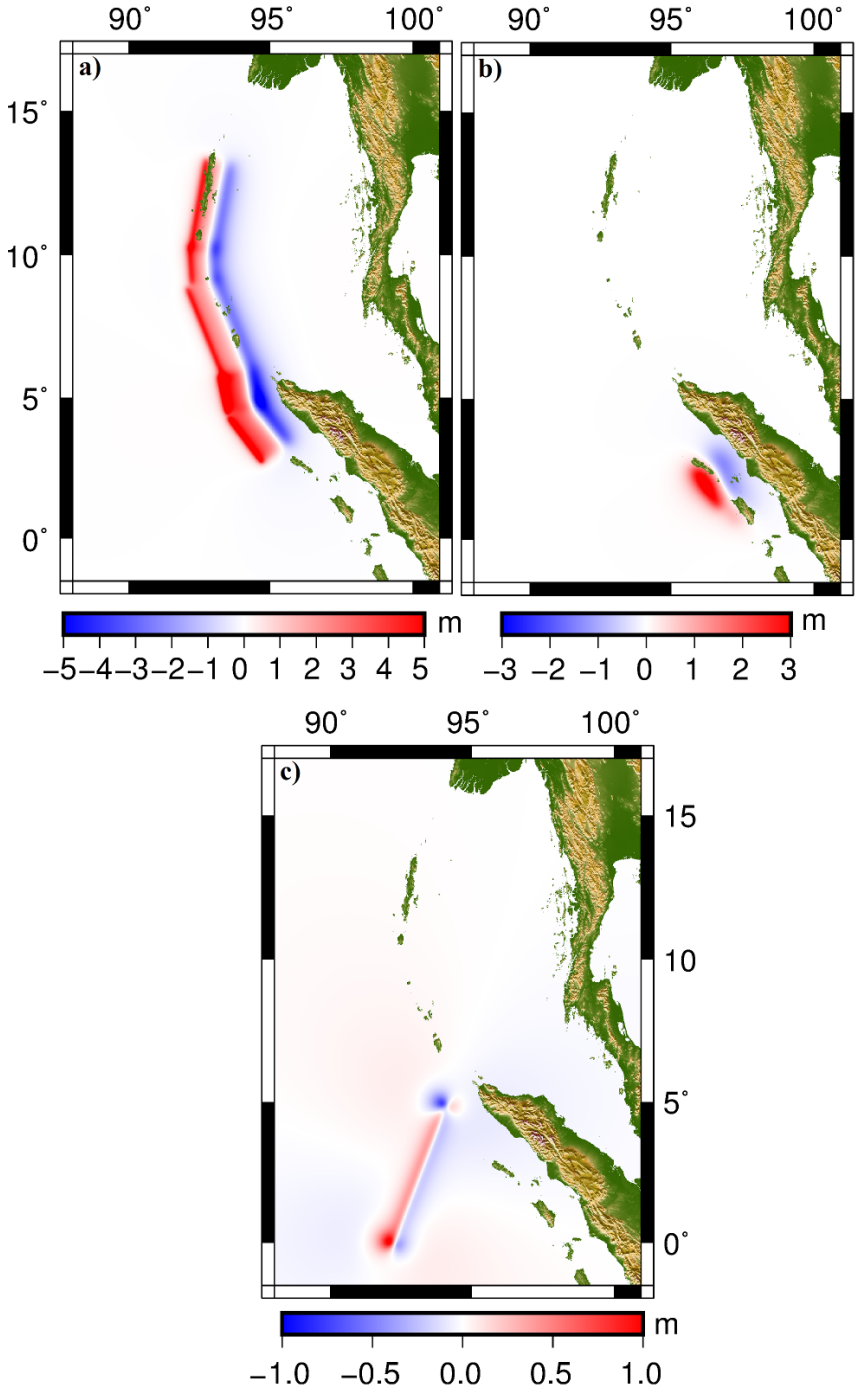

Figure 2.4: Initial condition for past tsunami in a) 2004, b) 2005 and c) 2012.

rupture areas were divided into five segments with a total seismic moment about $M_w = 8.66$. GPS static offsets were applied to produce the faults parameters. The strike and dip with values about 325 and 15 were adopted into five segments. Detail parameters for the 2005 earthquake can be seen in Table 2.2. The initial surface elevation of each event is shown in Figure 2.4.

In order to anticipate the possible impact caused by future tsunami at seismic gap which located around the Simeulue island that still locked (Meltzner et al., 2012). Three hypothetical scenarios with thrust mechanism were used to prevent future hazard in Aceh Province namely case A1, B1, and C1. Based on the United State Geological Survey (USGS) data, the past big earthquakes that occurred in Sumatra subduction zone have thrust mechanism (Geist et al., 2006) such as in 2004 and 2005 (can be seen in Figure 2.5 that indicated by a "beach ball" symbol).

For example, the values of strike, slip, and dip are about 329, 7, and 110, respectively. There were just two big earthquakes in 2012 with strike-slip mechanism. The magnitude of the hypothetical conditions is $M_w = 8.5$. This value was taken based on the probabilistic tsunami hazard assessment. The previous study indicated that the earthquake with magnitude $M_w = 8.5$ could occur with return period of 200-300 years (Sengara et al., 2008; Suppasri et al., 2012a,b) or 100 years (Burbidge et al., 2009). The dimension of estimated

Table 2.2: List of Multi Fault Parameters for Tsunami on 2005.

No	Coordinate		Fault parameters			D	Depth	W	L
	Long(°)	Lat (°)	Strike(°)	Dip(°)	Slip (°)	(m)	(km)	(km)	(km)
1	95.785	2.768	325	15	90	0.3	42	77.3	65
2	95.978	2.19	325	15	97	12.3	42	96.6	85
3	96.397	1.544	325	15	91	8.2	30	81.1	100
4	97.079	0.915	325	15	107	3.1	42	77.3	80
5	97.498	0.328	325	15	119	0.2	42	77.3	140

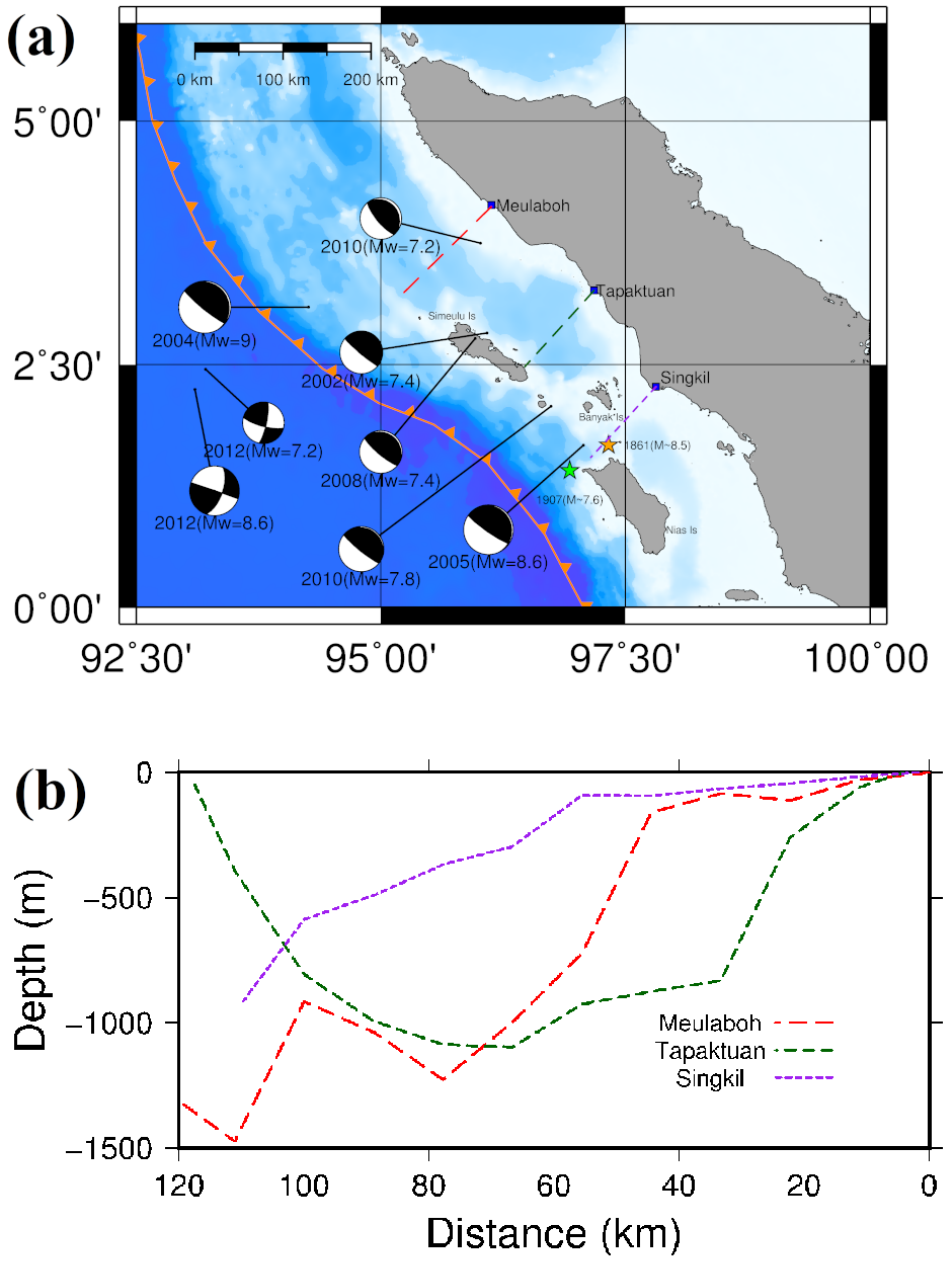

Figure 2.5: (a) Recent large ruptures with its focal mechanism (indicated by a "beach ball" symbol), study area for the western coast of Aceh Province and (b) bathymetry profile from land (0 km) to offshore (120 km).

fault plane is 80 km wide and 323 km long by using an analysis of relationship between a magnitude and a rupture dimension (Wells and Coppersmith, 1994) for the hypothetical cases.

The difference between these cases is on the epicenter location. The epicenters of last earthquake events around Simeulu Island were used for A1, B1, and C1. The location of case A1 is the same as 2005 event. Case B1 is located on the slightly northern side of the 2005 tsunami case. It is the same location of 2010 earthquake which did not cause high tsunami wave along Sumatra Island because of small magnitude. Case C1 is located on off Simeulu Island as same as the quake in 2002.

2.1.6 Earthquake Scaling Laws and Fault Dimensions

As described above, the tsunami simulations have been generated by using fault model to calculate deformation of seafloor due occurrence of earthquake. Analytical equations for finite rectangular sources itself require some input parameters to calculate deformation such as focal mechanism and rupture parameters (rupture length and dislocation). Focal parameter can be obtained by using information from seismograph, while rupture parameters of earthquake in seafloor are difficult to obtain. Hence empirical equations based in relation to an earthquake size are applied in this research to calculate rupture parameter, dislocation (D), fault length (L), and width length (W).

As it is understood recently that the earthquake's magnitude can be used to estimate rupture parameters. Hence, a lot of instruments were deployed in previous studies to measure earthquake's magnitude with different criteria and methods. Traditional magnitude scales such (M_s and M_b) are limited by both the frequency response of the Earth and the recording seismograph

consider seismic moment because it measure of the amount of radiated energy directly. Then, Hanks and Kanamori (1979) provided method to change the traditional magnitude scale becomes seismic moment and to introduce a formula to calculate moment magnitude scale from averaged seismic moment as follows:

$$M_W = \frac{2}{3} \log M_0 - 10.7 \tag{2.20}$$

where M_W is moment magnitude and M_0 is the seismic moment in dyne.cm.

The analysis to show empirical evidence of relationship between seismic moment and rupture parameters was proposed by Kanamori and Anderson (1975) that classified 41 earthquakes data into two groups based on position of epicenter, inter-plate, and intra-plate. Seismic moment and rupture dimension are plotted and to give result proportionally to effect of their magnitudes as shown in Figure 2.6. Hence, dislocation can be obtained by using concept of

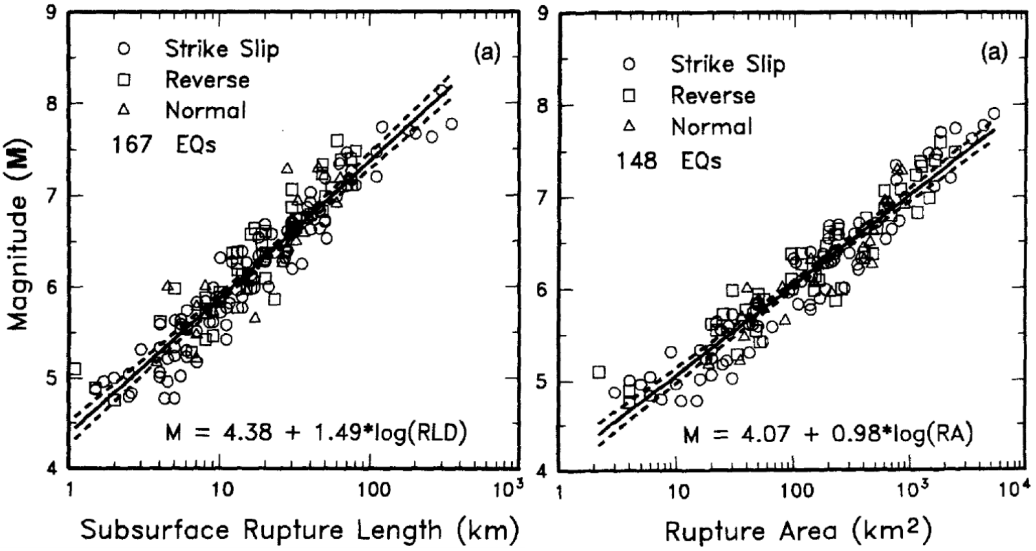

Figure 2.6: Correlation between Rupture Lenght, Area, and Magnitude (Kanamori and Anderson, 1975).

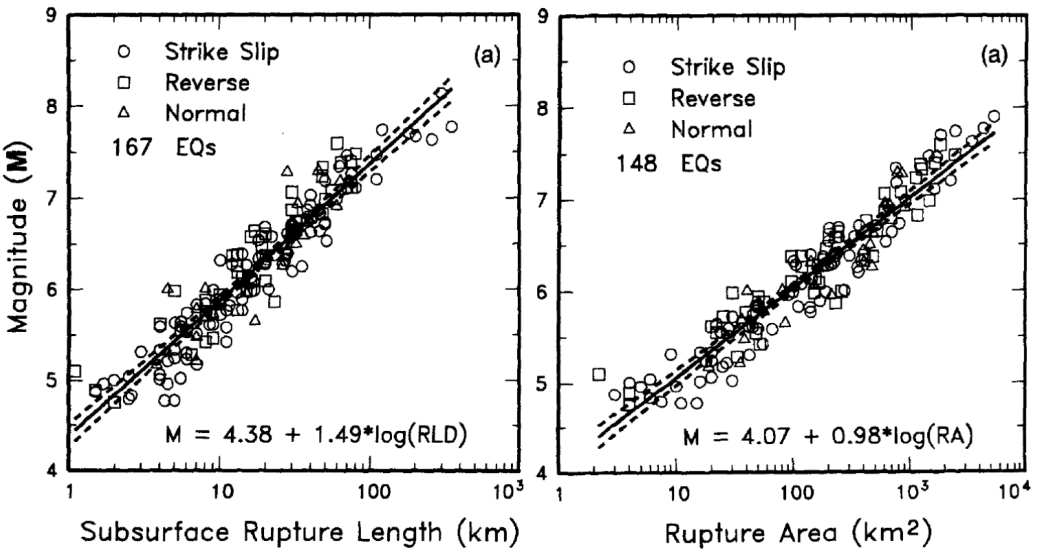

Figure 2.7: Relationship between The Earthquake Parameters of S and M_0 (Wells and Coppersmith, 1994).

seismic moment. This is the results of the equivalence between elastic dislocation and a double-force expression as follows:

$$M_0 = \mu DS = \mu DLW \tag{2.21}$$

whereμ is rigidity of earth's mantle, D is dislocation, S is a fault area, L is the length of fault plane and W is the width of the fault plane.

According to Kongko (2012), an empirical analysis of relationship between a magnitude and a rupture dimension develop by Wells and Coppersmith (1994) is widely used to calculate the rupture dimension. Based on the worldwide database of source parameters for 244 earthquakes occurrence with an epicenter depth less than 40 km and the magnitude above $M_W = 4.5$. The empirical relationship has been revised by using a log-linear regression between the earthquake magnitude (M_W) and the surface rupture length (L in km), subsurface rupture length, and rupture area (S in km^2) are well correlated. The relation

between earthquake magnitude and rupture parameters (L and S) for all events can be seen in Figure 2.7. The results are have a deviation standard about 0.25 to 0.35 and an acceptance level at 95 % based on a statistic. Therefor the empirical relationship can be used to calculated the subsurface rupture length. Based on the relation the empirical equations will be used in this research are as follow:

$$\log(L) = a + bM_w \tag{2.22}$$

where a = -2.57, -2.42, -1.88, and -2,44, and b = 0.62, 0.58, 0.5, and 0.59 for strike slip, reverse, normal, and all events, respectively.

$$\log(S) = a + bM_w \tag{2.23}$$

where a = -3.42, -3.99, -2.87, and -3.49, and b = 0.9, 0.98, 0.82, and 0.91 for strike slip, reverse, normal, and all event, respectively.

$$W = S/L \tag{2.24}$$

2.2 Study area

2.2.1 Big area

The western coast of Aceh

The western coast of Aceh, especially at three cities namely Meulaboh, Tapaktuan, and Singkil, is used as a case study to investigate the influence of small island against the tsunami wave. This area is located inside the Sumatra subduction area. The area had experienced the tsunami disaster in 2004 and 2005. Although this area has potential to be exposed the tsunami

attack, several cities in this area experienced the different tsunami impact. For instance, Tapaktuan city, which located nearby the earthquake epicenter as shown in Figure 2.5a, received insignificant damage by the tsunami wave compared to other cities along it.

These cities have a unique morphological condition that able to affect the tsunami wave. There are the presence of a small island, bathymetric profile, and dimension offshore island, as shown in Figure 2.5. Meulaboh city is facing directly the Indian Ocean. On the other hand, Tapaktuan and Singkil cities are obstructed by islands, namely Simeulu and Banyak Islands. The both islands have different dimensions. The length of Simeulu Island is about 98 km, and that of Banyak Island is about 37 km. Meulaboh and Singkil have a flat slope in a coastal region. In other hand, Tapaktuan has a steep slope in front of a coast. Therefore, this bathymetric feature can result in an amplification and a reduction of tsunami wave in this area.

Pulo Raya island

Pulo Raya is a small island with an area of about 3.42 km^2, located about 1 km from the mainland of Sumatra. The island is part of the Aceh Jaya district in Aceh Province, as shown in Figure 2.8a. Prior to the 2004 tsunami, Pulo Raya had three villages: Lhok Siron, Lhok Meu, and Ujung Manek. About 82 families, 363 people lived on the island. The tsunami waves destroyed many of the island's facilities, such as a mosque, a school, and houses.

Eye witnesses reported that the first tsunami waves were not significantly high to damage the coastal area. However, the tsunami waves that reflected toward the island were amplified around it, and the runup reached the villages. The areas were destroyed by the tsunami, as indicated by the light green color

in Figure 2.8b.In order to avoid human casualties if another tsunamigenic earthquake occurs, the local government enhanced the tsunami mitigation on

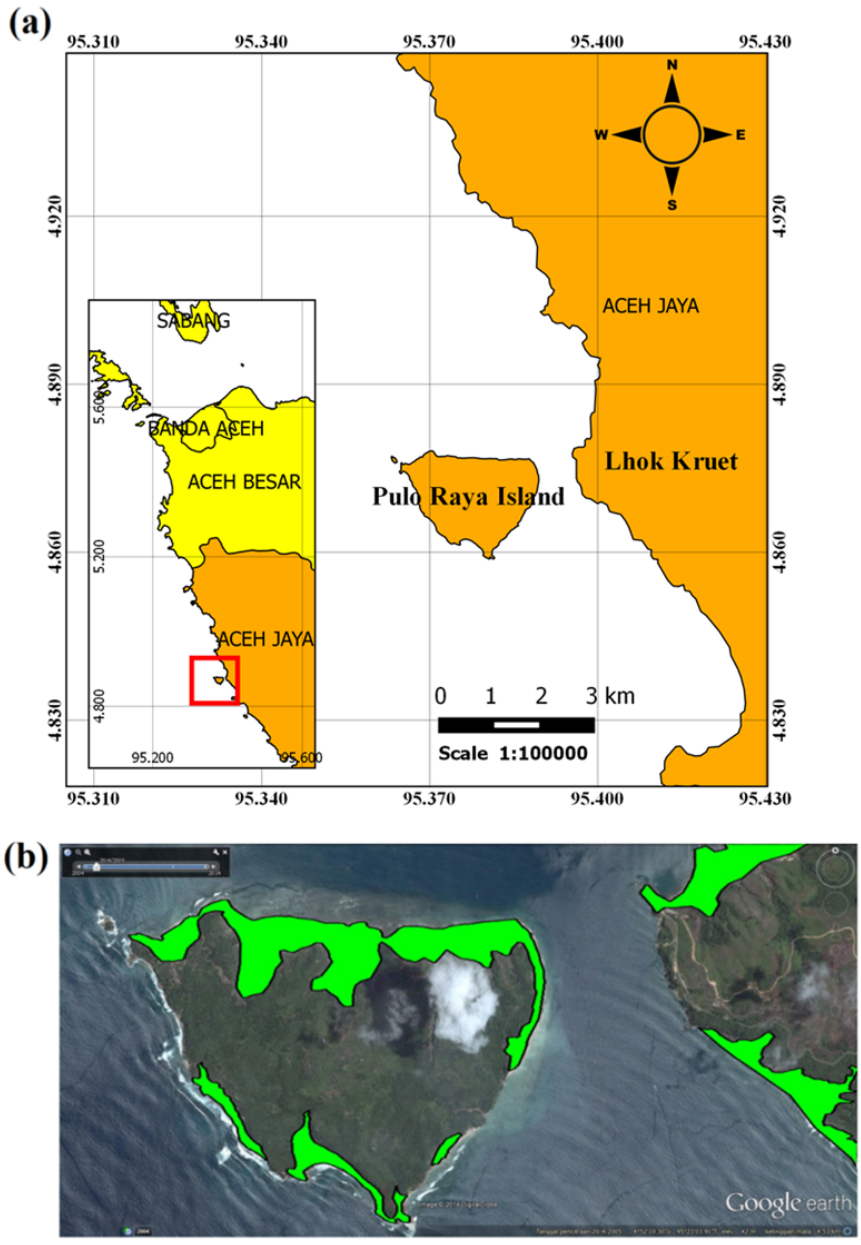

Figure 2.8: (a) Study area and (b) satellite image of Pulo Raya Island after the 2004 Indian Ocean tsunami (light green color indicates tsunami runup on the island).

Pulo Raya by enforced relocation. About 51 families, who survived the tsunami in 2004 by escaping to higher areas located behind their villages, were relocated to Lhok Kruet on the mainland.

The residents initially refused to relocate; most of them wanted to remain on Pulo Raya and continue their lives as before. However, the tsunami had caused changes in the island environment that led to erosion in several coastal areas; particularly, the northern coastal area where many people had lived prior to the tsunami. The erosion ultimately motivated residents to obey the spatial planning of the local government.

2.2.2 Small domain

Banda Aceh, which is located on the northern end of Sumatra Island, is the capital city of the Aceh Province of Indonesia (Figure 2.9). Banda Aceh is bordered by the Malaccaa strait, the Aceh Besar district, and the Indian Ocean on the north, south, and west, respectively. Banda Aceh is vulnerable to tsunami disaster because of its geographic location, which is close to the Sumatran subduction zone. Banda Aceh is characterized by relatively flat topography which can cause the tsunami waves to inundate areas further inland, as was the case during the 2004 Indian Ocean tsunami (Tursina et al., 2017).

Approximately 67 tsunami poles have been built in Banda Aceh for disaster education, as a tsunami memorial, and an evacuation sign by the local people and the Embassy of Japan in Indonesia through the Umi Abasiah Foundation. Each tsunami memorial pole illustrates the maximum tsunami wave height at that location based on local witnesses and watermarks. We used these data

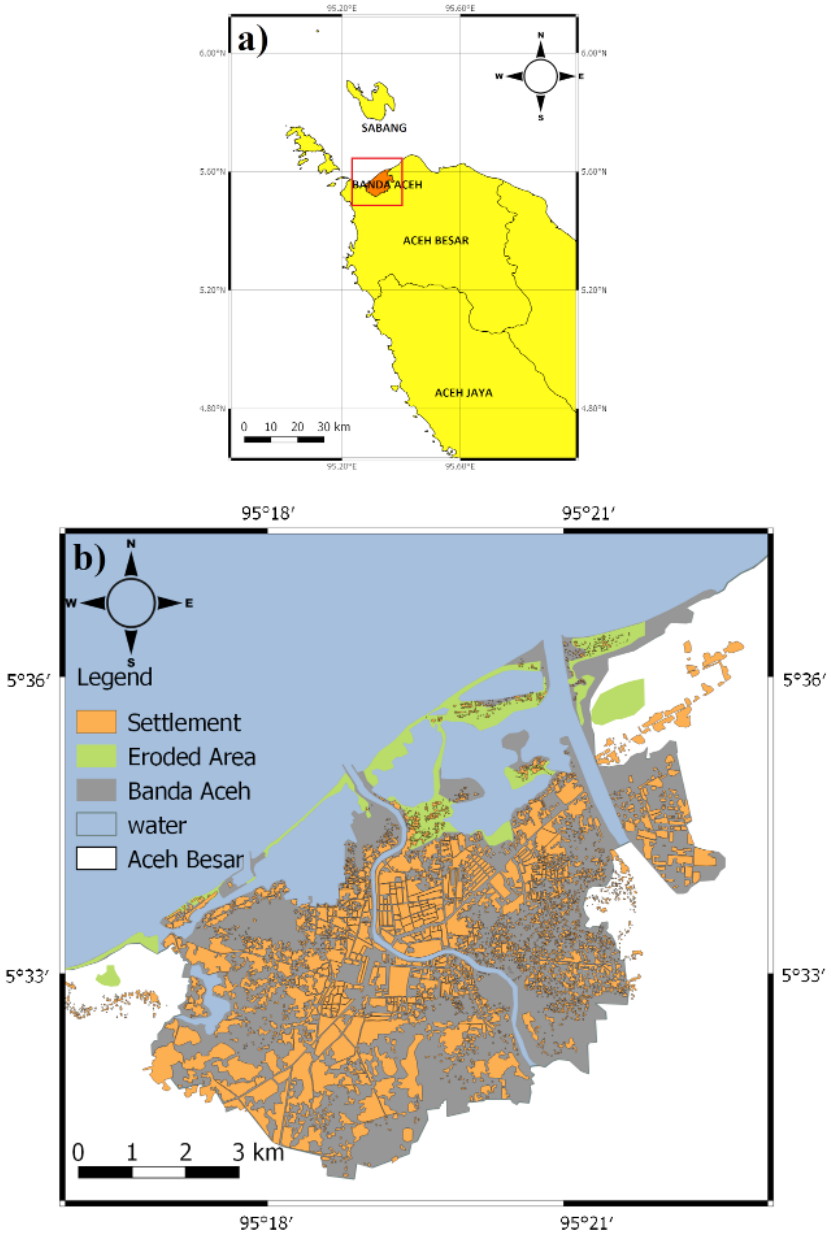

Figure 2.9: (a) Study area and (b) Banda Aceh city before and after the 2004 Indian Ocean Tsunami (green color indicates the land area eroded by the tsunami). This figure was modified from (Syamsidik et al., 2017a).

points to compare with our model results.

Banda Aceh is divided into eight sub-districts, four of which share boundaries with that coastal area, namely Meuraxa, Kuta Raja, Kuta Alam, and Syiah Kuala. Banda Aceh borders with Aceh Besar district, as indicated by white color in Figure 2.9b.The total Banda Aceh area is approximately 61.36 km^2, as indicated by orange color in Figure 2.9a. The city has a coastline of approximately 12 km. The pre-tsunami Banda Aceh coastal condition is indicated by gray and green colors in Figure 2.9b. After the tsunami event, the Banda Aceh coastal area underwent massive morphological changes within the area shown in green. The orange color in Figure 2.9 shows buildings within the Banda Aceh city. Due to the lack of knowledge about tsunami disasters, there was little land use management information for Banda Aceh before 2004.

2.2.3 Grid Setup and Input Data

The multi-layer system in the COMCOT-SED model was applied in this study to obtain accurate and detailed results for the specific simulation area. The multi-grid system, which is another term for Nested Grid, allows us to compose the numerical domain in varied size of grids and different Shallow Water Equations (either Liner/LSWE or NonLinear/NLSWE). Here, The COMCOT shows its practicality for this large simulation domain that could be run in a rather shorter running time and lower computer memory capacity. Figure 2.10 shows the sketch of nested grid setup in COMCOT-SED model.

Layer 1 and Layer 2 areas, which cover the big and small domains, were applied can be seen in Figure 2.11. Three of Layer 3 were adopted for the big domain such as Pulo Raya Island and the western cities and small domain such as Banda Aceh. The Pulo Raya Island, the western cities of Aceh Province,

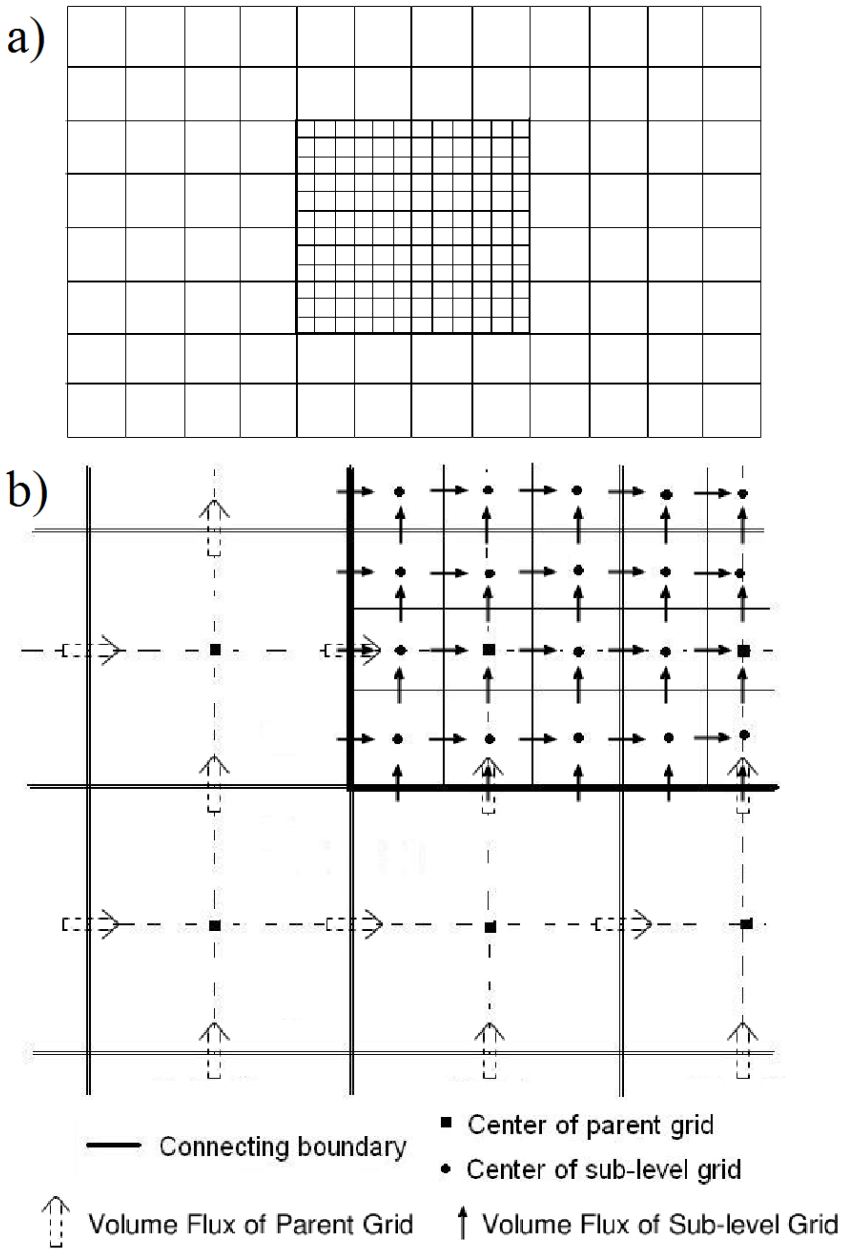

Figure 2.10: Sketch of Nested Grid Setup (Wang, 2009).

Banda Aceh were indicated as Layer 3.1, Layer 3.2, and Layer 3.3, respectively as shown in Figure 2.11.

As in the case of Pulo Raya, which is a small island, we used the advantages to concentrate on the tsunami impacts on the island and around the nearshore area of the island. As a result, reflected tsunami waves in Pulo Raya can be

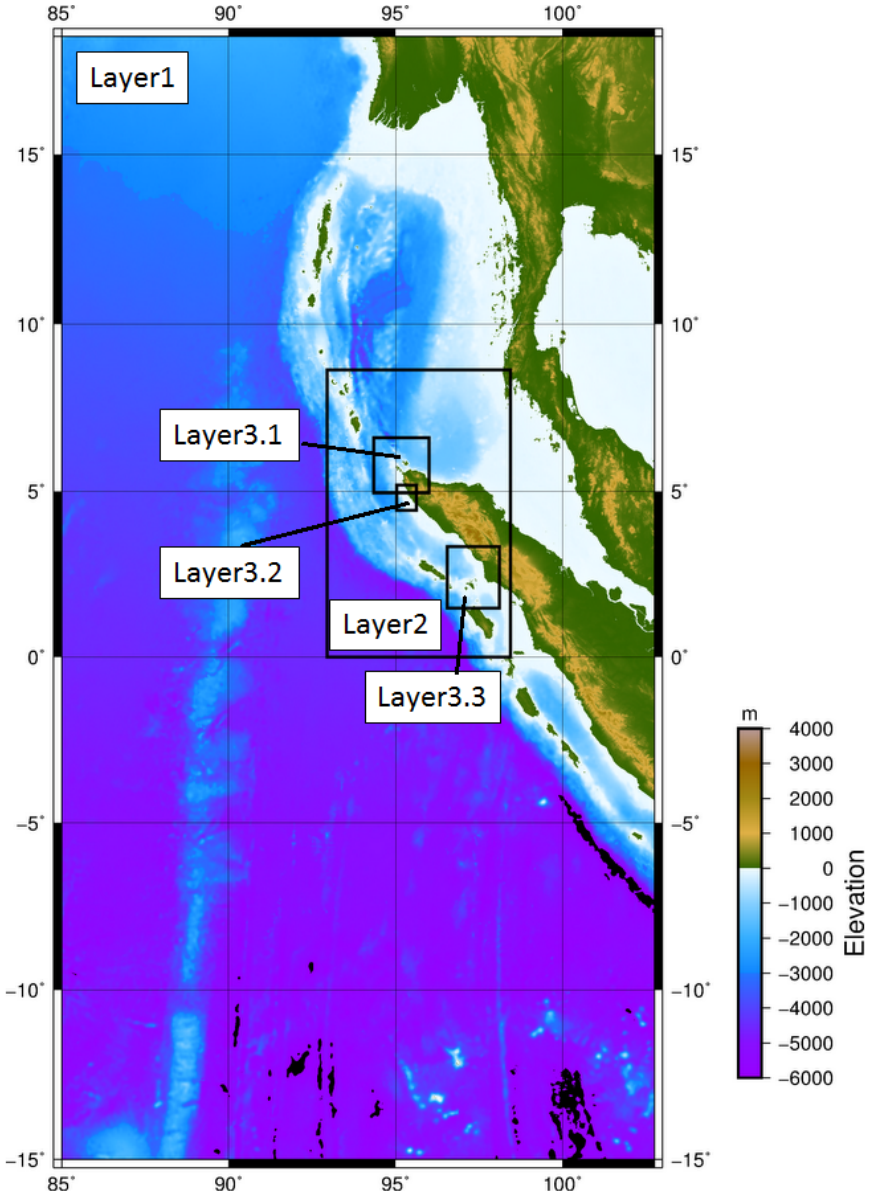

Figure 2.11: Simulation area around the Sumatra Island (Layer 1, Layer 2, Layer 3.1, Layer 3.2, and Layer 3.3).

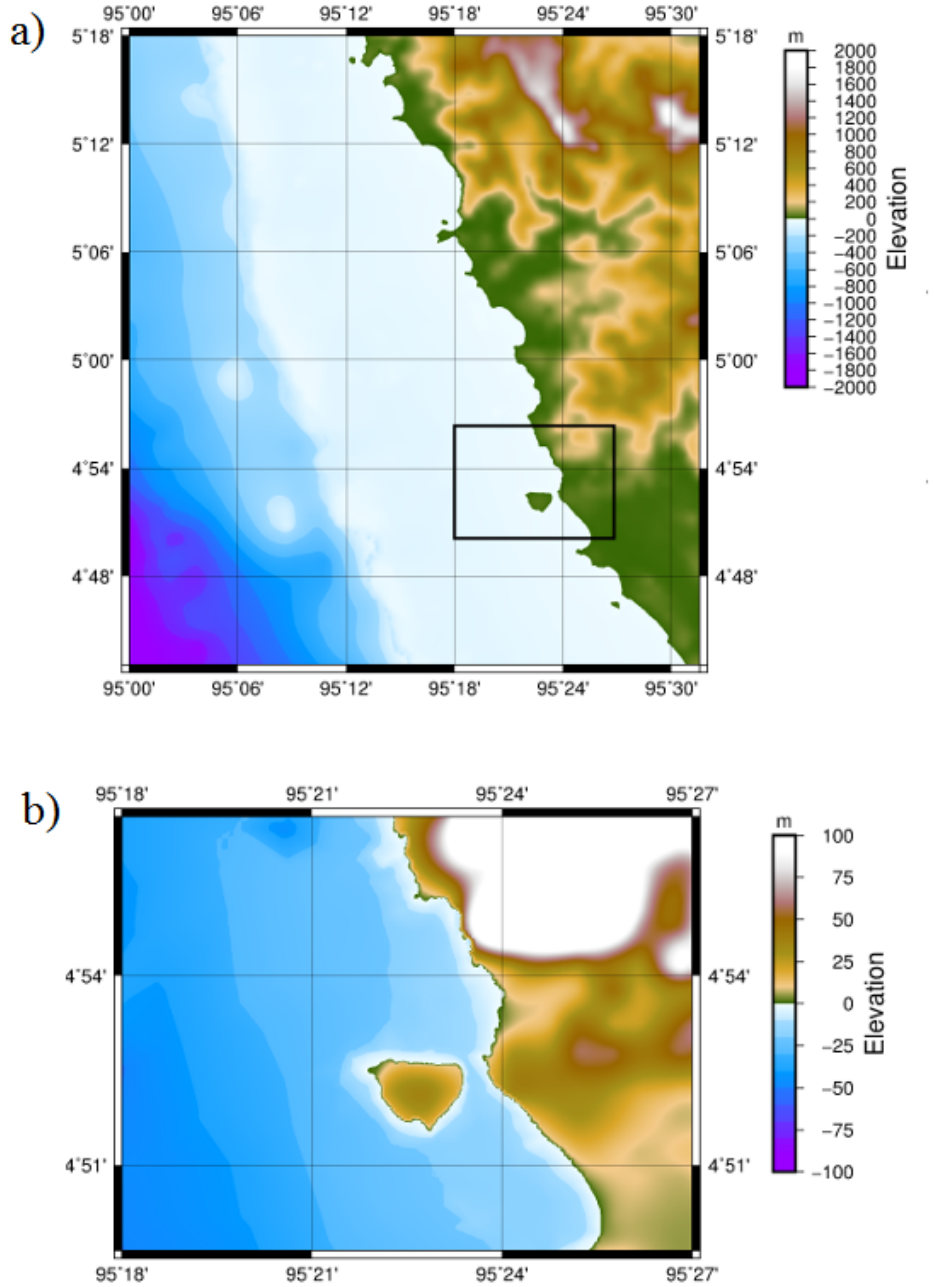

Figure 2.12: Nested grids for the Cornell Multigrid Coupled Tsunami Model simulation domain showing (a) Layers 3.2–4.2 and (b) Layer 4.2.

Table 2.3: Model Parameters of the Nested Grids Employed in the Numerical Simulations.

Layer No	Extent of grid (geographic, WGS 84)		Grid Size (m)	Grid Size Ratio	Coordinate System	Type SWE
	Long(°)	Lat (°)				
1	from 88 to 101	from 0 to 15	1840		Spherical	Linear
2	from 92 to 98	from 4 to 9	613.33	3	Spherical	Linear
3.1	from 94.5 to 96	from 5.25 to 6.7	204.4	3	Spherical	Linear
3.2	from 95.005 to 97.494	from 4.721 to 6.48	204.4	3	Spherical	Linear
3.3	from 95.01 to 95.52	from 4.72 to 5.21	204.4	3	Spherical	Non-linear
4.1	from 95.15 to 95.5	from 5.5 to 5.75	68.148	3	Cartesian	Non-linear
4.2	from 95.301 to 95.448	from 4.837 to 4.929	68.148	3	Spherical	Non-linear
5	from 95.275 to 95.386	from 5.507 to 5.646	17.037	4	Cartesian	Non-linear

observed based on high-resolution data. Therefore, four layers were used for the Pulo Raya Island, as shown in Figure 2.12.

Five nested grid layers were used to simulate the tsunami wave from the earthquake source to Banda Aceh city, as shown in Figure 2.13. A flow chart that show connection between of each layers can be seen Figure 2.14. As a result, the morphological changes in Banda Aceh can be observed based on high-resolution data. In layers 1 to 4, only the hydrodynamic model was applied. Both the hydrodynamic and sediment transport models were applied in layer 5. The time step with about 0.01 s was adopted in all layers for calculation stability. Table 2.3 shows the input parameters implemented on every layer in this study, such as grid size, simulation area, coordinate system, and SWE type.

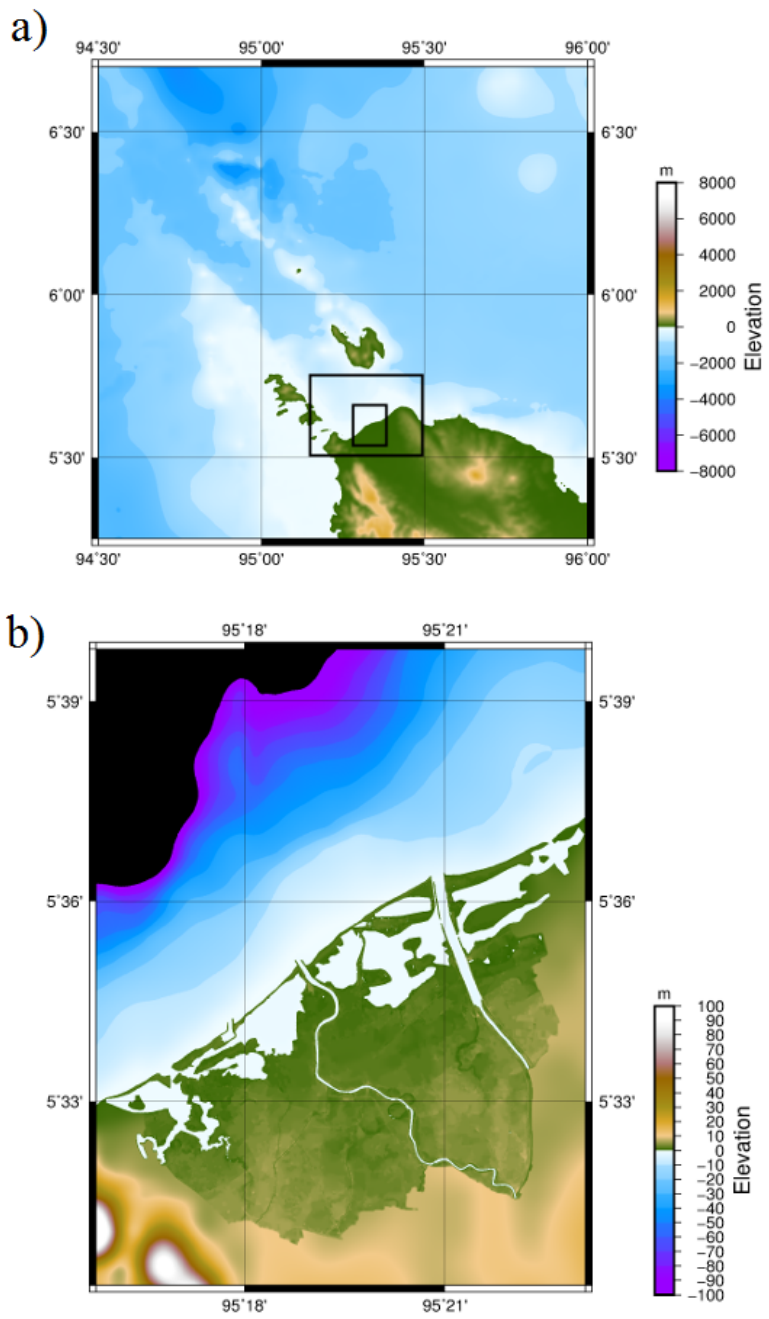

Figure 2.13: Nested grids for the Cornell Multigrid Coupled Tsunami Model coupled with a sediment module (COMCOT-SED) simulation domain showing (**a**) Layers 3.1–4.1 and (**b**) Layer 5.

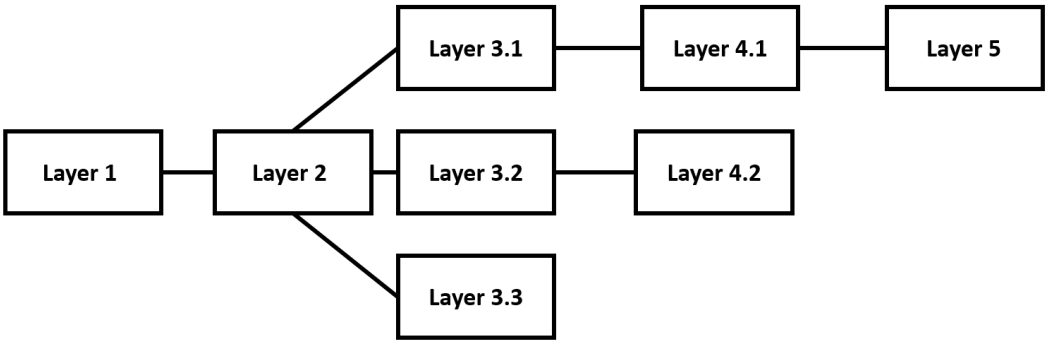

Figure 2.14: Flow Chart of Grid Setup.

Table 2.4: Software list.

No	Software Name	Utility
1	COMCOT-SED	Tsunami Numerical Simulation
2	Fortran	Preprocessing and Postprocessing
3	Generic Mapping Tools	Preprocessing and Postprocessing
4	Delft3D-Quickin	Manipulating Input Data
5	Quantum GIS	Digitizing and Georeferencing

Before processing tsunami numerical simulation with the COMCOT-SED model, several input data are required to undergo prepossessing. Therefore, open source softwares were used to do the prepossessing input data such as the batyhmetry and the topography in the COMCOT model. List of softwares has been used in the research can be seen in Table 2.4.

General Bathymetric Chart of the Ocean (GEBCO) data (Weatherall et al., 2015) were adopted in this study for the bathymetry and topography data for layers 1–2 and layers 1–5. The GEBCO data are open source for general bathymetry and topography data with a resolution of about 0.5 arcminute. Layers 2–5 have been implemented for different grid sizes, as shown in Table 2.5, that are smaller than the GEBCO data. Therefore, GMT (Generic Mapping Tools) (Wessel et al., 2013) software was used to interpolate the data

Table 2.5: List of data that used for layers 1-5.

Layer No	Topography	Bathymetry
1	GEBCO	GEBCO
2	GEBCO	GEBCO
3.1	GEBCO	nautical chart
3.2	GEBCO	nautical chart
3.3	GEBCO	nautical chart
4.1	GEBCO	nautical chart
4.2	GEBCO	nautical chart
5	GEBCO	nautical chart

for layers 2–5.

The topography data from GEBCO were selected despite having low accuracy, because it was impossible to get the data just before the 2004 tsunami for this study. The bathymetry for the (layers 3–5) was developed using nautical chart data measured by Dishidros of TNI AL Indonesia in 2001 with a map scale of approximately 1:100,000. The nautical chart map was digitized, using the geo-referenced function in Quantum GIS software (QGIS, 2009). Quickin and Refgrid software in Delft3D open source (Deltares, 2008) was used to combine the digitized bathymetry data from the nautical chart with a data from GEBCO in layers 3–5 (detail can be found in Table 2.5.

The sediment data were obtained from TDMRC (Tsunami and Disaster Mitigation Reseach Center) conducted at Ulee Lheu bay in 2006. The grain size d_{50} was specified as 0.18 mm for the sea area. The land area was assumed to have a similar grain size to the sea area. The entire area simulation for layer 5 was considered as erodible area.

Figure 2.15 shows the distribution of the Manning coefficients used in layer 5 as the innermost layer. A satellite image, based on Google Earth data in

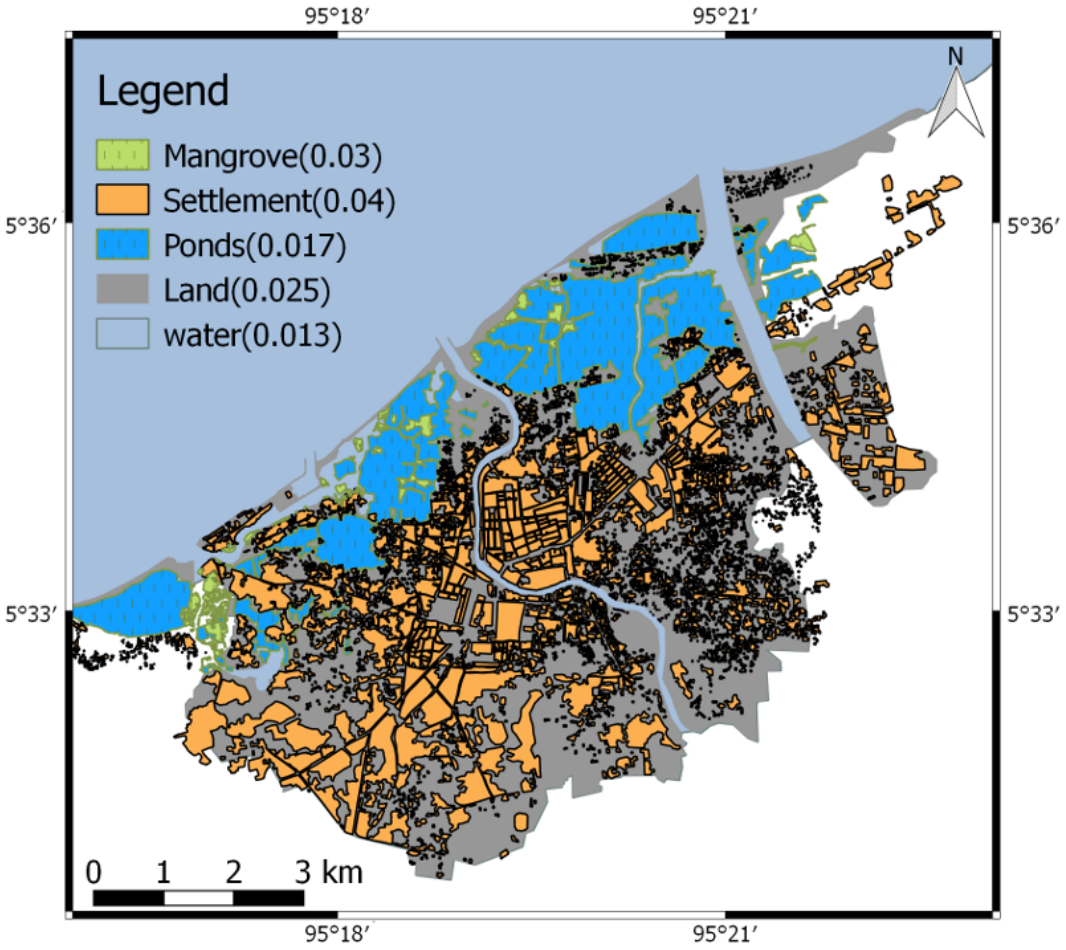

Figure 2.15: Distribution of Manning Coefficients in COMCOT-SED simulation.

2004, was applied to this study to show land use in Banda Aceh city. Different Manning coefficient values were obtained based on the land use classification in Banda Aceh city before the 2004 Indian Ocean tsunami. The Manning's values were adopted from previous studies by Syamsidik et al. (2017b); Li and Huang (2013), as shown in the Figure 2.15 legend. Settlements comprised most of the land area in Banda Aceh city. Ponds and mangrove areas existed on the backside of the coastal area, as indicated by blue and green colors. A uniform Manning coefficient value of 0.013 was used for layers 1–4.

2.2.4 Observation Points and Cross Section

An observation point is used as a virtual gauge to collect a fluctuation of seawater elevation. Several observation points were placed in the simulation area for big and small domain in order to obtain the Estimated Time of Arrival (ETA) and the maximum tsunami height. The ETA data used in this research were taken when the first tsunami wave reached its peak. For the western coast of Aceh, the observation points were putted along the shoreline.

For the Pulo Raya Island area, the observation points were divided into five areas. First, around the coastal area of the mainland in Layer 4.2, following the shoreline (points marked by red dots). Second, around Pulo Raya island. Points were placed eastern, western, northern, and southern of the island. These points are marked by green, purple, blue, and black dots, respectively. The other data widely used by tsunami researchers is tsunami elevation data measurement retrieved from Jason 1 satellite (the satellite track can be see in Gower (2005)). The satellite measured sea level elevation 2 hours after occurrence of the big earthquake in 2004. Hence, the simulation result has been validated by this data.

Simulation results have been validated by data from DART's (Deepocean Assessment and Reporting of Tsunami) buoy measurement at Cocos island and Phuket (DART, 2013)). Figure 2.16 shows a map of the buoys location. The DART buoy is an equipment which is functioned as tsunami warning system. The DART buoy has two-mode systems standard and event to report the data. The DART buoy regularly operates in a standard mode. The DART buoy measures water temperature and pressure then converts the data become sea water level and reports it with the time interval every 15 minutes.

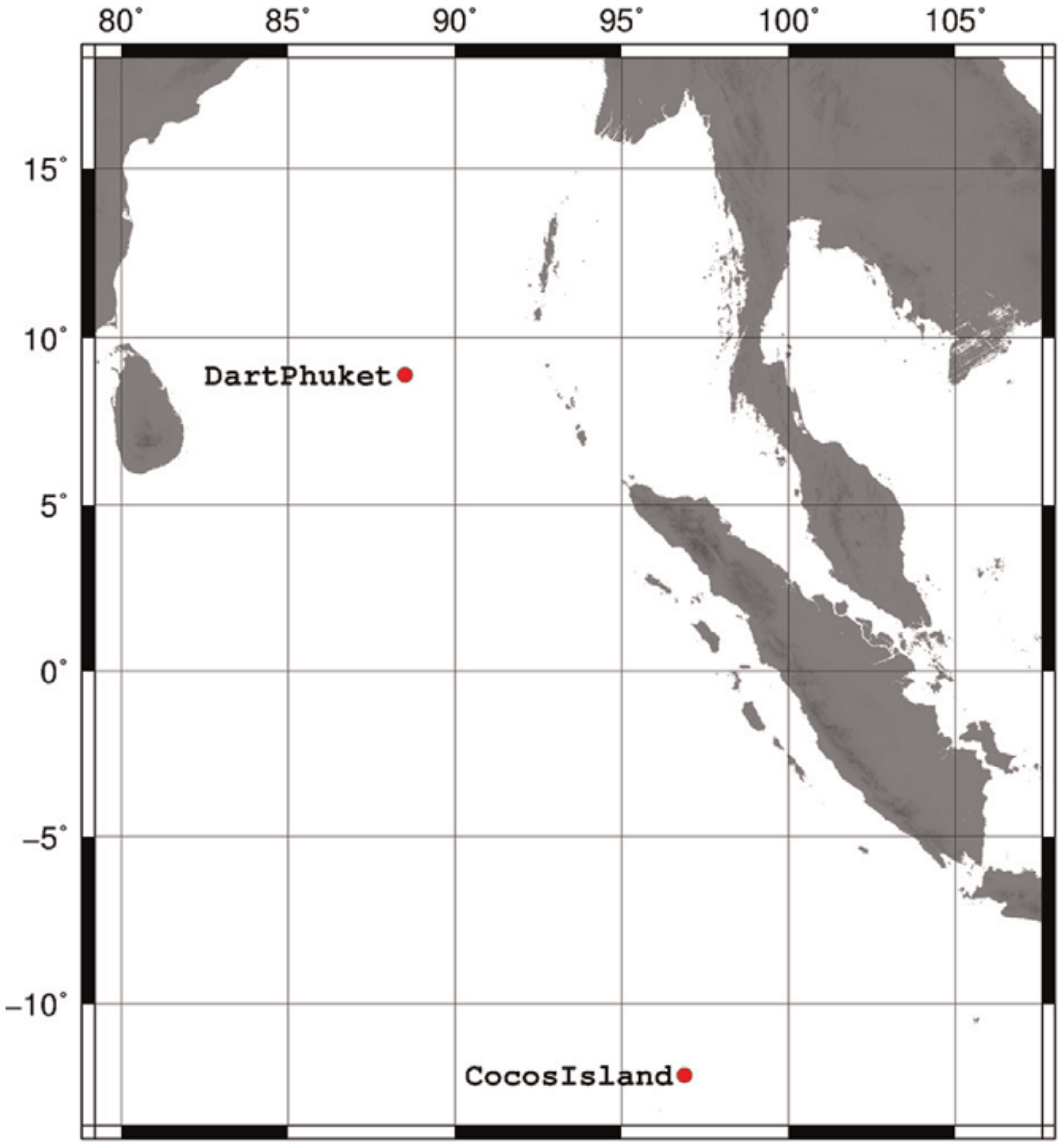

Figure 2.16: Locations of the numerical observation points and cross-sections.

If a big earthquake occurs, the DART buoy will be operated in event mode system and report the water elevation with time interval every 15 seconds. If there is no further earthquake, the system will return to the standard operation after reporting the data with the time interval 1 minute for 4 hours. The data not only can be used for early warning system but also for validating tsunami

simulation.

In Banda Aceh city as small domain, the observation points and cross-sections were placed on the simulation area to collect information such as water level and bed level on layer 5 also, as shown in Figure 2.17. The observation points (marked by red dots) were the same as the tsunami pole locations according to (Iemura et al., 2011; Syamsidik et al., 2017b). These locations were used to compare the maximum tsunami water level between the simulation results and the actual data. Three cross-sections perpendicular to the coastline were used to compare the coastal profile before and after the tsunami. The cross-sections were chosen because the tsunami wave caused massive damage at these locations.

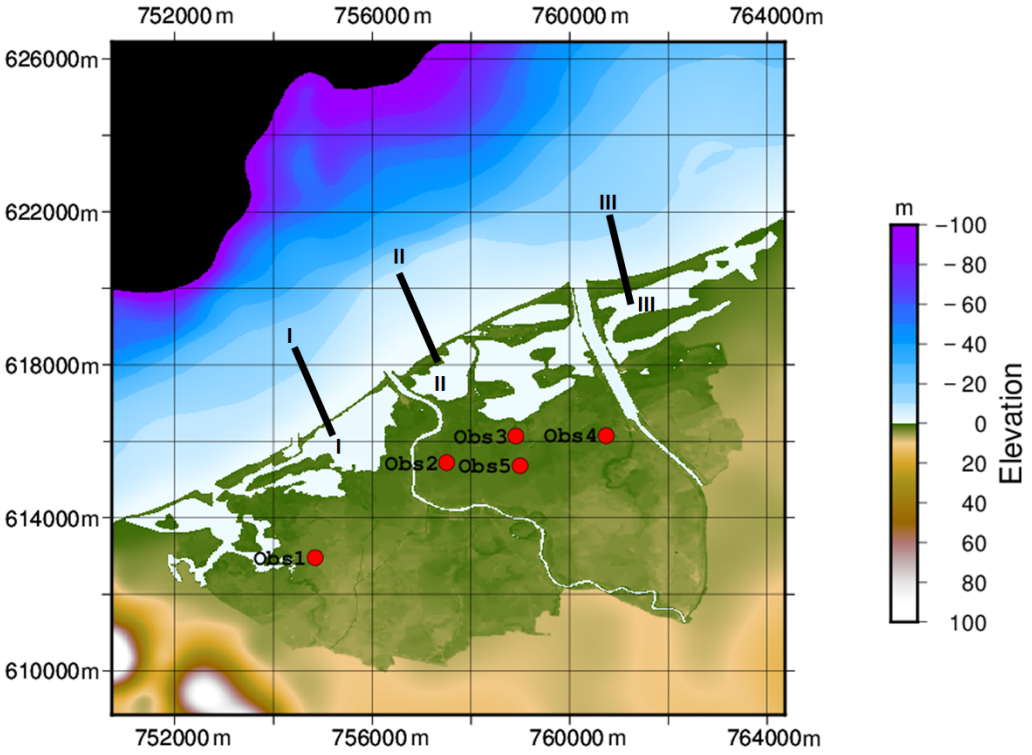

Figure 2.17: Locations of the numerical observation points and cross-sections.

References

Ammon, C. J., Ji, C., Thio, H.-K., Robinson, D., Ni, S., Hjorleifsdottir, V., Kanamori, H., Lay, T., Das, S., and Helmberger, D. (2005). Rupture process of the 2004 sumatra-andaman earthquake. *Science*, 308(5725):1133–1139.

Banerjee, P., Pollitz, F., Nagarajan, B., and Burgmann, R. (2007). Coseismic slip distributions of the 26 december 2004 sumatra–andaman and 28 march 2005 nias earthquakes from gps static offsets. *Bulletin of the Seismological Society of America*, 97(1A):S86–S102.

Burbidge, D., Cummins, P., Latief, H., Mleczko, R., Mokhtari, M., Natawidjaja, D., Rajendran, C., and Thomas, C. (2009). A probabilistic tsunami hazard assessment of the indian ocean nations. *Australian Government, Geoscience Australia, Professional Opinion*, (2009/11).

DART (2013). National data buoy center. available from: http://www.ndbc.noaa.gov/dart/dart.shtml. last accessed: 2016, march 4.

Deltares (2008). Delft3d-flow simulation of multi-dimensional hydrodynamic flows and transport phenomena including sediments, user manual. page 659.

Galappatti, G. and Vreugdenhil, C. (1985). A depth-integrated model for suspended sediment transport. *Journal of Hydraulic Research*, 23(4):359–377.

Geist, E. L., Bilek, S. L., Arcas, D., and Titov, V. V. (2006). Differences in tsunami generation between the december 26, 2004 and march 28, 2005 sumatra earthquakes. *Earth, planets and space*, 58(2):185–193.

Gower, J. (2005). Jason 1 detects the 26 december 2004 tsunami. *Eos, Transactions American Geophysical Union*, 86(4):37–38.

Grilli, S. T., Ioualalen, M., Asavanant, J., Shi, F., Kirby, J. T., and Watts, P. (2007). Source constraints and model simulation of the december 26, 2004, indian ocean tsunami. *Journal of Waterway, Port, Coastal, and Ocean Engineering*, 133(6):414–428.

Hanks, T. and Kanamori, H. (1979). A moment magnitude scale: Journal geophysical research.

Iemura, H., Pradono, M. H., Sugimoto, M., Takahashi, Y., and Husen, A. (2011). Tsunami height memorial poles in banda aceh and recommendations for disaster prevention. In *Proceedings of the International Symposium on Engineering Lessons Learned from the*.

Kanamori, H. and Anderson, D. L. (1975). Theoretical basis of some empirical relations in seismology. *Bulletin of the seismological society of America*, 65(5):1073–1095.

Kongko, W. (2012). *South Java Tsunami Model Using Highly Resolved Data and Probable Tsunamigenic Sources*. Leibniz Universität Hannover, Franzius-Institut für Wasserbau und Küsteningenieurwesen.

Li, L. and Huang, Z. (2013). Modeling the change of beach profile under tsunami waves: a comparison of selected sediment transport models. *Journal of Earthquake and Tsunami*, 7(01):1350001.

Li, L., Huang, Z., and Qiu, Q. (2014). Numerical simulation of erosion and deposition at the thailand khao lak coast during the 2004 indian ocean tsunami. *Natural hazards*, 74(3):2251–2277.

Li, L., Huang, Z., Qiu, Q., Natawidjaja, D. H., and Sieh, K. (2012a). Tsunami-induced coastal change: scenario studies for painan, west sumatra, indonesia. *Earth, planets and space*, 64(10):2.

Li, L., Qiu, Q., and Huang, Z. (2012b). Numerical modeling of the morphological change in lhok nga, west banda aceh, during the 2004 indian ocean tsunami: understanding tsunami deposits using a forward modeling method. *Natural Hazards*, 64(2):1549–1574.

Mansinha, L. a. and Smylie, D. (1971). The displacement fields of inclined faults. *Bulletin of the Seismological Society of America*, 61(5):1433–1440.

Meltzner, A. J., Sieh, K., Chiang, H.-W., Shen, C.-C., Suwargadi, B. W., Natawidjaja, D. H., Philibosian, B., and Briggs, R. W. (2012). Persistent termini of 2004-and 2005-like ruptures of the sunda megathrust. *Journal of Geophysical Research: Solid Earth*, 117(B4).

Okada, Y. (1985). Surface deformation due to shear and tensile faults in a half-space. *Bulletin of the seismological society of America*, 75(4):1135–1154.

QGIS, D. T. (2009). Qgis geographic information system.

Roelvink, D., Reniers, A., Van Dongeren, A., Van Thiel de Vries, J., Lescinski, J., and McCall, R. (2010). Xbeach model description and manual. *Unesco-IHE Institute for Water Education, Deltares and Delft University of Tecnhology. Report June*, 21:2010.

Sengara, I. W., Latief, H., and Kusuma, S. B. (2008). Probabilistic seismic and tsunami hazard analysis for design criteria and disaster mitigation in rehabilitation and reconstruction of a coastal area in city of banda aceh. In

Geotechnical Engineering for Disaster Mitigation and Rehabilitation, pages 224–230. Springer.

Soulsby, R. (1997). *Dynamics of marine sands: a manual for practical applications*. Thomas Telford.

Suppasri, A., Futami, T., Tabuchi, S., and Imamura, F. (2012a). Mapping of historical tsunamis in the indian and southwest pacific oceans. *International Journal of Disaster Risk Reduction*, 1:62–71.

Suppasri, A., Imamura, F., and Koshimura, S. (2012b). Tsunami hazard and casualty estimation in a coastal area that neighbors the indian ocean and south china sea. *Journal of Earthquake and Tsunami*, 6(02):1250010.

Syamsidik, Oktari, R. S., Munadi, K., Arief, S., and Fajri, I. Z. (2017a). Changes in coastal land use and the reasons for selecting places to live in banda aceh 10 years after the 2004 indian ocean tsunami. *Natural Hazards*, 88(3):1503–1521.

Syamsidik, Tursina, Meutia, A., Al'ala, M., Fahmi, M., and Meilianda, E. (2017b). Numerical simulations of impacts of the 2004 indian ocean tsunami on coastal morphological changes around the ulee lheue bay of aceh, indonesia. *Journal of Earthquake and Tsunami*, 11(01):1740005.

Tursina, Syamsidik, and Kato, S. (2017). Projections of tsunami inundation area coupled with impacts of sea level rise in banda aceh, indonesia. *In American Institute of Physics Conference Series*, 1892(10).

Wang, X. (2009). User manual for comcot version 1.7 (first draft). *Cornel University*, 65.

Weatherall, P., Marks, K. M., Jakobsson, M., Schmitt, T., Tani, S., Arndt, J. E., Rovere, M., Chayes, D., Ferrini, V., and Wigley, R. (2015). A new digital bathymetric model of the world's oceans. *Earth and Space Science*, 2(8):331–345.

Wells, D. L. and Coppersmith, K. J. (1994). New empirical relationships among magnitude, rupture length, rupture width, rupture area, and surface displacement. *Bulletin of the seismological Society of America*, 84(4):974–1002.

Wessel, P., Smith, W. H., Scharroo, R., Luis, J., and Wobbe, F. (2013). Generic mapping tools: improved version released. *Eos, Transactions American Geophysical Union*, 94(45):409–410.

Chapter 3

Numerical Simulation of the 2004 Indian Ocean Tsunami

3.1 Verification of The 2004 Tsunami Simulation

3.1.1 Tsunami Wave Height

Tsunami on 2004 was validated by measurement data of satellite Jason1. The satellite measured the sea level around the Indian Ocean about two hours after the tsunami was first generated. The tsunami wave height comparison between the simulation result and satellite data (Gower, 2005) can be seen in Figure 3.1. The most trailing waves did not match in height and phase. This overestimated results appeared due to a complex of earthquake which was occurred in 2004.

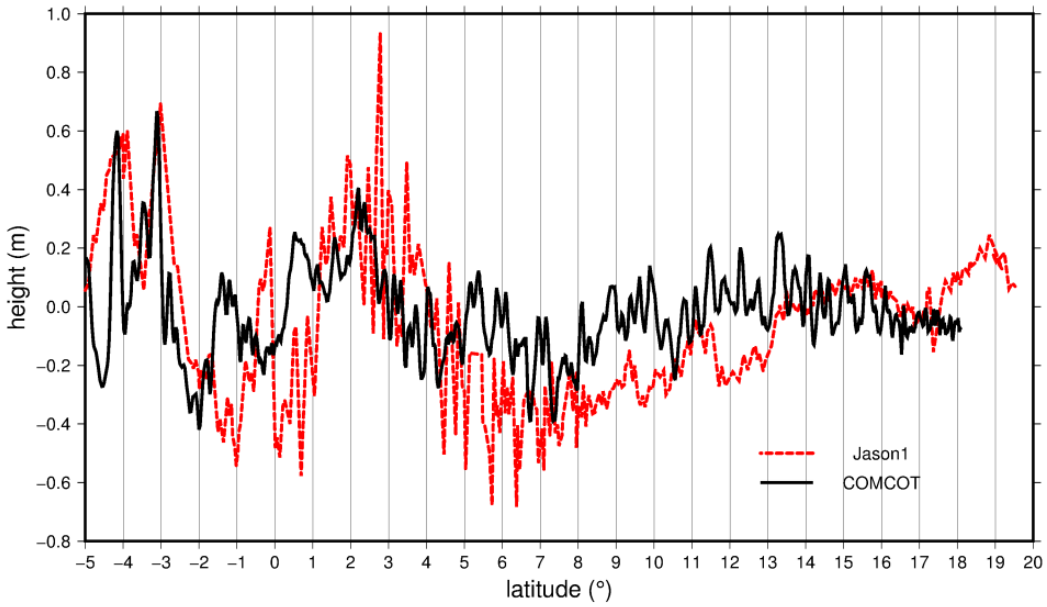

Figure 3.1: Tsunami height comparison between simulation results and satellite Jason1 in 2004 (Gower, 2005).

3.1.2 Inundation Distance

Banda Aceh city was inundated by the tsunami wave with the maximum inundation depth of approximately 7 m at the front of coastal land barrier and 4 m in the city area based on the simulation results, respectively (Figure 3.2). The tsunami wave flooded toward Banda Aceh city with a maximum inundation distance of about 4 km from the shoreline according to field observation (Tursina et al., 2017). The simulation results predicted a distance of about 5.5 km from the shoreline, which overestimated the inundation of the real event.

This can be explained because Banda Aceh city had a lot of structures around the coastal area which were not reproduced in the simulation, and they can reduce the tsunami wave energy and limit inundation further inland. The low accuracy of the data can cause differences between the simulation results

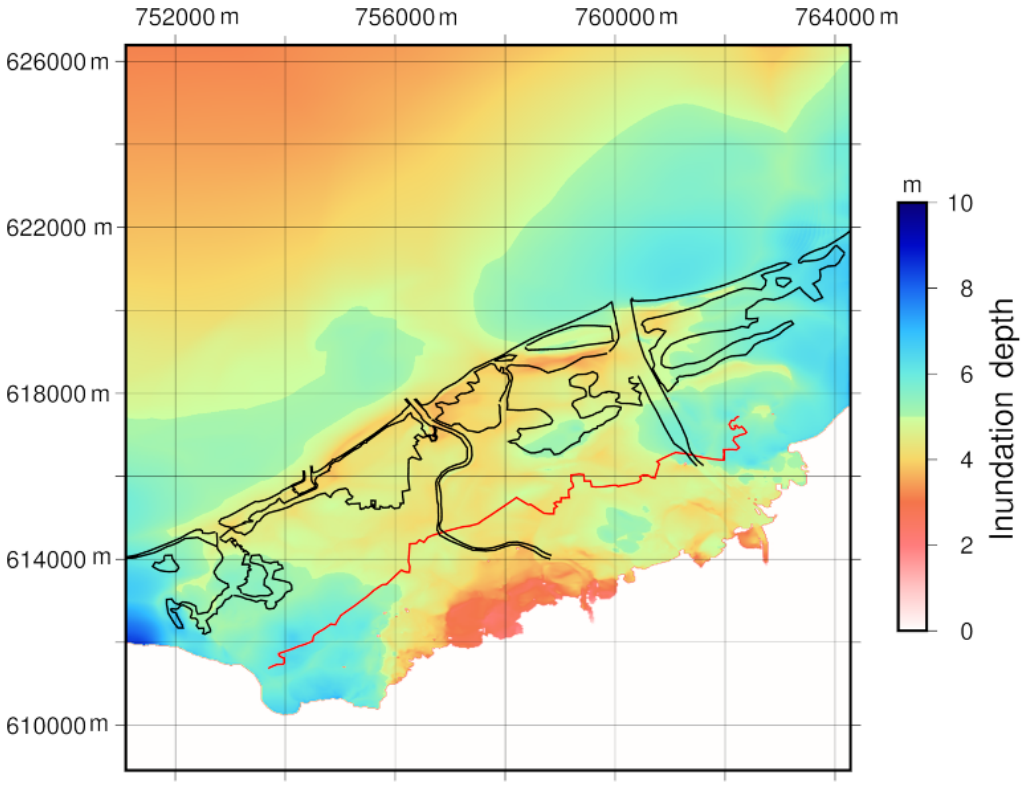

Figure 3.2: Map of the maximum inundation depth (m). The red line indicates the inundation limit based on the real event. The black line marks the Banda Aceh shoreline before the tsunami.

and field observation. The input data, especially the good accuracy of topography and bathymetry data in the simulation, can influence the inundation extent in the simulation results as indicated by previous researches (Tsubaki and Kawahara, 2013; Griffin et al., 2015).

3.1.3 Tsunami height at in-land locations

Figure 3.3 compares the simulated maximum tsunami height and measured height at the tsunami poles (Iemura et al., 2011). The simulated results at all points overestimate the measured results. However, the differences between the simulated result and the measured one at obs2, 3 and 5 are not so large. These

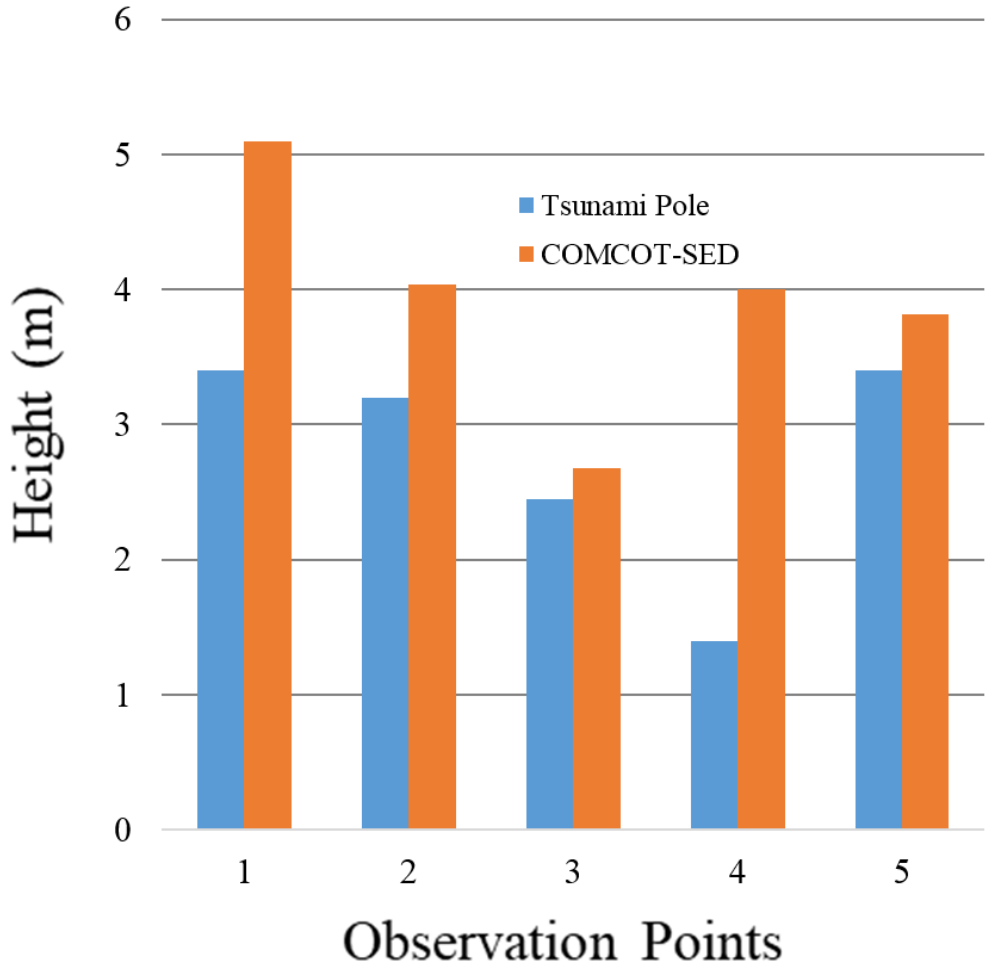

Figure 3.3: The calculated tsunami heights (orange bar) and tsunami pole (Iemura et al., 2011) (blue bar) in Banda Aceh city.

points are located in the middle of Banda Aceh city. Therefore, the tsunami inundation in the city area was simulated appropriately. On the contrary, a large difference is demonstrated at obs4. The location of obs4 is close to a large river.

In Figure 3.2 of the spatial distribution of the maximum inundation depth, a large inundation depth area, in blue color, extends further in the inland area

than the area close to the river mouth. Based on these results, it is suggested that the tsunami propagation in the river occurred up to the inland area and the significant overestimate of the maximum height was caused by the flood from the river in the simulation. This result also indicated the risk of river flooding caused by the tsunami in the inland area.

3.1.4 Coastal Profile Changes

Figure 3.4 shows sea bed profiles for the initial condition, the simulated result by COMCOT-SED, and measured data at cross-sections I-I, II-II, and III-III. The post-tsunami profile measurement was conducted in 2006 by the Public Works Department of Aceh two years after the tsunami event. In the initial condition, the shoreline position was at a distance of 600, 270, and 500 m from the ends of sections I-I, II-II, and III-III, respectively. In the simulated profiles, the coastal area directly facing the sea was eroded, reducing the height. In contrast, deposition occurred in the fishponds, as indicated by the black arrow in Figure 3.4a. Along this coast, the land barriers were eroded by the tsunami wave, and bed profiles in very shallow areas became flat at the distance from 0 to 300 m and from 0 to 550 m for sections II-II and III-III, respectively.

Comparing the simulation results to the 2006 bathymetry data indicates that the bathymetry profile underwent further changes. The disagreements can be caused possibly by other morphological changes in the 2004–2006 time range, low accuracy of the topography data before the tsunami, the uniform grain size applied for the simulation, and limitations of the current model. The low accuracy of topography data and limited information of grain size can influence the location of erosion and deposition in numerical calculation (Gus-

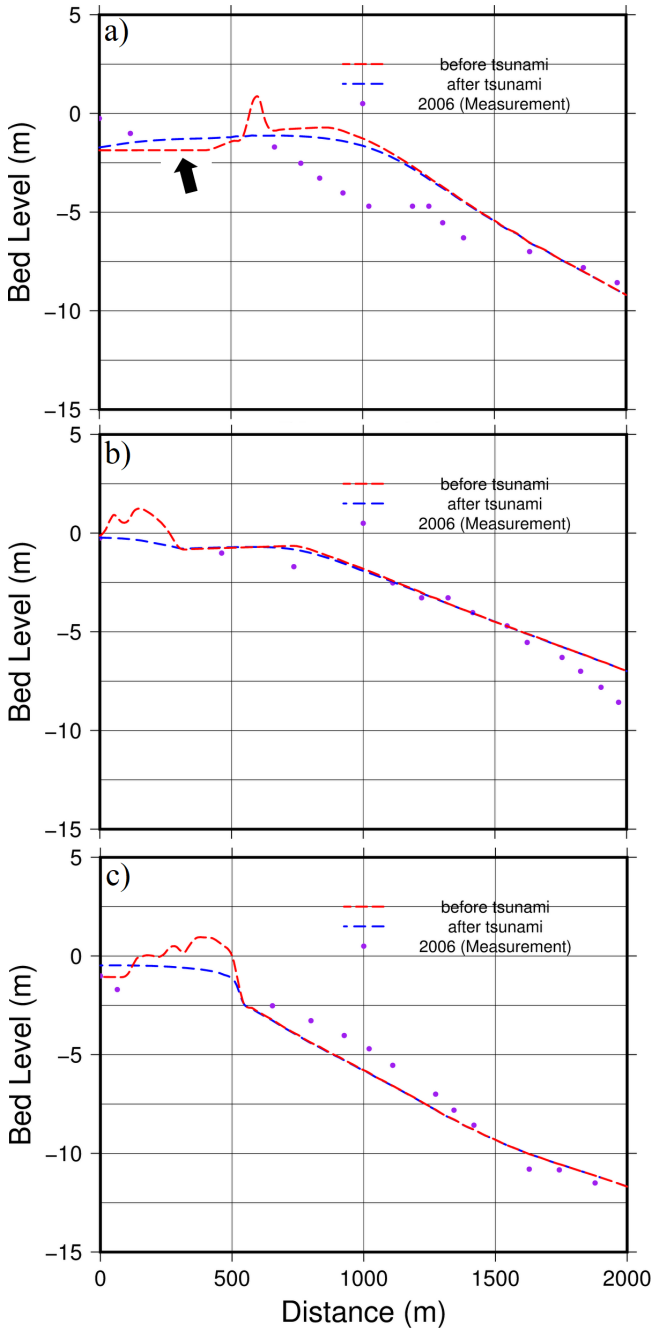

Figure 3.4: Bed profile for the initial condition (indicated by red line), after tsunami inundation (simulation) by the 2004 Indian Ocean Tsunami (indicated by blue line), and measured in 2006 (indicated by purple circles) in the cross-section; (a) I-I, (b) II-II and (c) III-III.

man et al., 2012).

The current model also has limitations in calculating the bed stress based on the Manning formula that possibly causes overestimation. Coupling the SWE and a Reynolds-averaged Navier–Stokes (RANS) model with a boundary-layer method indicates that the boundary-layer method is able to calculate the bed stress accurately compared to the Manning formula (Tanaka et al., 2016; Williams and Fuhrman, 2016). The advantage of the boundary-layer method was applied by Larsen et al. (2018) to predict the tsunami wave-induced scouring.

This suggests that it is important to apply the boundary-layer method in the model to calculate the sediment transport properly. In general, coastal erosion was indicated by the 2006 bathymetry data, as shown in Figure 3.4b,c with distances of 0–300 m and 50–600 m. This is shown by the simulation results at the cross-sections II and III, where the land barrier had been destroyed by the tsunami wave.

3.1.5 Destroyed Land Barrier

This part of the study used geospatial information, based on a Google Earth map released between 2004 and 2005, to validate the simulation result. Figure 3.5a,b displays the Banda Aceh coast condition in 2004, (a) before the tsunami and (b) afterwards. The topographic data in the simulation results are also shown in Figure 3.5c,d. Figure 3.5c is the initial topography (before the tsunami) and Figure 3.5d is the simulated topography after the tsunami impact. Figure 3.5a,c, and 3.5b,d should be compared. The northern coast area underwent massive morphological changes after the tsunami. The beach area from lines A1 to A2 and C1 to C2 in Figure 3.5d was completely eroded

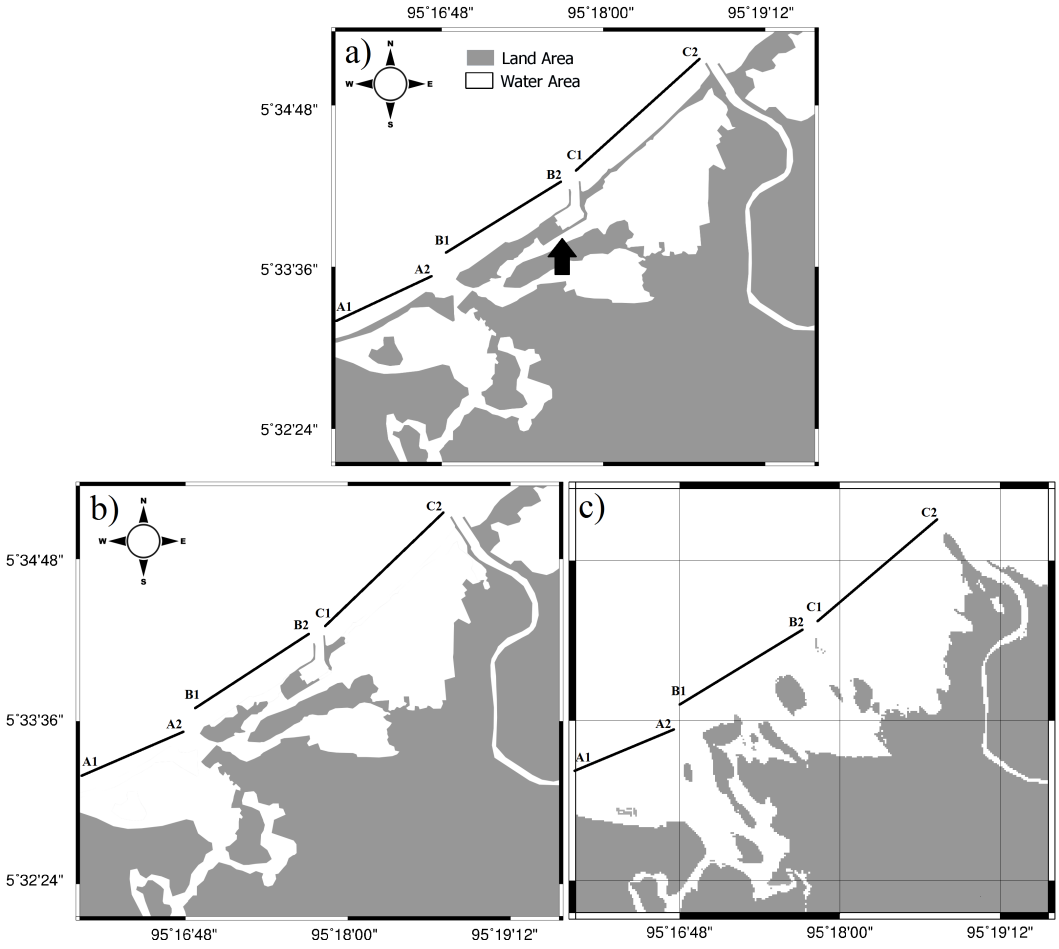

Figure 3.5: Coastal area comparison between the satellite images: (a) before, (b) after the tsunami in 2004, and numerical simulation: (c) after simulated by COMCOT-SED. The satellite images are taken from Google Earth with time history imagery setting on 23 July 2004 and 28 January 2005.

by the tsunami wave. This area was natural beach without any protection; therefore, the tsunami wave could erode easily in this area (Syamsidik et al., 2017a; Meilianda et al., 2010; Syamsidik et al., 2015).

The beach area from line B1 to line B2 shows differences between the satellite image and the simulation results. This could be because no structures were assumed and the whole area was consider erodible in the simulation but

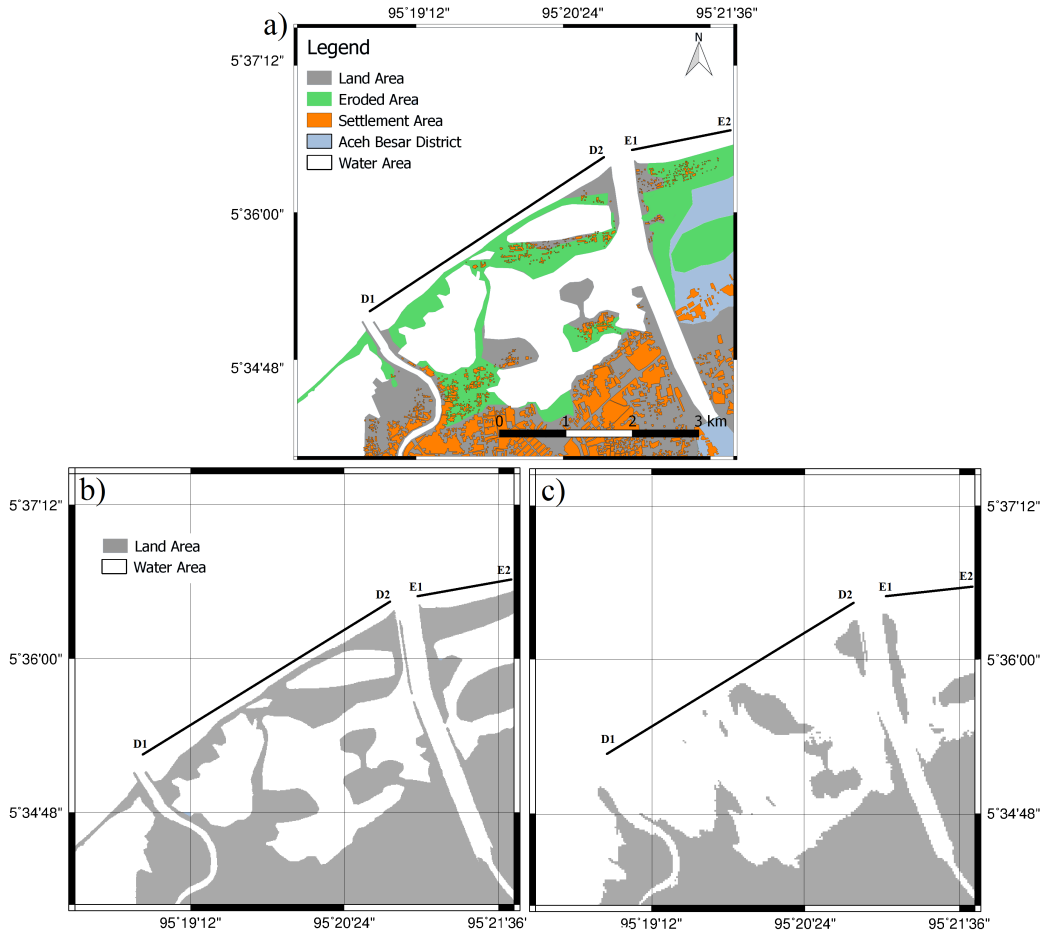

Figure 3.6: Coastal area comparison between the geospatial data and numerical simulation. (a) Green and a gray areas indicate the land condition before the tsunami in 2004. The green area indicates the eroded area after the tsunami in 2004. This figure was modified from (Syamsidik et al., 2017b). (b) before simulated and (c) after simulated by COMCOT-SED.

there were several hard structures on the ground before the tsunami, especially the area indicated by a black arrow shown in Figure 3.5a. At this area, a port structure complex prevented severe erosion from the tsunami waves.

Geospatial analysis results based on Syamsidik et al. (2017b) were used in this study to compare the simulation results, as shown in Figure 3.6a. The

coastal area in Syiah Kuala sub-district, indicated from point E1 to E2 as shown in Figure 3.6c, was destroyed by the tsunami wave based on the simulation results. The simulation results indicated a similar result to the geospatial analysis, indicating that this area was also massively impacted by the tsunami waves. This area was natural beach without any protection and was used as a settlement area before the 2004 tsunami. The coastal area was completely eroded during the tsunami event in 2004.

The coastal area from point D1 to D2, as shown in Figure 3.6, is located in Kuta Alam and Syiah Kuala district. These areas were fish/shrimp ponds and vegetation before the 2004 tsunami. A small, but dense, housing area also existed here before the tsunami. The simulation results indicated that this area underwent massive morphological changes due to the tsunami wave (Figure 3.6c). The land area, which had been used as ponds, vegetation, and a settlement area, was covered with water (Syamsidik et al., 2017b). The coastal area located behind the ponds did not receive massive morphological changes. The simulation results are consistent with the geospatial analysis in which the land barrier had been destroyed.

3.2 Analysis and Discussion

3.2.1 Large Domain

Tsunami Propagation Process

Figure 3.7 shows the tsunami propagation process during the Indian Ocean Tsunami on 2004. Meulaboh was a nearest city to the earthquake's epicenter with distance 94 km in 2004. Without the present of a small island in the front, Meulaboh city was directly facing the fault area in 2004. In case of

parameters used to generate the tsunami in 2004, the fault area is extended from the northern of Simeulu Island. Therefore, the tsunami wave did not come directly in front of the Simeulu Island. The tsunami wave reach at Meulaboh and Tapaktuan after around 51 min where the wave height reach around 0.5 m as shown in Figure 3.8.

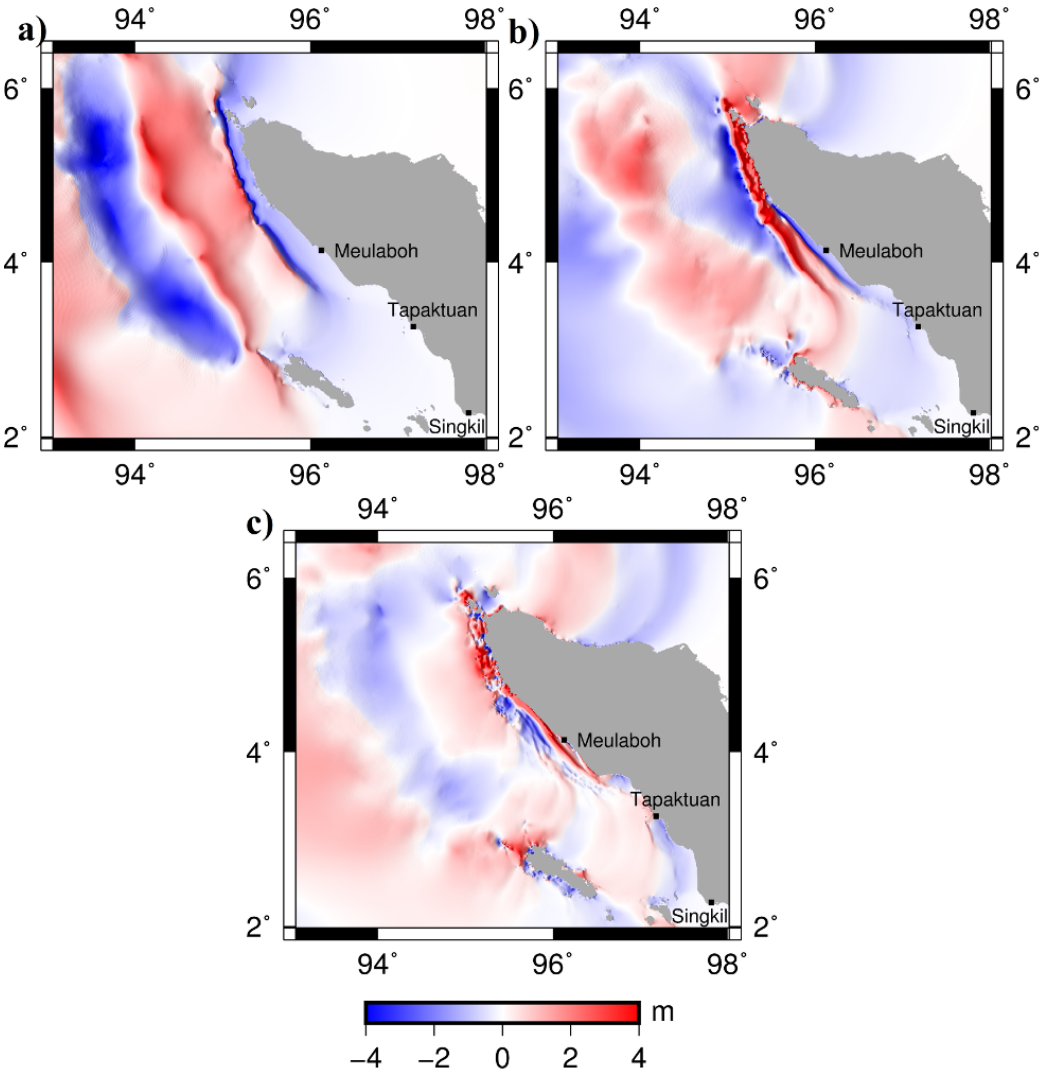

Figure 3.7: Snapshots of tsunami propagation process in 2004 at: (a)t=14 mins, (b)t=33 mins, and (c) t=51 mins.

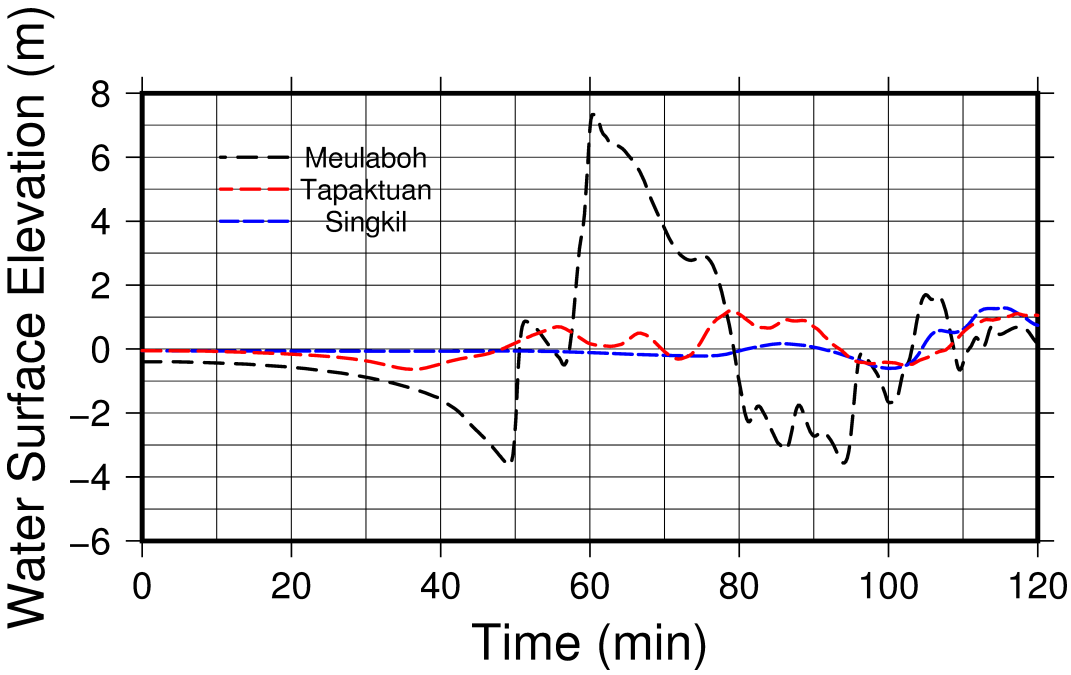

Figure 3.8: Tsunami wave height at Meulaboh, Tapaktuan, and Singkil for the tsunami in 2004 based on simulation.

The tsunami wave reaches to the Tapaktuan coast after propagation through the strait between the Simeulu and Sumatra Island, as shown in Figure 3.7c. The tsunami wave trapped behind the island arrived at Tapaktuan. Therefore, the amplification process by the island did not happened. According to in-depth interview with local people around Tapaktuan, they witnessed that the tsunami wave inundated to the land. However, that tsunami did not cause massive damage at Tapaktuan. They also said that the wave was similar to storm waves which could lift up fishing boats.

The tsunami wave energy was reduced during propagating toward the Singkil city. The tsunami also did not cause massive damage at Singkil and the Banyak Island which located in front of the city. As shown in Figure 3.8, tsunami wave was reach bellow 2 m at Tapaktuan and Singkil. The tsunami

propagation results indicated that the offshore small island can give influence toward Tapaktuan and Singkil cities. This condition contrary with previous study that showed the city which located behind the small island will be receive higher impact (Hill et al., 2012; Stefanakis et al., 2014). In order to prevent the future of tsunami hazard in these cities, several scenarios have been used to investigate further the influence of the small island that discuss in Chapter 4.

The tsunami propagation process toward Pulo Raya Island can be seen in Figure 3.9. The results indicated that the tsunami wave in 2004 caused significant damage at Pulo Raya, especially at the lee side of the small island (Liu et al., 1995; Imamura et al., 1995; Xie et al., 2019; Yeh et al., 1993, 1994). The distance between the source and Pulo Raya was about 90 km, and the initial tsunami wave (which occurred about 18 min after the earthquake) was about 0.5 m at the island. The tsunami wave then propagated from the west of Aceh Jaya (see Figure 3.9), and after 18 min of simulation, the tsunami wave arrived at the western coast of Pulo Raya with a height of about 7 m.

As the tsunami arrived at the western coast of the island, the tsunami waves were blocked by the island, and the wave separated to the north and south of the island as shown in Figure 3.9a. The flow marked by the colored arrow in the figure indicates the tsunami continued to propagate toward the northern and southern coast of Lhok Kruet on the mainland. The tsunami waves arrived at the northern and southern coast of Lhok Kruet with interval times about 20 to 22 min after the tsunami reached Pulo Raya.

When the tsunami hit the mainland, it was reflected back to the ocean and caused a flow vortex to the north as shown in Figure 3.9c. The tsunami flow

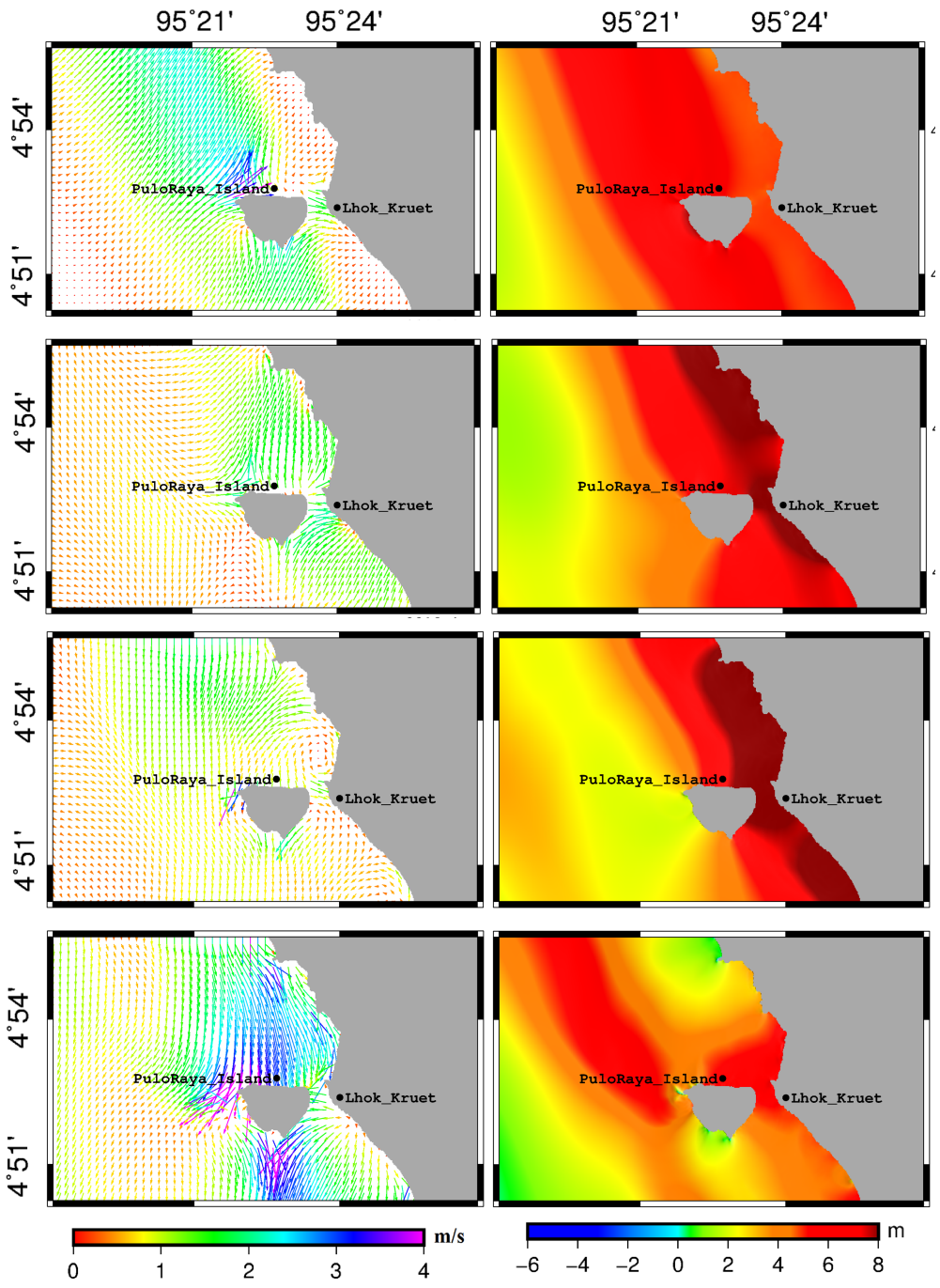

Figure 3.9: Snapshot of velocity maps (left) and tsunami propagation process (right) at (a1 and a2) t = 16 min, (b1 and b2) t = 19 min, (c1 and c2) t = 21 min, and (d1 and d2) t = 25 min.

that rotated around the northern part of Lhok Kruet changed its direction to the southern coast as it was carried away by a tsunami wave that reflected from the northern to southern coast of Aceh Province. Pulo Raya, located near Lhok Kruet, held the tsunami flow as shown in Figure 3.9d. As shown in the figure, the tsunami flow struck the northern coast of Pulo Raya with a velocity of about 4 m/s. Most of the tsunami flow did not hit directly to this area when it reached to the island at the first time about 18 min after the earthquake occur. Tsunami waves were again reflected back to the ocean. Further investigation of the reflected wave is discuss in Chapter 4.

3.2.2 Small domain

Sedimentation and Erosion

Figure 3.10 shows a map of erosion and deposition thickness by tsunami inundation 90 min after the tsunami (earthquake) occurrence according to the COMCOT-SED model. The results predict that the tsunami wave caused morphological changes along the entire Banda Aceh coast; especially severe erosion is shown in the red color areas. The most eroded area is along the eastern part of the coast of Banda Aceh because of direct attack of the tsunami waves. The western part of the coast of Banda Aceh was relatively shielded by a headland and a group of small islands. The sediment eroded by the tsunami wave near the coast line was transported to the land side and deposited in the ponds and lagoons behind the coast, as indicated by blue color in Figure 3.10. The sediments were deposited on the settlement area. This condition indicated that the high manning coefficient for settlement area able to reduce tsunami wave force (Syamsidik et al., 2017c). Less erosion and deposition occurred in coastal areas behind the coastal land barrier and pool areas.

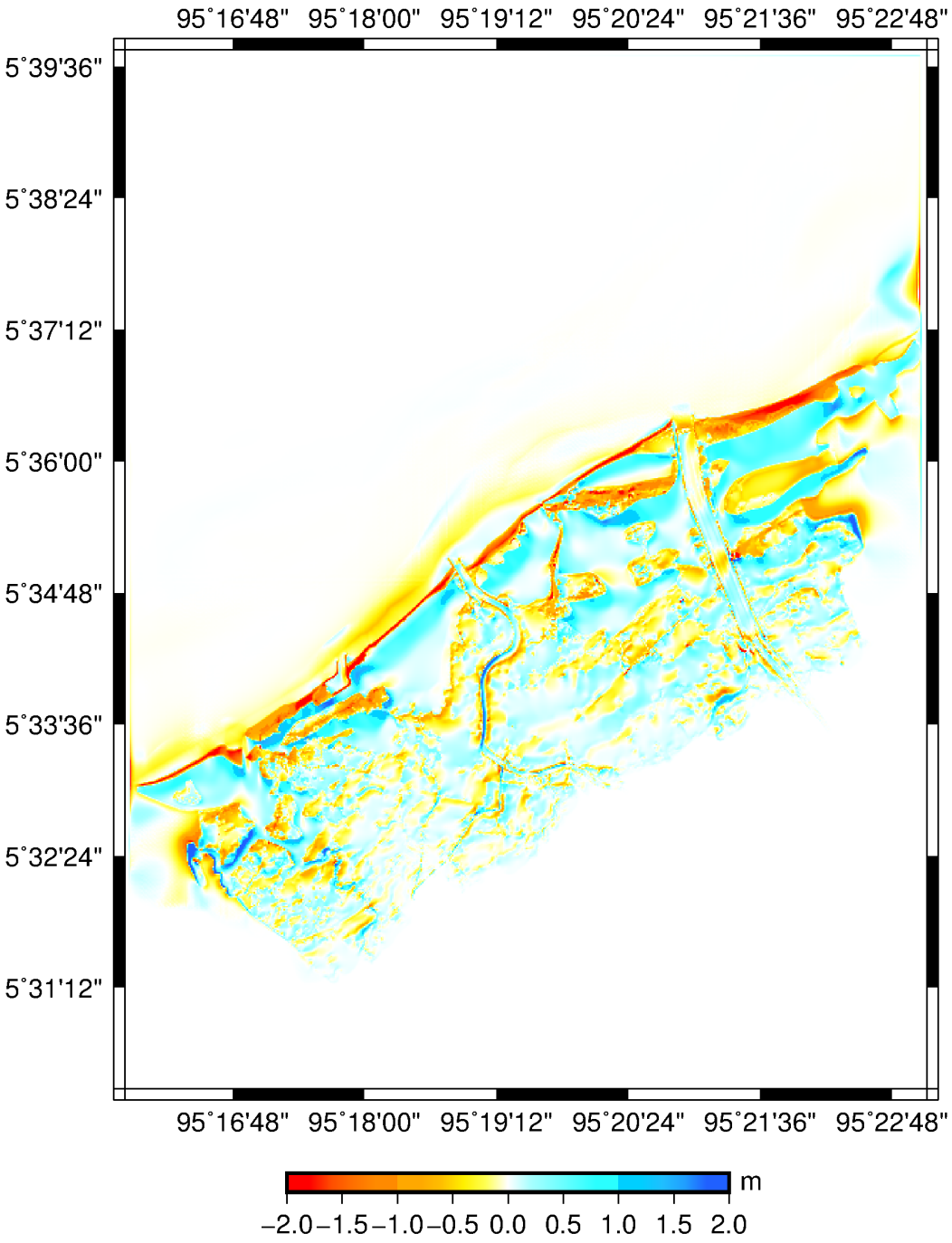

Figure 3.10: Map of erosion and deposition areas. Red color indicates negative (erosion) and blue indicates positive (deposition).

Problems for Tsunami disaster in Banda Aceh

The problem for tsunami disaster in Banda Aceh is linked to the lack of knowledge about it. After the tsunami event, the Banda Aceh coastal area underwent massive morphological changes. There was little land use management information for Banda Aceh before 2004. The natural beach areas without any protection in Banda Aceh, which facing directly to the sea, were completely destroyed by the tsunami wave. Even now, the local community has returned and rebuilt a new settlement in the area that eroded by the tsunami wave in 2004.

Suggestion for Tsunami disaster mitigation and prevention

Numerical simulation can be used to investigate morphological changes due to tsunami waves in the high-risk area. This model can predict areas of sedimentation and erosion caused by a tsunami wave. This study shows that the numerical model can simulate destruction of the land barrier by the 2004 tsunami. Unfortunately, the land barrier on Banda Aceh coast was used by the local community as a settlement.

The 2004 tsunami wave destroyed not only the land barrier but also the settlement area in Banda Aceh. The information of erosion and sedimentation location that obtained from simulation results can be used by local governments for land use management to help avoid a disaster such as the one in Banda Aceh during the 2004 Indian Ocean tsunami. A hard structure such as elevated road along the Banda aceh coastal area can be applied to prevent the coastal morphological changes due to the tsunami wave (Suppasri et al., 2016; Syamsidik et al., 2019).

References

Gower, J. (2005). Jason 1 detects the 26 december 2004 tsunami. *Eos, Transactions American Geophysical Union*, 86(4):37–38.

Griffin, J., Latief, H., Kongko, W., Harig, S., Horspool, N., Hanung, R., Rojali, A., Maher, N., Fuchs, A., and Hossen, J. (2015). An evaluation of onshore digital elevation models for modeling tsunami inundation zones. *Frontiers in Earth Science*, 3:32.

Gusman, A. R., Tanioka, Y., and Takahashi, T. (2012). Numerical experiment and a case study of sediment transport simulation of the 2004 indian ocean tsunami in lhok nga, banda aceh, indonesia. *Earth, Planets and Space*, 64(10):3.

Hill, E. M., Borrero, J. C., Huang, Z., Qiu, Q., Banerjee, P., Natawidjaja, D. H., Elosegui, P., Fritz, H. M., Suwargadi, B. W., and Pranantyo, I. R. (2012). The 2010 m_w 7.8 mentawai earthquake: Very shallow source of a rare tsunami earthquake determined from tsunami field survey and near-field gps data. *Journal of Geophysical Research: Solid Earth*, 117(B6):p. B06402.

Iemura, H., Pradono, M. H., Sugimoto, M., Takahashi, Y., and Husen, A. (2011). Tsunami height memorial poles in banda aceh and recommendations for disaster prevention. In *Proceedings of the International Symposium on Engineering Lessons Learned from the*.

Imamura, F., Gica, E., Takahashi, T., and Shuto, N. (1995). Numerical simulation of the 1992 flores tsunami: Interpretation of tsunami phenomena in northeastern flores island and damage at babi island. *Pure and Applied Geophysics*, 144(3):555–568.

Larsen, B. E., Arbøll, L. K., Kristoffersen, S. F., Carstensen, S., and Fuhrman, D. R. (2018). Experimental study of tsunami-induced scour around a monopile foundation. *Coastal Engineering*, 138:9–21.

Liu, P. L.-F., Cho, Y.-S., Briggs, M. J., Kanoglu, U., and Synolakis, C. E. (1995). Runup of solitary waves on a circular island. *Journal of Fluid Mechanics*, 302:259–285.

Meilianda, E., Dohmen-Janssen, C. M., Maathuis, B., Hulscher, S. J., and Mulder, J. (2010). Short-term morphological responses and developments of banda aceh coast, sumatra island, indonesia after the tsunami on 26 december 2004. *Marine Geology*, 275(1-4):96–109.

Stefanakis, T. S., Contal, E., Vayatis, N., Dias, F., and Synolakis, C. E. (2014). Can small islands protect nearby coasts from tsunamis? an active experimental design approach. *Proceedings of the Royal Society A: Mathematical, Physical and Engineering Sciences*, 470(2172):20140575.

Suppasri, A., Latcharote, P., Bricker, J. D., Leelawat, N., Hayashi, A., Yamashita, K., Makinoshima, F., Roeber, V., and Imamura, F. (2016). Improvement of tsunami countermeasures based on lessons from the 2011 great east japan earthquake and tsunami-situation after five years. *Coastal Engineering Journal*, 58(4):1640011–1.

Syamsidik, Fahmi, M., Fatimah, E., and Al'ala, M. (2017a). A decade process of coastal land use changes in peukan bada-aceh after the 2004 indian ocean tsunami. *IOP Conference Series: Earth and Environmental Science*, 56(1):012012.

Syamsidik, Iskandar, A., and Rasyif, T. M. (2015). Progress of coastal line rehabilitation after the indian ocean tsunami around banda aceh coasts.

In: Shaw R (ed) Recovery from the Indian Ocean Tsunami, disaster risk reduction, pp:175–189.

Syamsidik, Oktari, R. S., Munadi, K., Arief, S., and Fajri, I. Z. (2017b). Changes in coastal land use and the reasons for selecting places to live in banda aceh 10 years after the 2004 indian ocean tsunami. *Natural Hazards*, 88(3):1503–1521.

Syamsidik, Suppasri, A., Al'ala, M., Luthfi, M., and Comfort, L. K. (2019). Assessing the tsunami mitigation effectiveness of the planned banda aceh outer ring road (borr), indonesia. *Natural Hazards and Earth System Sciences*, 19(1):299–312.

Syamsidik, Tursina, Meutia, A., Al'ala, M., Fahmi, M., and Meilianda, E. (2017c). Numerical simulations of impacts of the 2004 indian ocean tsunami on coastal morphological changes around the ulee lheue bay of aceh, indonesia. *Journal of Earthquake and Tsunami*, 11(01):1740005.

Tanaka, H., Adityawan, M. B., Mitobe, Y., and Widiyanto, W. (2016). A new computation method of bottom shear stress under tsunami waves. *Journal of Coastal Research*, 75(sp1):1247–1252.

Tsubaki, R. and Kawahara, Y. (2013). The uncertainty of local flow parameters during inundation flow over complex topographies with elevation errors. *Journal of Hydrology*, 486:71–87.

Tursina, Syamsidik, and Kato, S. (2017). Projections of tsunami inundation area coupled with impacts of sea level rise in banda aceh, indonesia. *In American Institute of Physics Conference Series*, 1892(10).

Williams, I. A. and Fuhrman, D. R. (2016). Numerical simulation of tsunami-scale wave boundary layers. *Coastal Engineering*, 110:17–31.

Xie, X., Chen, C., Li, L., Wu, S., Yuen, D. A., and Wang, D. (2019). Tsunami hazard assessment for atoll islands inside the south china sea: A case study of the xisha archipelago. *Physics of the Earth and Planetary Interiors*, 290:20–35.

Yeh, H., Imamura, F., Synolakis, C., Tsuji, Y., Liu, P., and Shi, S. (1993). The flores island tsunamis. *Eos, Transactions American Geophysical Union*, 74(33):369–373.

Yeh, H., Liu, P., Briggs, M., and Synolakis, C. (1994). Propagation and amplification of tsunamis at coastal boundaries. *Nature*, 372(6504):353.

Chapter 4

Influence of Small Island and Reflected Wave along Sumatra Island for Tsunami Disaster Reduction

4.1 Small Island Function

Indonesia is archipelago country which consist lot of islands with more than 17,000. Aceh province, which located in the northern of Sumatra island, has several offshore islands near the western coast of Aceh province such as Simeulu and Banyak islands. Meulaboh, Tapaktuan, and Singkil cities are located along the western coast that facing directly to Sumatra subduction zone. The Indian Ocean Tsunami in 2004 was give significant damage on Meulaboh city. However, Tapaktuan and Singkil did not receive any big damage from the 2004 tsunami. The simulation results in Chapter 3 indicated that the tsunami wave

height at the the Meulaboh, Tapaktuan, and Singkil reach about 7, 1, and 1 m, respectively.

Resident believe that the small island that located in front of the cities able to protect against tsunami. Disaster management and education in these cities are not enough because of no damage experience. This condition caused difficulty to carry out any disaster mitigation program such as prepares an escape route, an escape building, etc in order to prevent the tsunami hazard at Tapaktuan city (Syamsidik et al., 2015). Minor mitigation activity from the local government can decrease awareness and preparedness of local community at Tapaktuan toward the tsunami disaster. In another hand, numerical study by Stefanakis et al. (2014); Hill et al. (2012) indicated that the small island can amplify the tsunami wave to the mainland behind it rather than give protection.

The small Island's communities itself are among the most tsunami vulnerable societies in term of preparedness towards tsunami. Around the active the Sunda-subduction zone, there are many small islands where the population number is large. Managing the coastal area in the small island case would indeed require a thorough consideration. Assuming that the lee side of the island is a safest place from tsunami attack was proven incorrect if the distance of the small island is significantly close to the mainland. Some of them have the first arrival time of the tsunami waves less than 10 minutes (Syamsidik and Istiyanto, 2013).

This adds to a more complexity of efforts to increase the small island community's preparedness toward tsunami hazards. The simulation results in Chapter 3 revealed that although the small islands are assumed to hydro-

dynamically shelter the main island at the lee side of the island, the reflecting waves have created a similar destructive effect on the Pulo Raya island. The amplification of tsunami waves when it comes to the setting of Pulo Raya Island is similar to what was found in the 1867 tsunami around the Virgin Island in the Caribbean (Zahibo et al., 2003). In the case of tsunami wave trains (where the waves could be more than one), the amplification effects are more likely. Therefore, a comprehensive investigation of the effect of the small island on the tsunami wave height at the mainland which directly protected by the isle and the reflected wave toward the small island were discussed in the Chapter 4.

4.2 Verification of the 2005 and 2012 Tsunami Simulation

The tsunami wave in 2005 and 2012 were validated by using DART buoy data at Cocos island and Phuket (DART, 2013). The numerical results for a tsunami scenario in 2005 based on multi faults model that issued by Banerjee et al. (2007) are shown in Figure 4.1a. Figure 4.1a shows that A leading first wave overestimated with measurement data by DART buoy at Cocos Island. On other hand, a second wave until a middle of trailing wave about 3 hour after the earthquake are well match with measurement. After that, the trailing waves become overestimated with troughs and crests of measurement data. This happened due to lack resolution of the nearshore bathymetry used around Cocos island. The time series analysis between DART buoy data and simulation result for the 2012 case are shown in Figure 4.1b. The wave height between 0.5 - 3 hour were overestimated with the DART buoy data. However, the wave height around 3-4 hour give good comparison between the data. The

both of time series data indicated that the wave propagation to the observed study are relatively reliable.

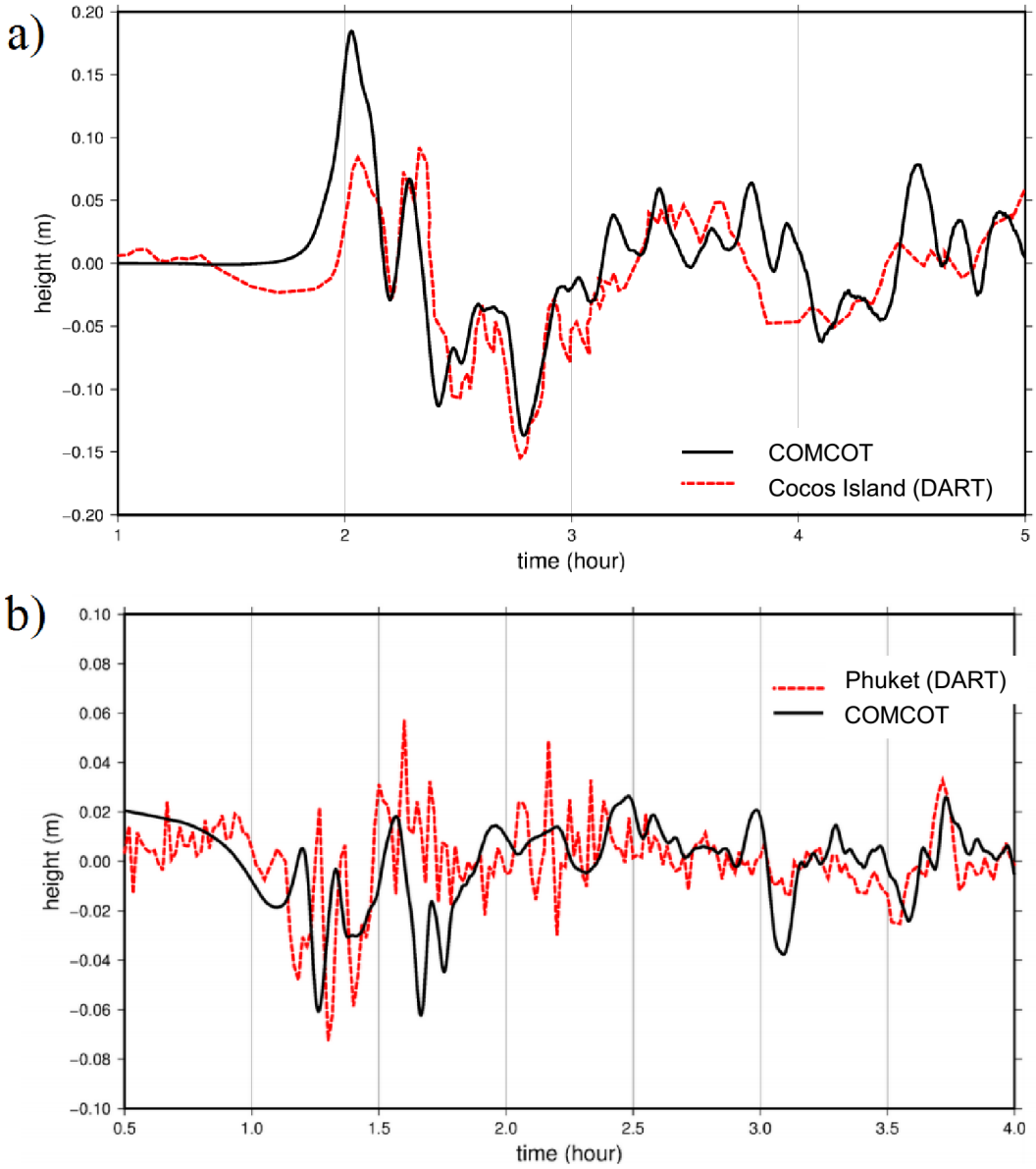

Figure 4.1: Tsunami Height Comparison between COMCOT-SED model and DART data at : a) Cocos island for the 2005 case and b) Phuket for the 2012 case.

4.3 Effect of fault area position

4.3.1 Case of tsunami in 2005

After the tsunami in 2004, another earthquake occurred in Sumatra subduction zone near Simeulue, Nias, and Banyak Islands with magnitude $M_W = 8.6$ on March 28, 2005. Tsunami was generated due to earthquake movement, which caused dislocation with about 12.3 m. Firstly tsunami propagated to Simeulue and Nias Islands about 14 min after the earthquake and caused tsunami around it, as shown in Figure 4.2. The tsunami waves, which described with blue color, were propagated to Singkil city through Banyak Island. The wave was divided by Banyak Island and caused the wave propagated to the right and left sides of the island. After the wave passed through the island, the wave that comes from the both sides of the island focused at the behind of island (Stefanakis et al., 2014). Then, the focused wave caused the higher run-up on Singkil city that located just behind the isle, as shown in Figure 4.2b.

In another hand, the focused wave did not occur at Tapaktuan city. The initial condition showed that the tsunami wave was triggered from southeast of Nias Island to northwest of Simeulu Island. The tsunami waves from the northwest of Simeulu as shown in Figure 4.2b and Figure 4.2c were propagated to the northwest of Aceh and turn into the lee side of Simeulu Island. However before the wave completely turns, the tsunami wave which propagated from the strait between the Simeulu Island and Tapaktuan has already propagated through it. The tsunami waves that hit the Tapaktuan city have just come from the strait between Simeulu and Banyak Island.

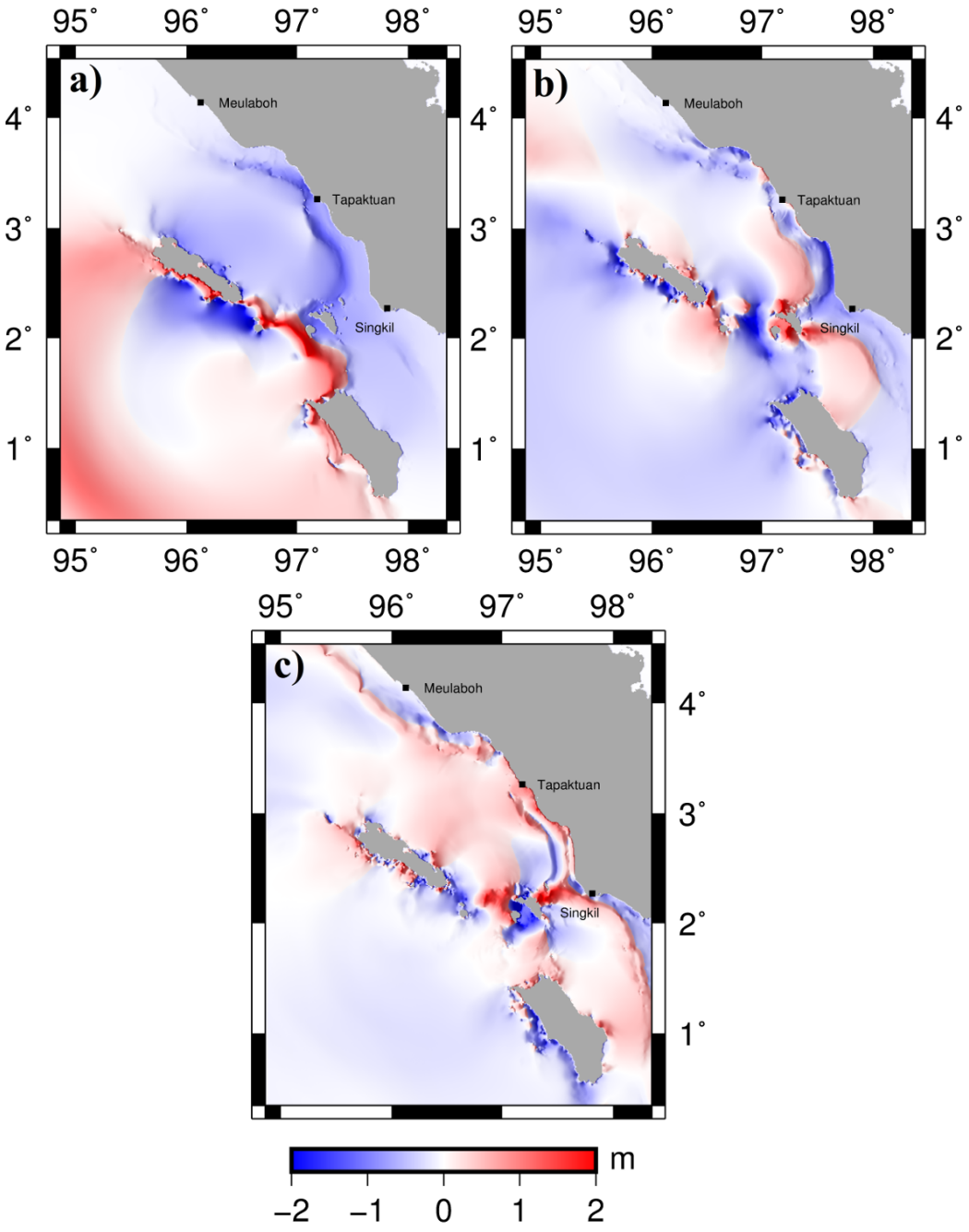

Figure 4.2: Snapshots of tsunami propagation proces in 2005 at southwestern coast of Aceh at: (a) t = 14 min, (b) t = 33 min, and (c) t = 51 min.

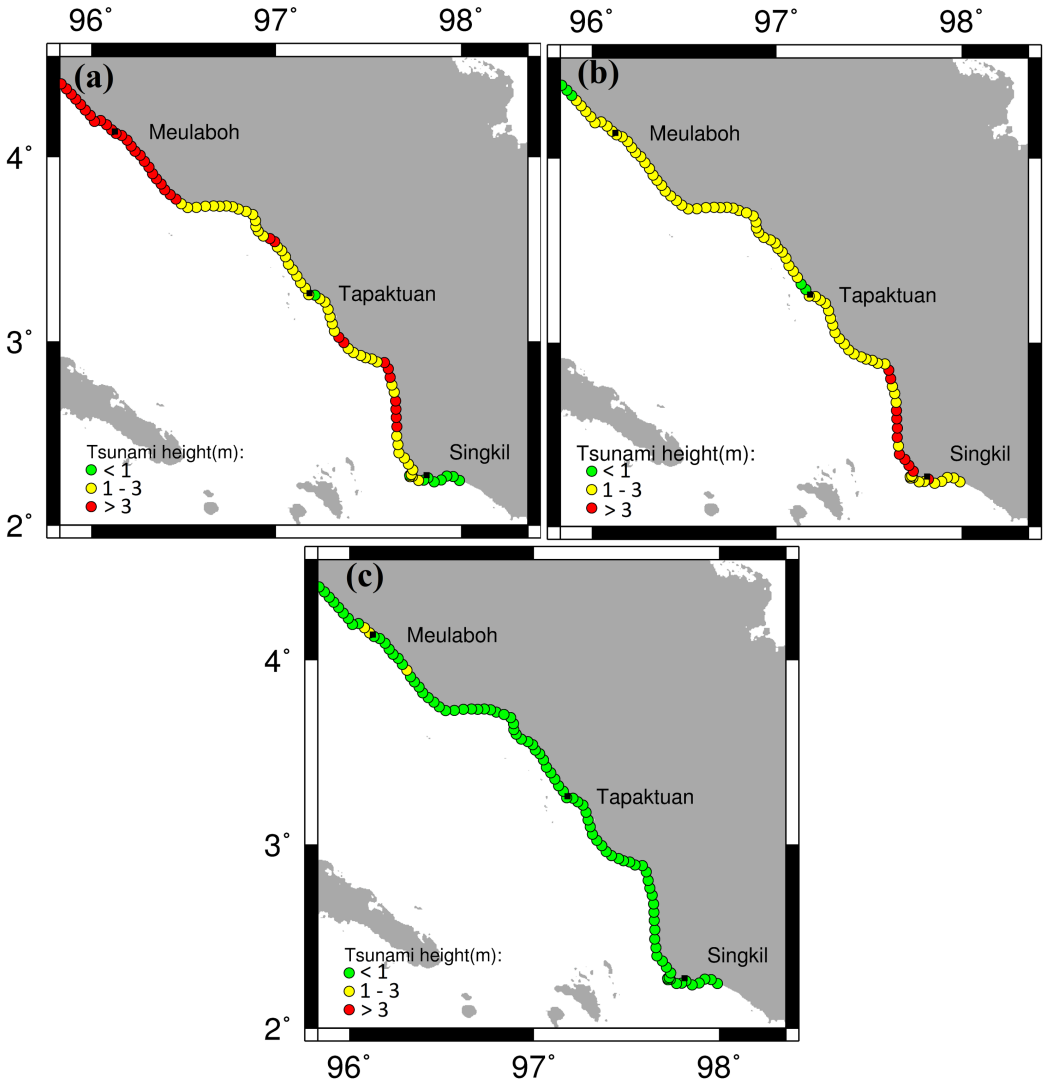

Figure 4.3: The maximum tsunami wave height along the southwestern coast of Aceh for tsunami case in: (a) 2004; (b) 2005; and (c) 2012.

Figure 4.3b shows the maximum tsunami height along Sumatra Island by 2005 tsunami. As it has been confirmed by field measurements, the tsunami height at Tapaktuan was calculated lower than the neighboring coast, especially Singkil. In case of 2005 tsunami, the wave height at Singkil which is located on the southern area of Tapaktuan becomes higher by going around

the southern end of Simeulu Island. On the other hand, the high wave does not arrive at Tapaktuan.

4.3.2 Case of tsunami in 2012

Two big earthquakes occurred again in April 11, 2012 after 8 years of Indian Ocean Tsunami in 2004. They occurred at the west of Aceh Province outside the Sumatra subduction zone with earthquake epicenter at (2.311N, 93.063E) and (0.773N, 92.452E) with magnitudes $M_w = 8.6$ and $M_w = 8.2$, respectively. The focal mechanism of the earthquakes was strike slip. Hence, those earthquakes had been predicted not to cause damage such as the case of in 2004 (Duputel et al., 2012). Tsunami waves were propagated faster to the northwestern coast of Aceh province because the rupture area was extended northeast. Hence, several people around there such as in Banda Aceh had saw receding water after several minutes of the main shock.

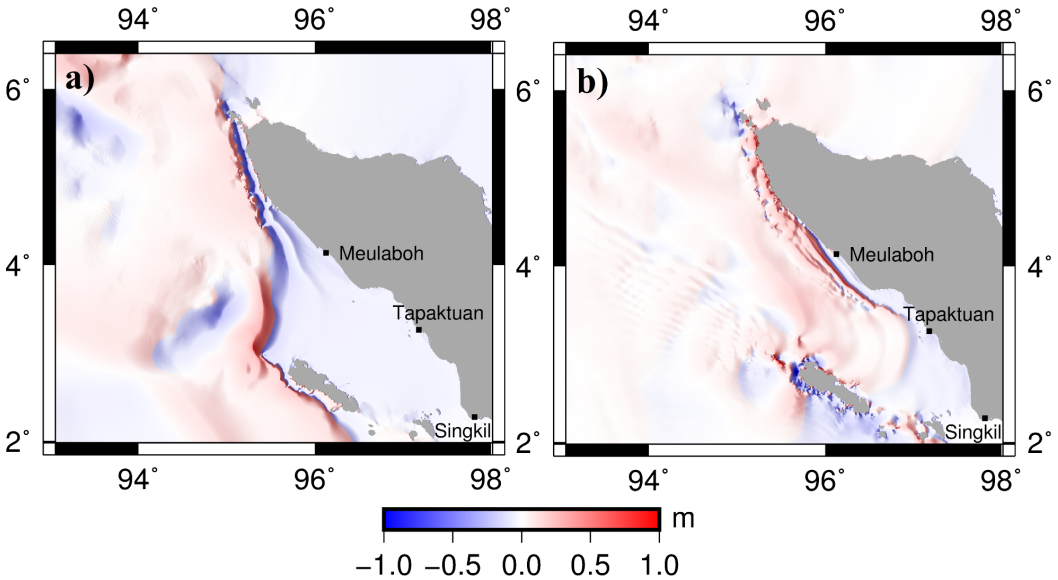

Figure 4.4: Snapshots of tsunami propagation process in 2012 at southwestern coast of Aceh at: (a) t = 30 min and (b) t = 58 min, after the earthquake.

Based on the simulations, the tsunami waves had occurred in Meulaboh and had not caused damage in coastal area as shown in Figure 4.3c. The tsunami wave reached at the cities with height about less than 1 m. While in Tapaktuan and Singkil, tsunami had not occurred. Tsunami wave was blocked by the Simeulu Island and the wave was reflected by the island toward the southern part of Sumatra. Half of tsunami wave that were not blocked was propagated through strait between Sumatra and Simeulue Islands. Even though it able to propagate through the Banyak Island, the focused wave which occurred around Banyak island did not cause massive damage at Singkil. That can be seen in Figure 4.4b.

4.3.3 Hypothetical model for future hazard

The hypothetical case is used the earthquake with $M_w = 8.5$. That value is taken according to Sengara et al. (2008); Suppasri et al. (2012a,b); Burbidge et al. (2009). Based on the simulation results, the tsunami propagation process for case A1 is similar with the tsunami in 2005 as shown in Figure 4.5a. Singkil become the worst area that impacted by the tsunami wave. In other hand, the tsunami wave is lower in Tapaktuan and Meulaboh. However, the focused wave is occurred in the case of model B1 and C1. That indicated by the propagation process as shown in Figure 4.5. The tsunami waves for model B1 and C1 were propagated faster than model A1 because almost the entire rupture area for model A1 was blocked by Simeulue Island.

Figure 4.6 shows the results of maximum tsunami height at the cities under the past and hypothetical scenarios. Case B1 indicates higher than Case A1 and C1 for Tapaktuan city. By the examination of tsunami propagation process, Simeulu Island seemed to act as a shelter for the area around Tapaktuan

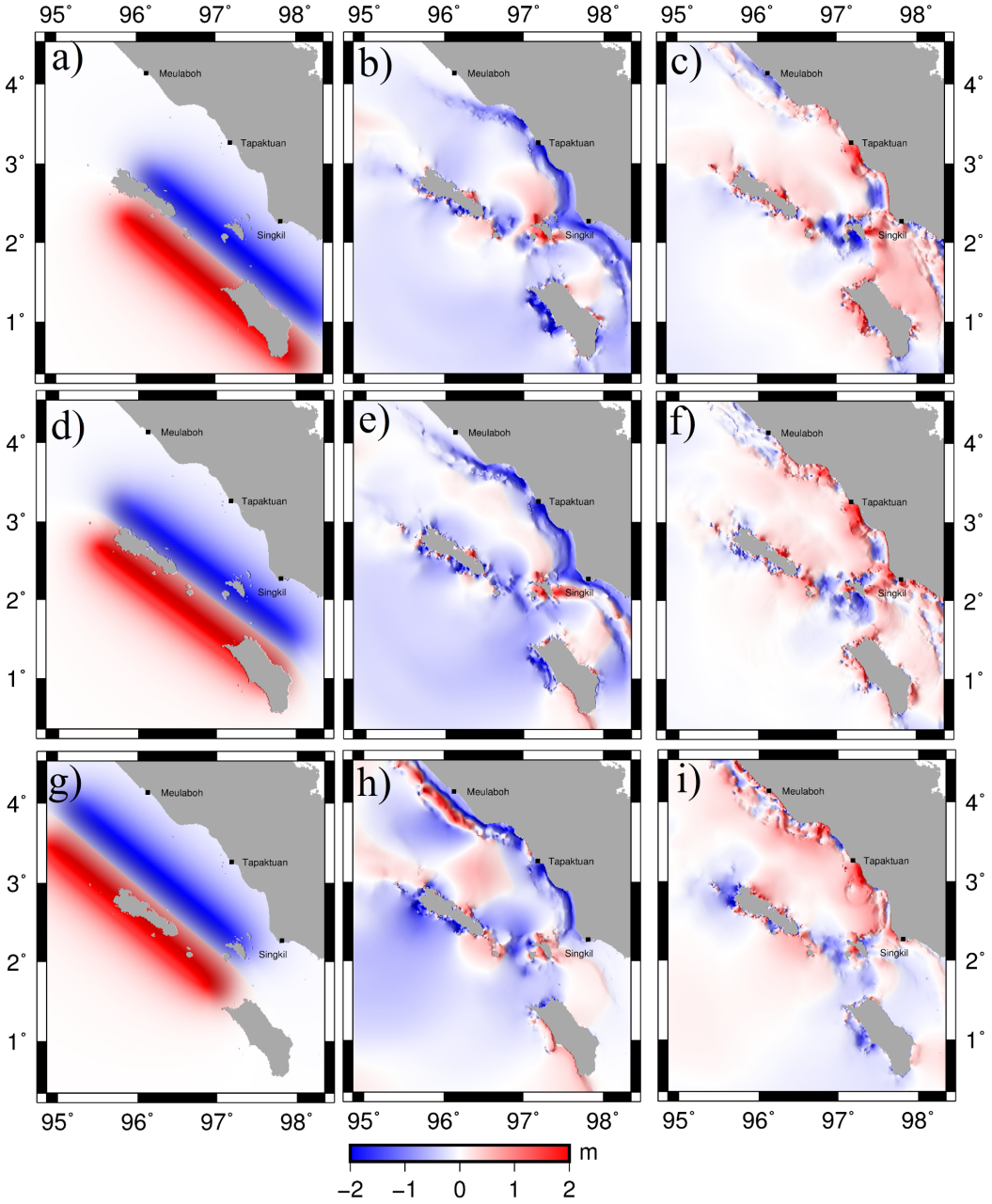

Figure 4.5: Snapshots of tsunami propagation proces for case: A1 (a) t = 0 min, (b) t = 30 min, and (c) t=60 min, B1 (d) t = 0 min, (e) t = 30 min, and (f) t=60 min, and C1 (g) t = 0 min, (h) t=30 min, and (i) t =60 min.

in Case A1 and C1. Banyak Island and flat topography caused the tsunami am-

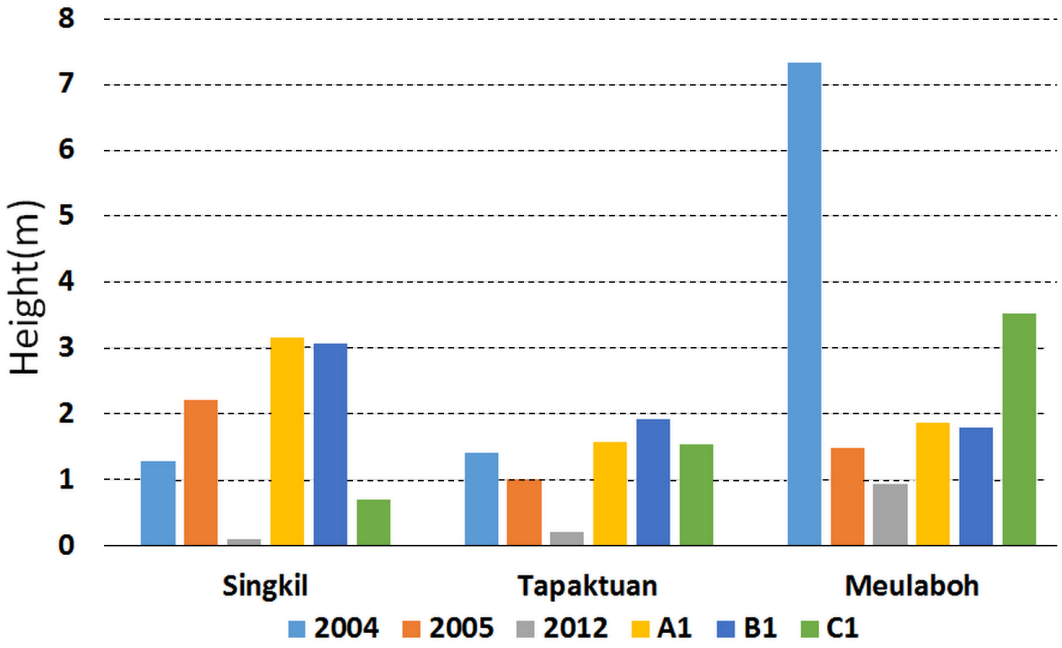

Figure 4.6: Tsunami wave height at Singkil, Tapaktuan, and Meulaboh.

plification in the Singkil city. Meulaboh city, which directly facing the Indian Ocean, becomes the vulnerable area toward the tsunami disaster. When the fault area is located exceed to northwest of the Simeulu island. The tsunami wave will be able to propagate directly to the Meulaboh city as same as the tsunami in 2004. This phenomena indicated that Whether island able to prevent the tsunami waves becomes higher depends on the position between the island and rupture area (Riyaz et al., 2010).

4.4 Effect of Reflected Wave

4.4.1 Maximum Tsunami Height

The maximum tsunami wave was observed at observation points around the northern coast of Lhok Kruet, which has a concave shoreline. This area is

indicated by black arrows on Figure 4.7a. The tsunami wave that propagated around the concave shoreline was amplified due to bathymetry conditions. The maximum tsunami height reached about 11 m at the concave shoreline compared to the area nearby that it just reached about 9 m. The tsunami inundation area in Lhok Kruet, based on a Google map released in 2005, was one of the worst affected by the tsunami in Aceh Jaya (Figure 4.7d). The inundation area was turned to soil, whereas other areas are seen to still be in their green condition, as before the tsunami occurred. The tsunami inundation area reached about 2.3 km from the shoreline.

The maximum tsunami wave height around Pulo Raya Island varied. The maximum tsunami heights at the coastal area facing directly to the Indian Ocean and at the back side of the island were about 7 m and 9 m, respectively (see the purple and green lines in Figure 4.7b). The back side of the island had value as same as the mainland. This indicates that the tsunami wave was amplified at the back side of the island. The tsunami wave that arrived at the mainland was reflected back to the island. The small gap of about 800 m between the mainland and the small island also caused the maximum tsunami height to be about the same around this area. At the top and bottom sides of the island, the maximum tsunami height reached about 8 m and 7 m, respectively, as shown in Figure 4.7c. The maximum tsunami waves were at the top side of the island when the tsunami wave arrived at the mainland after 22 min of simulation. The comparison between the maximum tsunami height after 22 and 25 min of simulation can be seen in Figure 4.8. The graph indicates that the tsunami wave arrived at the northern coast of the island with the maximum height at the time the tsunami waves reflected back to the ocean. This condition was proven based on previous studies in the case of the

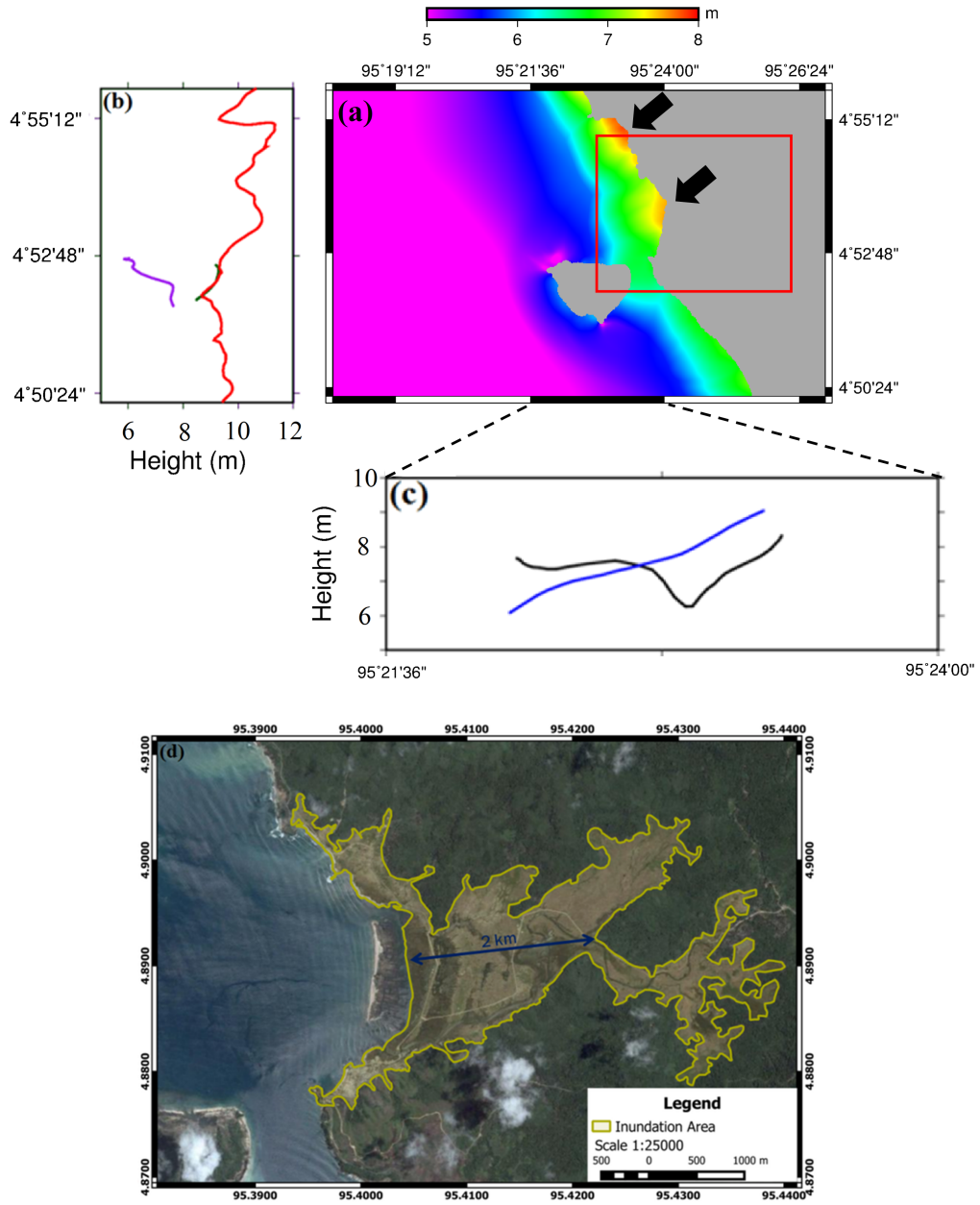

Figure 4.7: (a) Maximum tsunami height for Layer 2 of the computational domain. (b) Maximum tsunami height at the mainland (red line), western of the island (purple line), and eastern of the island (green line). (c) Maximum tsunami height at northern of the island (blue line) and southern of the island (black line). (d) Inundation area in Lhok Kruet.

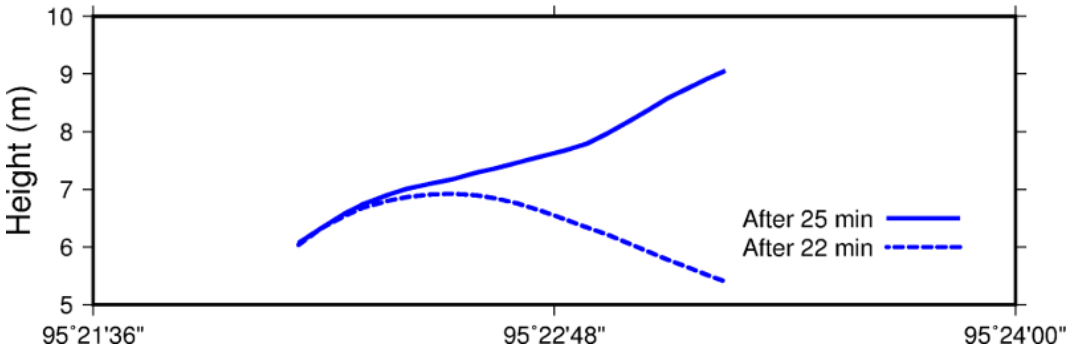

Figure 4.8: Comparison of tsunami height at the northern coast of Pulo Raya after the tsunami propagated at about 22 and 25 min.

1992 Folres Islands tsunami (Yeh et al., 1993, 1994; Liu et al., 1995; Imamura et al., 1995).

4.4.2 Hydraulic Pressure and Inundation Area

This research used hydraulic pressure and the inundation area (based on the Google map) to explain the tsunami's destruction of most of the infrastructure on the northern coast of Pulo Raya. The northern coast of Pulo Raya is located on the lee side of the island, where the maximum tsunami wave was small, but the velocity is large. (Imamura et al., 1995) found that velocity is more important than maximum tsunami height for calculating hydraulic pressure. The propagation process discussed previously indicates that the current velocity when the tsunami waves arrived at the mainland was not much larger than the tsunami wave that reflected back toward the island. The observation point which located at the middle of the northern coast of the island was used to calculate the hydraulic pressure.

Tsunami height, velocity vector, and hydraulic pressure values were obtained based on simulation at observation points, as shown in Figure 4.9. The results indicate that the tsunami wave at the observation point in the middle

of the northern coast of Pulo Raya had a positive value of velocity. This indicates that the tsunami wave was propagated from the south to the north. The tsunami wave that arrived at the northern coast of Pulo Raya was propagated

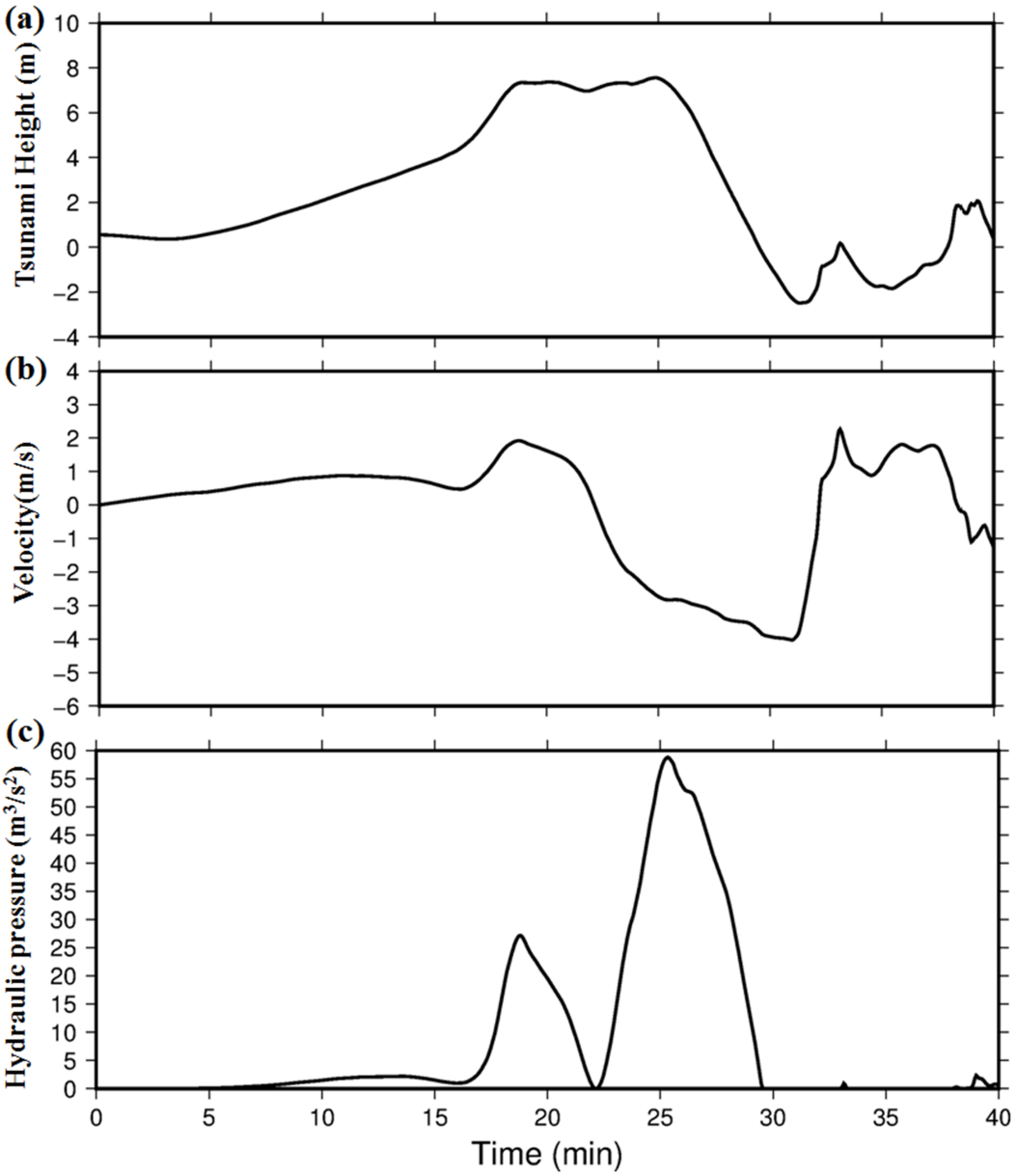

Figure 4.9: (a) Simulated of water level during the Indian Ocean tsunami at the Northern coast of Pulo Raya island, (b) velocity, and (c) hydraulic pressure.

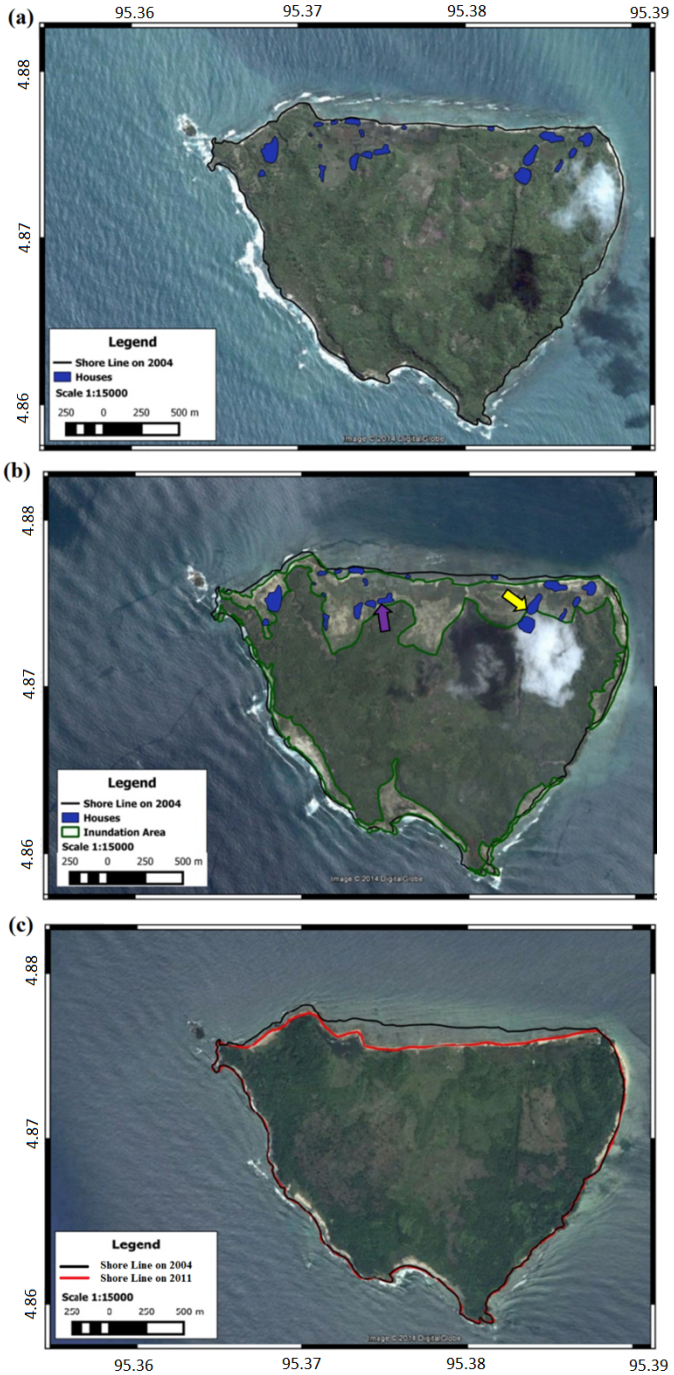

Figure 4.10: Pulo Raya Island condition in (a) 2004, before tsunami; (b) 2005, after tsunami; and (c) 2011.

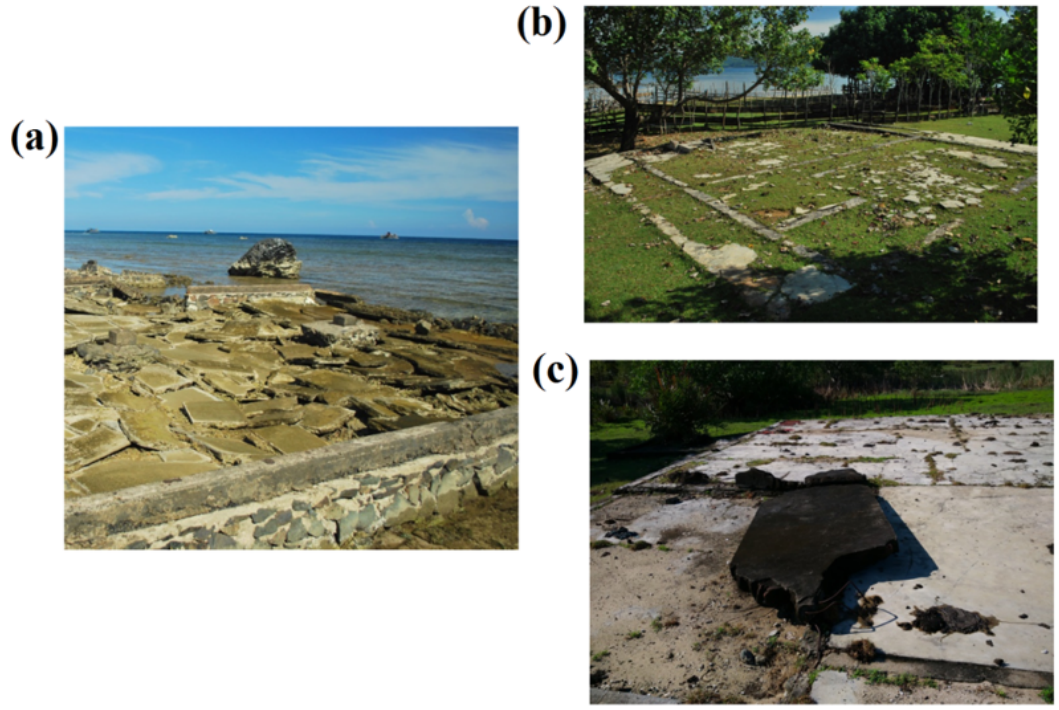

Figure 4.11: Buildings destroyed by the tsunami impact in 2004 at (a) northern, (b) northern, and (c) north eastern coasts of Pulo Raya.

to the east and north, as shown previously in Figure 3.9 of Chapter 3. However, the velocity became negative at the observation point after about 21 min of simulation. This indicates that the tsunami wave was propagated from the north to the south, directly focusing on the northern coast of Pulo Aceh with hydraulic pressure of about 50 m^3/s^2.

Geospatial information based on Google maps released between 2004 and 2011 was used in this research. Figure 4.10a shows the Pulo Raya island condition in 2004, including the shoreline and infrastructure (marked by black lines and the blue polygon) before it was impacted by the tsunami. Most of the infrastructure on the island was located on the northern coast near the shoreline. The map released in 2005 (see Figure 4.10b) shows that most of the

infrastructure was inside the inundation area, which is marked by the green polygon. The tsunami destroyed most of the infrastructure, including houses, a hospital, and a mosque. It also caused erosion on the northern coast, as shown in Figure 4.10c. The black line shows the shoreline condition in 2004, and the red line shows the shoreline condition in 2011, after seven years of erosion. In this time frame, the shoreline retreated about 145 m.

The hydraulic pressure correlates well with the observed condition of buildings after the tsunami. (Imamura et al., 1995) found that hydraulic pressure over 5 to 9 m^3/s^2 can lead to building damage of 50% or more. The foundation of a mosque located in the middle of the northern coast is one example of hydraulic pressure wrecking an upper structure, as shown in Figure 4.11a. Several foundations of houses are also visible on the northern and northeastern coast of Pulo Raya, as shown in Figure 4.11b and 4.11c. Even 175 m to 225 m from the shoreline, the hydraulic pressure was strong enough to completely overthrow the upper structure of houses during the tsunami.

References

Banerjee, P., Pollitz, F., Nagarajan, B., and Burgmann, R. (2007). Coseismic slip distributions of the 26 december 2004 sumatra–andaman and 28 march 2005 nias earthquakes from gps static offsets. *Bulletin of the Seismological Society of America*, 97(1A):S86–S102.

Burbidge, D., Cummins, P., Latief, H., Mleczko, R., Mokhtari, M., Natawidjaja, D., Rajendran, C., and Thomas, C. (2009). A probabilistic tsunami hazard assessment of the indian ocean nations. *Australian Government, Geoscience Australia, Professional Opinion*, (2009/11).

DART (2013). National data buoy center. available from: http://www.ndbc.noaa.gov/dart/dart.shtml. last accessed: 2016, march 4.

Duputel, Z., Kanamori, H., Tsai, V. C., Rivera, L., Meng, L., Ampuero, J.-P., and Stock, J. M. (2012). The 2012 sumatra great earthquake sequence. *Earth and Planetary Science Letters*, 351:247–257.

Hill, E. M., Borrero, J. C., Huang, Z., Qiu, Q., Banerjee, P., Natawidjaja, D. H., Elosegui, P., Fritz, H. M., Suwargadi, B. W., and Pranantyo, I. R. (2012). The 2010 m_w 7.8 mentawai earthquake: Very shallow source of a rare tsunami earthquake determined from tsunami field survey and near-field gps data. *Journal of Geophysical Research: Solid Earth*, 117(B6):p. B06402.

Imamura, F., Gica, E., Takahashi, T., and Shuto, N. (1995). Numerical simulation of the 1992 flores tsunami: Interpretation of tsunami phenomena in northeastern flores island and damage at babi island. *Pure and Applied Geophysics*, 144(3):555–568.

Liu, P. L.-F., Cho, Y.-S., Briggs, M. J., Kanoglu, U., and Synolakis, C. E. (1995). Runup of solitary waves on a circular island. *Journal of Fluid Mechanics*, 302:259–285.

Riyaz, M., Park, K.-H., Ali, M., and Kan, H. (2010). Influence of geological setting of islands and significance of reefs for tsunami wave impact on the atoll islands, maldives. *Bulletin of Engineering Geology and the Environment*, 69(3):443–454.

Sengara, I. W., Latief, H., and Kusuma, S. B. (2008). Probabilistic seismic and tsunami hazard analysis for design criteria and disaster mitigation in rehabilitation and reconstruction of a coastal area in city of banda aceh. In

Geotechnical Engineering for Disaster Mitigation and Rehabilitation, pages 224–230. Springer.

Stefanakis, T. S., Contal, E., Vayatis, N., Dias, F., and Synolakis, C. E. (2014). Can small islands protect nearby coasts from tsunamis? an active experimental design approach. *Proceedings of the Royal Society A: Mathematical, Physical and Engineering Sciences*, 470(2172):20140575.

Suppasri, A., Futami, T., Tabuchi, S., and Imamura, F. (2012a). Mapping of historical tsunamis in the indian and southwest pacific oceans. *International Journal of Disaster Risk Reduction*, 1:62–71.

Suppasri, A., Imamura, F., and Koshimura, S. (2012b). Tsunami hazard and casualty estimation in a coastal area that neighbors the indian ocean and south china sea. *Journal of Earthquake and Tsunami*, 6(02):1250010.

Syamsidik and Istiyanto, D. C. (2013). Tsunami mitigation measures for tsunami prone small islands: lessons learned from the 2010 tsunami around the mentawai islands of indonesia. *Journal of Earthquake and Tsunami*, 7(01):1350002.

Syamsidik, Rasyif, T. M., and Kato, S. (2015). Development of accurate tsunami estimated times of arrival for tsunami-prone cities in aceh, indonesia. *International Journal of Disaster Risk Reduction*, 14:403 – 410.

Yeh, H., Imamura, F., Synolakis, C., Tsuji, Y., Liu, P., and Shi, S. (1993). The flores island tsunamis. *Eos, Transactions American Geophysical Union*, 74(33):369–373.

Yeh, H., Liu, P., Briggs, M., and Synolakis, C. (1994). Propagation and amplification of tsunamis at coastal boundaries. *Nature*, 372(6504):353.

Zahibo, N., Pelinovsky, E., Yalciner, A., Kurkin, A., Koselkov, A., and Zaitsev, A. (2003). The 1867 virgin island tsunami: observations and modeling. *Oceanologica Acta*, 26(5-6):609–621.

Chapter 5

Conclusion and Future Research

The main objective of this study is to enhance the local community awareness and preparedness toward the tsunami wave hazard especially in Aceh province, Indonesia. In order to achieve this goal, several study have been conducted, which aim at performing a investigation of effects of the small island, the hydrodynamic process of reflected wave on small islands, and morphological changes due to tsunami wave. Conclusions and recommendations based on results and findings through the study above are elucidated in this chapter as follow.

5.1 Conclusion

Several conclusions have been taken based on the simulation model results as follow:

- The amplification due to the offshore island happens when the tsunami wave propagates from both sides of the island. That indicated by 2005 tsunami in Singkil city

- The small island has a possibility to cause the amplification when the fault area is symmetry in front of the island. The tsunami wave is able to propagate through the island and focused its wave behind it.
- The simulation results indicate that the reflected wave, together with the tsunami wave velocity, triggered hydraulic wave pressure that destroyed the infrastructure along the northern coast of Pulo Raya.
- The simulation results show that the tsunami wave caused massive morphological changes to the Banda Aceh coastal area. The land barrier area, which was in a natural condition, was almost completely eroded by the tsunami wave. The simulation results agreed well with geospatial data.
- Numerical simulation can be used to investigate morphological changes due to tsunami waves in the high-risk area. This model can predict areas of sedimentation and erosion caused by a tsunami wave. This study shows that the numerical model can simulate destruction of the land barrier by the 2004 tsunami

5.2 Recommendations

Based on the limitation and results of the study, some recommendations for future research and practice are offered as follow:

5.2.1 Recommendations for future research

- A low accuracy of the data can cause big different between simulation result and observation data. A high resolution data for Topography and bathymetry is required to obtain more accurate result. This study has

limitation on using single grain size for simulating sediment transport. A multi grain size is suggested to applied for future study.

- The current model was used the Manning equation to calculate the bed stress. A boundary-layer method is suggested to used in order to get more accurate result for further study.

- Further study is needed to investigate the morphological changes caused by future tsunamis, based on the current condition of Banda Aceh city, to enhance tsunami disaster mitigation by analyzing the sensitivity of the input data that are applied in the sediment transport model.

- The sediment transport calculation requires a lot of computational resources. There is a need to develop the model by using Graphic Processing Unit (GPUs) to reduce computational time.

5.2.2 Recommendations for practice

- Small changes of the location of epicenter in future tsunami scenarios will result in different tsunami impact along Sumatra island due to the influence of small islands. This condition indicates that it will be dispensable for the appropriate disaster management and education to grasp the function of small islands along Sumatra island about future scenarios.

- The small Islands communities are among the most tsunami vulnerable societies in term of preparedness towards tsunami. As Indonesia has many populated small islands, local communities and the governments need to be aware of the complex phenomena that control the impacts of tsunamis on small islands in order to minimize the effects of future tsunamis.

- The information of erosion and sedimentation location that obtained from simulation results can be used by local governments for land use management to help avoid a disaster such as the one in Banda Aceh during the 2004 Indian Ocean tsunami.